Magnetospheric Science Objectives of the Juno *Mission*

F. Bagenal, A. Adriani, F. Allegrini, S. J. Bolton, B. Bonfond, E. J. Bunce, J. E. P. Connerney, S. W. H. Cowley, R. W. Ebert, et al.

Space Science Reviews

ISSN 0038-6308

Space Sci Rev
DOI 10.1007/s11214-014-0036-8

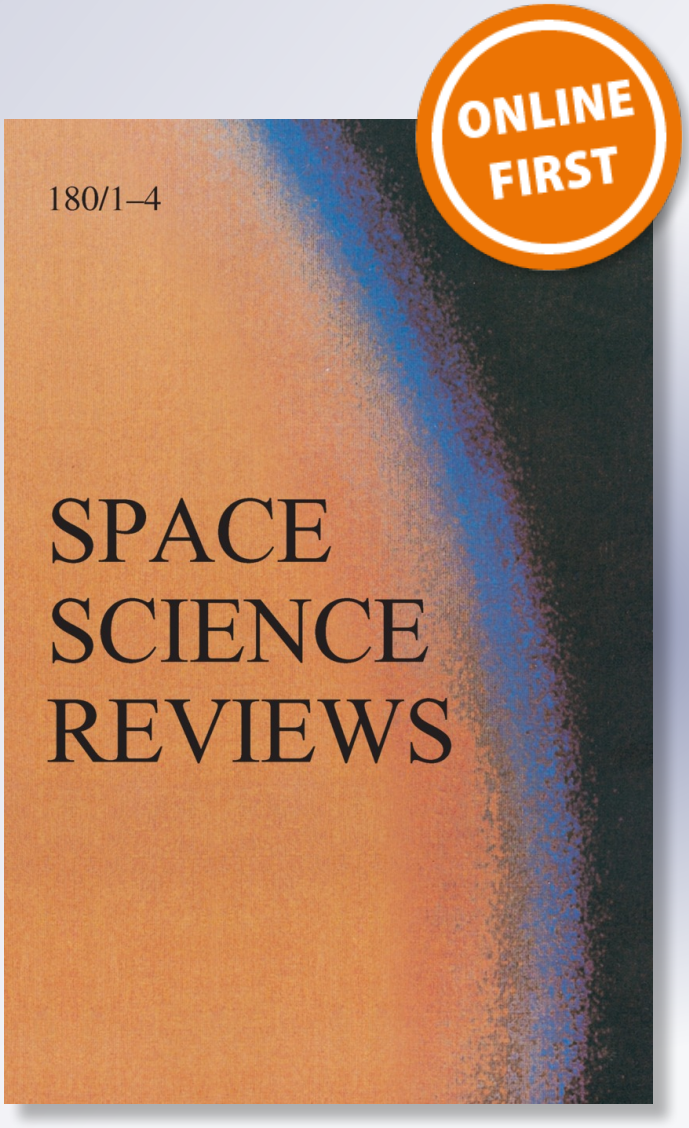

Springer

Space Sci Rev
DOI 10.1007/s11214-014-0036-8

Magnetospheric Science Objectives of the *Juno* Mission

F. Bagenal · A. Adriani · F. Allegrini · S.J. Bolton · B. Bonfond · E.J. Bunce · J.E.P. Connerney · S.W.H. Cowley · R.W. Ebert · G.R. Gladstone · C.J. Hansen · W.S. Kurth · S.M. Levin · B.H. Mauk · D.J. McComas · C.P. Paranicas · D. Santos-Costa · R.M. Thorne · P. Valek · J.H. Waite · P. Zarka

Received: 1 July 2013 / Accepted: 16 January 2014

Abstract In July 2016, NASA's *Juno* mission becomes the first spacecraft to enter polar orbit of Jupiter and venture deep into unexplored polar territories of the magnetosphere. Focusing on these polar regions, we review current understanding of the structure and dynamics of the magnetosphere and summarize the outstanding issues. The *Juno* mission pro-

F. Bagenal (✉)
University of Colorado, Boulder, CO, USA
e-mail: bagenal@colorado.edu

A. Adriani
INAF-IAPS, Rome, Italy

F. Allegrini · S.J. Bolton · R.W. Ebert · G.R. Gladstone · D.J. McComas · D. Santos-Costa · P. Valek · J.H. Waite
Southwest Research Institute, San Antonio, TX, USA

F. Allegrini · D.J. McComas · P. Valek
University of Texas, San Antonio, TX 78249, USA

B. Bonfond
Laboratory for Planetary and Atmospheric Physics, University of Liège, Liège, Belgium

E.J. Bunce · S.W.H. Cowley
University of Leicester, Leicester, UK

J.E.P. Connerney
Goddard Space Flight Center, Greenbelt, MD, USA

C.J. Hansen
Planetary Science Institute, Tucson, AZ, USA

W.S. Kurth
University of Iowa, Iowa City, IA, USA

S.M. Levin
Jet Propulsion Lab, Pasadena, CA, USA

Published online: 21 February 2014

file involves (a) a several-week approach from the dawn side of Jupiter's magnetosphere, with an orbit-insertion maneuver on July 6, 2016; (b) a 107-day capture orbit, also on the dawn flank; and (c) a series of thirty 11-day science orbits with the spacecraft flying over Jupiter's poles and ducking under the radiation belts. We show how *Juno's* view of the magnetosphere evolves over the year of science orbits. The *Juno* spacecraft carries a range of instruments that take particles and fields measurements, remote sensing observations of auroral emissions at UV, visible, IR and radio wavelengths, and detect microwave emission from Jupiter's radiation belts. We summarize how these *Juno* measurements address issues of auroral processes, microphysical plasma physics, ionosphere-magnetosphere and satellite-magnetosphere coupling, sources and sinks of plasma, the radiation belts, and the dynamics of the outer magnetosphere. To reach Jupiter, the *Juno* spacecraft passed close to the Earth on October 9, 2013, gaining the necessary energy to get to Jupiter. The Earth flyby provided an opportunity to test *Juno*'s instrumentation as well as take scientific data in the terrestrial magnetosphere, in conjunction with ground-based and Earth-orbiting assets.

Keywords Jupiter · Magnetosphere · Juno

1 Introduction

1.1 Overview

The vast and complicated magnetosphere of Jupiter was first detected in 1954, before Van Allen's *Explorer 1* discovery of the Earth's radiation belts, via bursts of radio emission at decameter wavelengths (Burke and Franklin 1955). Subsequent radio observations at decimeter wavelengths revealed synchrotron emission from trapped electrons (Field 1959; Drake and Hvatum 1959). These early radio measurements showed that Jupiter has a strong magnetic field (opposite in polarity to the Earth's) tilted about 10° from the spin axis and that energetic (>MeV) electrons are trapped near the equator close to the planet (see for example review by Carr et al. 1983). These very energetic particles pose a formidable hazard for spacecraft exploring Jupiter's inner magnetosphere.

The peculiar role of Io was first pointed out in the observations by Bigg (1964) that bursts of radio emission were modulated by the position of the moon along its orbit around Jupiter. The magnetometers and particle detectors on *Pioneer 10* (1973) and *Pioneer 11* (1974) exposed the vastness of Jupiter's magnetosphere and made in situ measurements of energetic ions and electrons. The *Voyager 1* fly-by in 1979 revealed Io's prodigious volcanic activity, thus explaining why this innermost Galilean moon plays such a strong role. Key information about the Io plasma torus and Io-induced aurora came from a variety of Earth- and space-based telescopes at wavelengths across the spectrum. Additional data came from subsequent traversals of Jupiter's magnetosphere by the *Ulysses* (1992), *Cassini* (2000) and *New Horizons* (2007) spacecraft, but it was the 33 orbits of *Galileo* (1995–2003) around Jupiter that

B.H. Mauk · C.P. Paranicas
Applied Physics Lab., The Johns Hopkins University, Laurel, MD, USA

R.M. Thorne
Atmospheric Sciences, UCLA, Los Angeles, CA, USA

P. Zarka
LESIA, Observatoire de Paris-CNRS-UPMC-UPDn, 92190 Meudon, France

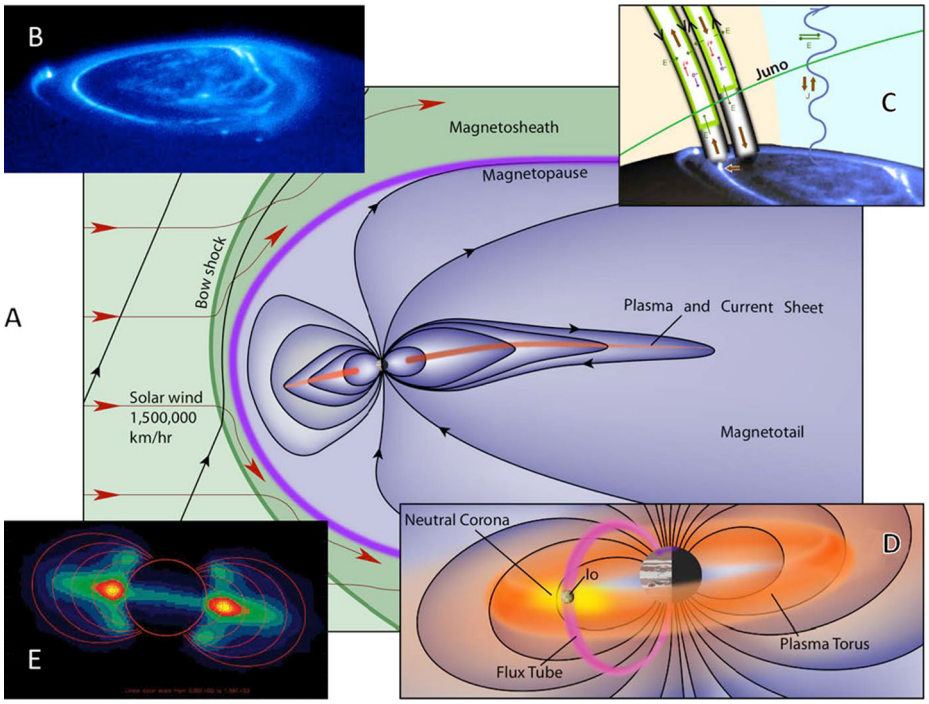

Fig. 1 (**A**) The magnetosphere of Jupiter extends 63–92 Jovian radii in the direction towards the Sun, with a tail that stretches beyond the orbit of Saturn >4 AU, and occupies a volume over a thousand times that of the Sun. (**B**) Intense auroral emissions are signatures of the coupling between the planet and the magnetospheric plasmas. (**C**) The *Juno* spacecraft will fly through the regions where the auroragenerating particles are excited. (**D**) The magnetosphere is dominated by a ∼1 ton/s source of plasma from Io's volcanic gases that forms a toroidal cloud around Jupiter. (**E**) Close to the planet are strong radiation belts comprising energetic (MeV) electrons that emit synchrotron emission

mapped out the equatorial magnetospheric structures and monitored their temporal variability.

Jupiter's strong magnetic field makes the magnetosphere of Jupiter the largest object within the heliosphere (Fig. 1), stretching in the direction towards the Sun for typical distances of 63–92 R_J (the radius of Jupiter, $R_J = 71492$ at the 1 bar level, see the Appendix). Over a ton/second of Io's SO_2 atmosphere escapes the satellite. The escaping neutrals are dissociated, ionized and trapped by the magnetic field. The resulting dense (∼2000 particles/cm^3) torus of plasma, roughly corotates with Jupiter's ∼10 hour spin period. The ions of sulfur and oxygen (Ti ∼100 eV) are excited by the ∼5 eV thermal electrons and radiate ∼1.5 terawatts of UV emission. Rather than cooling on expansion, the iogenic plasma is heated (by an as-yet-unknown process) to temperatures of ∼10 s keV as it is transported radially outwards (via flux tube interchange motions) on timescales of weeks. Coupling of the magnetospheric plasma to Jupiter's rotating atmosphere dominates the dynamics of the magnetosphere, the ensuing strong centrifugal forces producing an extended, equatorially-confined plasmadisk. Associated with the electrical currents that couple the magnetospheric and ionospheric plasmas are intense auroral emissions that span the spectrum from X-rays to radio. The hot plasma in Jupiter's plasmadisk inflates the magnetosphere, making it larger and more compressible than a magnetic dipole alone. While the vast

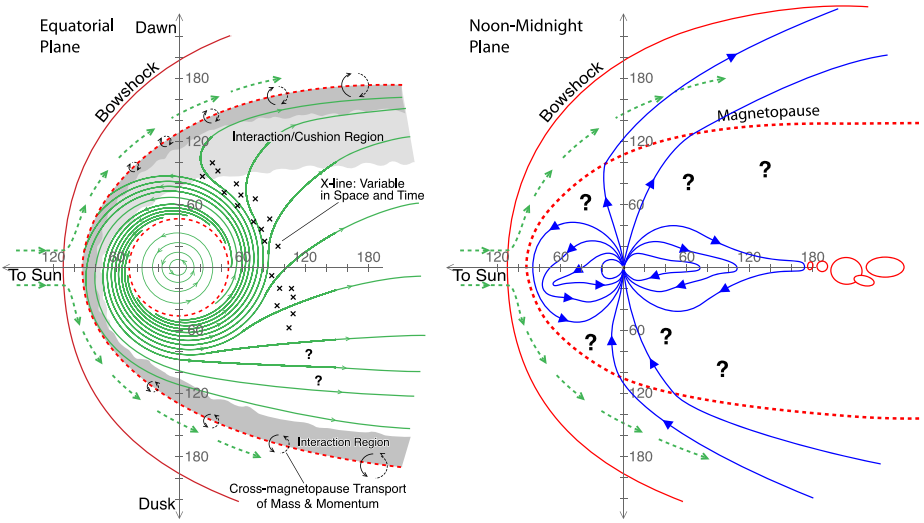

Fig. 2 Magnetospheric structure and dynamics. While the equatorial plane (*left*, **A**) has been traversed multiple times and is well mapped, the polar region (see *noon-midnight plane on right*, **B**) has barely been explored and major questions remain. *Blue lines* show magnetic field, *green lines* indicate flows and *red lines* show boundaries between plasma regimes. *On the left*, the *green lines* indicate averaged motions of material: mostly corotating with the planet inside $\sim 50\ R_J$, outside of which the bulk of the plasma spirals outward, eventually being lost down the tail or through the magnetopause. To conserve magnetic flux through the equatorial plane, fluxtubes that are largely empty must circulate inwards and return flux to the inner magnetosphere. (Based on Vasyliūnas 1983; Delamere and Bagenal 2010)

magnetosphere presents a substantial obstacle to the solar wind, the nature of the interaction between the solar wind and magnetospheric plasma remains an issue of debate.

Figure 2 shows some current ideas of the global structure and dynamics of the magnetosphere comprising: a rotation-dominated inner/middle plasmadisk, magnetic coupling to Jupiter's atmosphere/ionosphere, slow diffusive radial transport, a sporadic x-line across the magnetotail, plasmoids ejected down the tail and interaction regions in boundary layers on the flanks. These components are discussed further in Sect. 3. While the equatorial plane has been traversed multiple times and is well mapped, the polar region has barely been explored and major questions remain.

The pre-*Galileo* understanding is presented in Dessler (1983)'s book *Physics of the Jovian Magnetosphere* and the advances made by the *Ulysses* and *Galileo* missions are reviewed in seven chapters of *Jupiter: The Planet, Satellites and Magnetosphere* (edited by Bagenal et al. 2004). In this paper we summarize the current understanding of Jupiter's magnetosphere, the outstanding issues and the methods *Juno* employs to address them. An overview of the whole *Juno* mission is provided by Bolton et al. (2014, this issue). The *Juno* instruments that make in situ magnetospheric measurements are the magnetometer MAG (Connerney et al. 2014, this issue), the electric and magnetic wave detectors Waves (Kurth et al. 2014, this issue), the electron and ion detectors JADE (McComas et al. 2014a, this issue), and the energetic particle detectors JEDI (Mauk et al. 2014, this issue). Remote sensing measurements of the aurora are carried out at UV wavelegths by UVS (Gladstone et al. 2014, this issue), in the IR by JIRAM (Adriani et al. 2014, this issue) and at visible wavelengths by *Juno*Cam (Hansen et al. 2014, this issue). Emissions from the radiation belts are detected via emissions in the microwave region of the spectrum by the MWR instrument (Janssen et al. 2014, this issue).

1.2 Comparative Magnetospheres

Reviews of planetary magnetospheres range in their approach to the subject from considering it a topic in space plasma physics (exploiting the breadth of planetary environments as a laboratory to explore space plasmas) to a branch of planetary science (presenting the space environment as a component of planetary objects). Basic, qualitative introductions are given by Van Allen and Bagenal (1999) and by Kivelson and Bagenal (2007). Deeper studies of comparative magnetospheres span from the abstract to the specific (Siscoe 1979; Vasyliūnas 2004, 2009, 2011; Kivelson 2007; Walker and Russell 1995; Bagenal 1992, 2009; Russell 2004, 2006; Kurth and Gurnett 1991).

The interaction between a planetary object and the surrounding plasma depends on the properties of both the object and the plasma flow in which it is embedded. A planet with a significant internal magnetic field forms a magnetosphere that extends the planet's influence beyond its surface or cloud tops. The interaction of the supersonic solar wind with a planetary magnetic field (either generated by an internal dynamo or induced externally) produces a bow shock (BS) upstream of the planet. Behind the bow shock, the slowed, heated magnetosheath plasma is deflected around the magnetospheric obstacle. The magnetospheric boundary—the magnetopause (MP)—has historically been regarded to first order as an impenetrable boundary. However, the amount of mass, momentum and magnetic flux exchanged across the magnetopause is an active area of research at Earth and other planets. The distance between the center of the planet and the magnetopause in the direction of the Sun, R_{MP}, is generally determined by a balance between the ram pressure of the solar wind and the internal pressure of the magnetosphere (combining both magnetic and plasma pressures). Whatever the details of the interaction, in all explored cases there is a "wake" or "tail"—the magnetotail—that can extend at least several hundred times R_{MP} downstream in the solar wind.

Figure 3 illustrates the huge range in scale of planetary magnetospheres. The magnetospheres of the giant planets encompass most of their extensive moon systems, including the four Galilean moons of Jupiter, many icy satellites (importantly Enceladus), and Titan at Saturn. Earth's Moon, however, resides almost entirely outside the magnetosphere, spending less than 5 % of its orbit crossing the magnetotail. The R_{MP} of Earth is about 10 R_{E} which is only a little larger than the radius of the planet Saturn. The R_{MP} of Saturn is about 20 R_{S} which is about 17 R_{J}, a modest fraction of Jupiter's magnetopause distance (R_{MP} of Jupiter ranges between typical scales of 63 and 92 R_{J}).

Table 1 lists the basic parameters characterizing the magnetospheres of Earth, Jupiter, and Saturn. The classical scale of a planet's magnetosphere, R_{CF}, as derived by Chapman and Ferraro (1930), comes from balancing the ram pressure of the solar wind with the magnetic pressure of a dipole planetary field. A simple pressure balance between the ram pressure of the solar wind $(\rho V^2)_{\mathrm{sw}}$ and the magnetic pressure of a dipole field $(B^2/2\mu_0)$ produces a weak variation in the dayside magnetopause distance R_{MP} such that $R_{\mathrm{MP}} \propto (\rho V^2)_{\mathrm{sw}}^{-1/6}$ (for a solar wind mass density $\rho_{\mathrm{sw}} = m_{\mathrm{p}} n_{\mathrm{sw}}$ and speed V_{sw}). That is, a dipole magnetosphere is very "stiff" with modest response to large changes in the solar wind.

As shown in Table 1 and illustrated in Fig. 3, this Chapman-Ferraro magnetopause distance works well for Earth but underestimates the sizes of the giant planet magnetospheres, particularly for Jupiter. If the pressure of the energetic particle populations P inside the magnetosphere, dominates over the local magnetic field pressure $(B^2/2\mu_0)$, then $\beta = P/(B^2/2\mu_0) > 1$ and the particle pressure inflates and stretches out the magnetic field, generating strong currents in the equatorial plasma disk. Figure 3 illustrates how the substantial internal plasma pressure at Jupiter (and to a lesser extent at Saturn) expands the

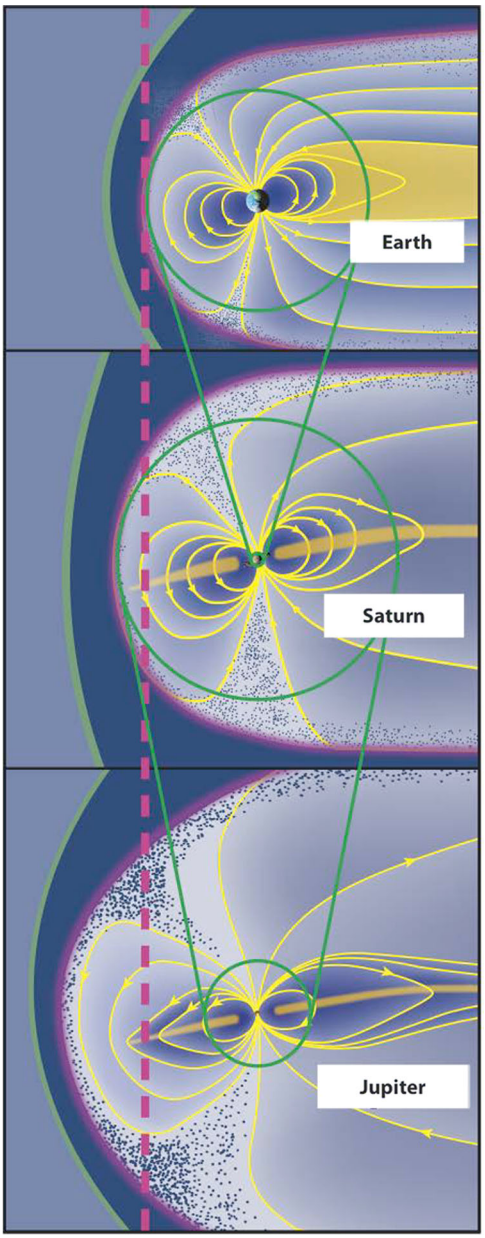

Fig. 3 Comparison of the magnetospheres of Earth, Saturn and Jupiter. The *green circles* show how the magnetosphere of Earth scales to the planet Saturn and how the magnetosphere of Saturn scales to the inner 20 % of Jupiter's magnetosphere. The *dashed vertical line* shows the scale of each magnetosphere for a pure dipole magnetic field with no internal plasma

magnetosphere well beyond that of a dipole internal field. At Jupiter, values of β greater than unity are found beyond $\sim$15 R_J, increasing to $\beta > 100$ by 45 R_J (Mauk et al. 2004). Not only does the plasma pressure dominate the magnetic pressure, but the radial profile of plasma pressure is also considerably flatter than the $R^{-1/6}$ variation in magnetic pressure for a dipole field. It is the high plasma pressure in the plasma disk that doubles the scale of Jupiter's magnetosphere from the dipolar stand-off distance of $\sim$42 R_J to over 90 R_J. Careful statistical analysis (combined with modeling) of how the magnetopause standoff distance at

Table 1 Comparison of magnetospheres of Earth, Jupiter and Saturn

	Earth	Jupiter	Saturn
Radius, R_P (km)	6,373	71,492[a]	60,268
Distance from Sun[b] (AU)	1	5.2	9.5
Spin period (hours)	24	9.92492	10.56[c]
Solar wind density, n_{sw} (cm^{-3})	7	0.2	0.07
Magnetic moment[d] (M_E)	1	20,000	600
Equatorial magnetic field, B_o (nT)	30,600	430,000	21,400
Plasma source (kg/s)	5	260–1400[e]	12–250[e]
Plasma source (ions/s)	2×10^{26}	$>10^{28}$	$3–5 \times 10^{26}$
Dipole R_{CF}[f] (R_P)	10 R_E	46 R_J	20 R_S
Observed R_{MP} (R_P)	8–12 R_E	63–92 R_J	22–27 R_S
Plasma Transport Time[g]	hours-days	11–60 days[e]	5–40 days[e]
Auroral UV Emission Power (W)	10^{10}	10^{12}	10^{11}
Auroral Radio Emission Power (W)[h]	$\sim 4 \times 10^7$	8×10^{10} DAM 4×10^{10} HOM 5×10^8 bKOM 2×10^8 nKOM 5×10^9 QP	4×10^8

[a] We define 1 $R_J = 71{,}492$ km (see discussion in the Appendix)

[b] Semi-major axis of orbit. 1 AU $= 1.5 \times 108$ km

[c] Voyager value. The rotation rate of Saturn is an important issue of scientific debate

[d] $M_{Earth} = 7.9 \times 10^{25}$ Gauss $cm^3 = 7.9 \times 10^{15}$ Tesla m^3

[e] Summarized by Bagenal and Delamere (2011)

[f] R_{CF} is calculated using $R_{CF} = \xi(B_o^2/2\mu_o \rho_{sw} V_{SW}^2)^{1/6}$ for typical solar wind conditions of $\rho_{sw} = m_p n_{sw}$ given above and $V_{SW} \sim 400$ km s^{-1} and ξ an empirical factor of $\sim$1.4 to match Earth observations (Walker and Russell 1995)

[g] Typical residence time in the magnetosphere. Plasma stays inside the Earth's plasmasphere for days but is convected through the outer magnetosphere in hours

[h] Zarka et al. (2001a, 2004). DAM = decametric, HOM = hectometric, bKOM = broadband kilometric, nKOM = narrowband kilometric emissions. QP = quasi-periodic bursts of emission

Jupiter varies with solar wind conditions by Joy et al. (2002) revealed a bimodal distribution with high probabilities at 63 and 92 R_J. Furthermore, the observed magnetopause locations indicate a variation in R_{MP} with solar wind ram pressure $R_{MP} \propto (\rho V^2)_{sw}^{-\alpha}$ where α is found to be between 1/3.8 and 1/5.5, a stronger function than for a dipole (Slavin et al. 1985; Huddleston et al. 1998; Joy et al. 2002; Alexeev and Belenkaya 2005). Consequently, a factor 10 increase in ram pressure at Earth shrinks R_{MP} to 70 % of the nominal value while at Jupiter the tenfold variations in solar wind pressure often observed at 5 AU cause the dayside magnetopause to move by a factor of $\sim$2. At Saturn the magnetospheric plasma pressures are less than Jupiter but the plasma β is still greater than unity beyond 8 R_S (e.g. Sergis et al. 2010) and has values of $\beta = 2–5$ in the plasma sheet. The more modest values of β at Saturn are consistent with the magnetopause stand-off distance varying as $(\rho V^2)_{sw}^{-1/5}$ (Kanani et al. 2010).

Saturn's magnetosphere is similarly dominated by a satellite source of plasma (Enceladus) and rotational dynamics. The major difference, apart from scale, is that the material escaping Enceladus (mostly water products) remain largely neutral and forms an extended corona. The densities of plasma in the Enceladus torus remain relatively low. The modest size of Saturn's magnetosphere also means that the solar wind has a stronger influence on magnetospheric dynamics at Saturn. For reviews of the magnetosphere of Saturn see chapters by Gombosi et al. (2009), Kurth et al. (2009), Mauk et al. (2009), Mitchell et al. (2009) in *Saturn from Cassini-Huygens* (edited by Dougherty et al. 2009). These reviews summarize our understanding after the primary phase of the *Cassini* mission to Saturn. In 2008 Cassini made the only traversal by a spacecraft of an auroral radio source at a planet other than the Earth (Lamy et al. 2010; Mutel et al. 2010; Schippers et al. 2011). The properties of the auroral plasma and microphysical processes at a giant planet were uniquely documented. These studies serve as a reference for comparisons with *Juno* in-situ measurements at Jupiter. The later phases of the *Cassini* mission involve a series of high latitude orbits that will hopefully elucidate structures and processes in the polar magnetosphere, though not as polar *Juno*'s orbits around Jupiter and probably not passing through the auroral acceleration regions.

As elaborated below, the giant, rotation-dominated magnetosphere of Jupiter is very different from the small, solar-wind-dominated magnetosphere of Earth. Nevertheless, we expect all magnetospheres to be governed by the same underlying plasma processes. Thus, as *Juno* ventures into Jupiter's polar regions we are also guided by the experience derived from Earth missions such as *IMP, ISEE, DE, POLAR* and particularly the *VIKING* and *FAST* missions (e.g., Bahnsen et al. 1989; Roux et al. 1993; McFadden et al. 1999) whose extensive measurements have provided the basis of our understanding of the physical processes in polar regions.

1.3 Polar Regions

Figure 1 (inset B) shows a UV image from the *Hubble Space Telescope* (Clarke et al. 2004) that illustrates the complex structure of the Jovian aurora. As discussed below, the auroral emissions at X-ray to radio wavelengths suggest that a variety of physical processes are occurring in the polar magnetosphere, including beams of ions and electrons carrying electrical currents, waves generated locally as well as traveling through the region, localized parallel electric fields as well as many transient features (sketched in the top right inset C in Fig. 1, loosely based on *FAST* observations at Earth).

Figure 4 shows the trajectories of the seven previous flyby missions (left) and the 33 orbits of *Galileo* (right) in the Jupiter system. Since the flyby missions used the orbital momentum of Jupiter for a gravitational boost to their next target they all passed on the dusk (or trailing) side of the planet except *Ulysses* that used Jupiter to get out of the ecliptic plane. (Aside: note that *Pioneer 11* left the Jupiter system moving towards the Sun rather than away. The spacecraft took 4½ years to traverse the solar system and encounter Saturn on the opposite side of the Sun as Jupiter.) As illustrated in the lower plots in Fig. 4, the only spacecraft that passed close to Jupiter's polar region was *Pioneer 11*. However, when the *Pioneer 11* trajectory is plotted in magnetic coordinates, it is clear that the spacecraft did not traverse the region of auroral currents (Fig. 5 from Trainor et al. 1975). Thus, *Juno* is the first spacecraft to explore the regions where auroral currents flow, particles are accelerated, and radio emissions are generated.

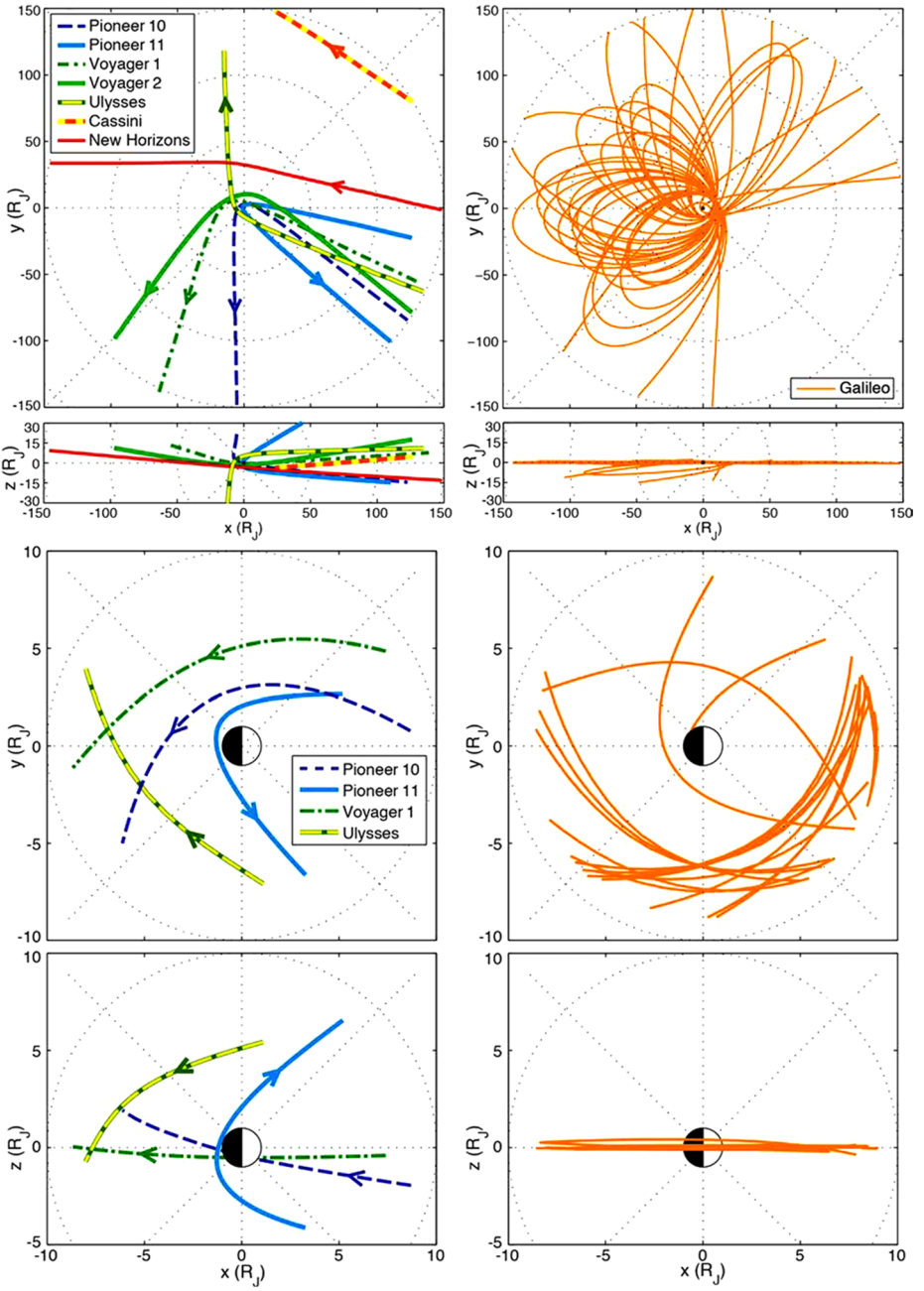

Fig. 4 Trajectories of (*left*) flyby missions and (*right*) orbiter Galileo. The top 4 plots show positions within 150 R_J of Jupiter. The bottom 4 are limited to within 9 R_J. Note that the Sun is to the right

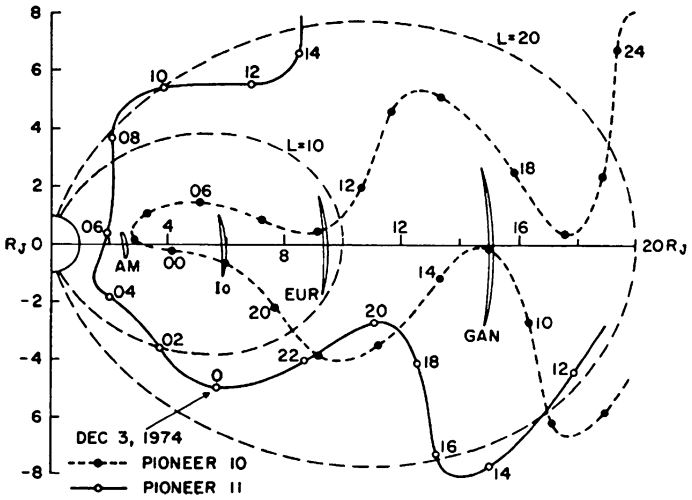

Fig. 5 Projection of the trajectories of Pioneer 10 and Pioneer 11 on a magnetic meridian plane of Jupiter based on the (dipolar) D2 magnetic field model. The region sampled by Pioneer 10 was within 20° of the magnetic equator, whereas the Pioneer 11 trajectory was at much higher latitudes, usually above 40° but less than 80° (from Trainor et al. 1975). The *dashed lines* show the magnetic field lines that map from 10 and 20 R_J at the magnetic equator to the planet. Since the main aurora are generated around the $L = 20$ flux shell and beyond, the Pioneer 11 barely entered these auroral field lines for a couple hours at distances of 4 to 6 R_J from the planet, probably above the acceleration region

1.4 Outstanding Issues

Above we have provided a brief description of the magnetosphere of Jupiter that is based primarily on observations made in the equatorial regions. The lack of in situ measurements over the poles raises many outstanding issues about the polar magnetosphere:

- What is the high latitude structure of the magnetosphere? Is it fundamentally similar to the Earth or radically different?
- Where and how are the particles that excite the aurora accelerated?
- Where and how is auroral radio emission generated?
- What causes the very transient polar aurora?
- How much of the planetary field connects to the solar interplanetary magnetic field? What is the size and variability of Jupiter's polar cap?
- How is the main aurora related to magnetospheric dynamics and/or changes in the solar wind?
- What mechanisms accelerate particles to radiation belt energies? What processes control the structure and dynamics of the radiation belts?
- How is the magnetosphere coupled to the solar wind? What are the mechanisms and quantities of mass and momentum transfer across the magnetopause?
- What is the role of coupling of the solar wind to the magnetosphere in magnetospheric dynamics? How deep does the influence penetrate or is the interaction confined to a boundary layer?
- How do the polar regions couple to the long magnetotail observed by *Voyager 2* and *New Horizons*?

In the rest of this paper we first address the geometry of *Juno*'s orbits in the Jovian magnetosphere and then describe how *Juno* addresses these scientific issues.

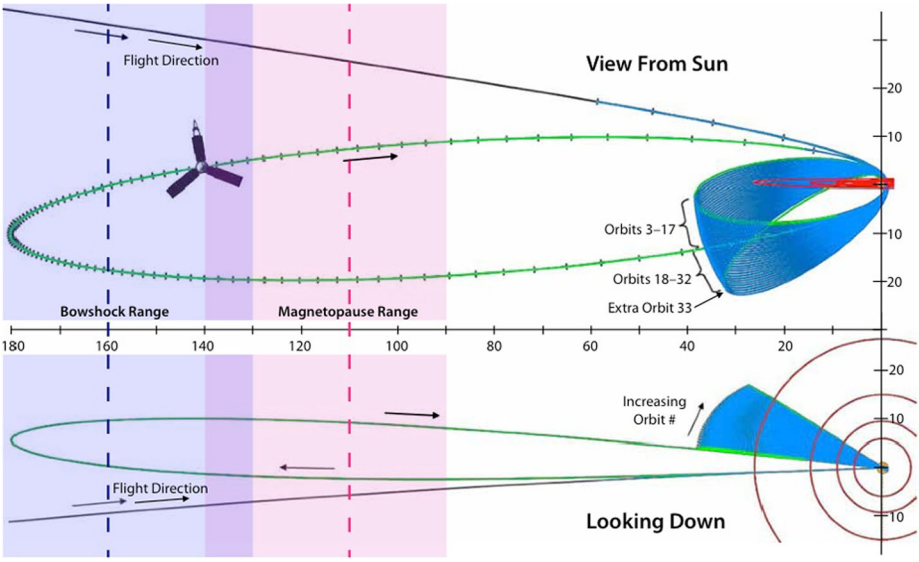

Fig. 6 Geometry of *Juno's* orbits viewed with the dawn flank on the left, (*top*) from the Sun with north up, and (*bottom*) looking down on the system, the Sun below. The *pink* (*purple*) *dashed lines* show the average positions of the magnetopause (bow shock) derived by Joy et al. (2002) with the corresponding shaded regions showing the statistical ranges of their locations on the dawn terminator. The *black* shows where data will be gathered on approach to Jupiter. After Jupiter orbit insersion, the *green line* (with daily tick marks) shows the 107-day capture orbit. The smaller science orbits (3–33, *in blue*) precess both in local time and latitude at about 1° per orbit. Orbits of Galilean moons Io, Europa, Ganymede and Callisto are shown in *red*. The *Juno* spacecraft (not to scale) spins in an anti-clockwise direction as viewed in the top panel at 2 rpm

2 *Juno*'s Trajectory Through the Magnetosphere

2.1 Orbit Overview

The *Juno* spacecraft was launched on August 5, 2011 and, after an Earth flyby on October 9, 2013, arrives at Jupiter on July 5, 2016 (Bolton et al. 2014, this issue). After orbit insertion, *Juno* spends the next 106 days on a capture orbit that takes *Juno* out to 180 R_J on the dawn flank of the magnetosphere (Fig. 6).

After the second close pass of Jupiter on October 19, 2016, *Juno* starts a series of 33 highly eccentric 11-day period science orbits (apojove distance of 38 R_J, perijove of 1.05 R_J) that last until October 2017. All orbits are close to polar, inclined less than a degree from the poles. Jupiter's motion around the Sun over the 1-year duration of the mission, results in the apojoves of the *Juno* orbits moving earlier in local time from close to 0600 (dawn) to 0400 LT. The rotational flattening (oblateness) of the planet Jupiter causes *Juno*'s orbit to precess, so that the semi-major axis tilt with respect to the equatorial plane shifts progressively southward from $-4.6°$ to $-33.5°$, eventually bringing the spacecraft progressively farther into the hazardous radiation belts. After each perijove there is an orbit trim maneuver that is designed to bring *Juno* back to Jupiter at a precise time so that each successive pass is at a Jovian longitude displaced by $180 + 24 = 204°$ (S3LH or 156° S3RH, see Appendix for description of coordinate systems) from the previous perijove. After spanning once around the planet in 24° intervals there is a phase shift to fill in the coverage with a final 12° longitude resolution. This allows instruments on the spacecraft to systematically

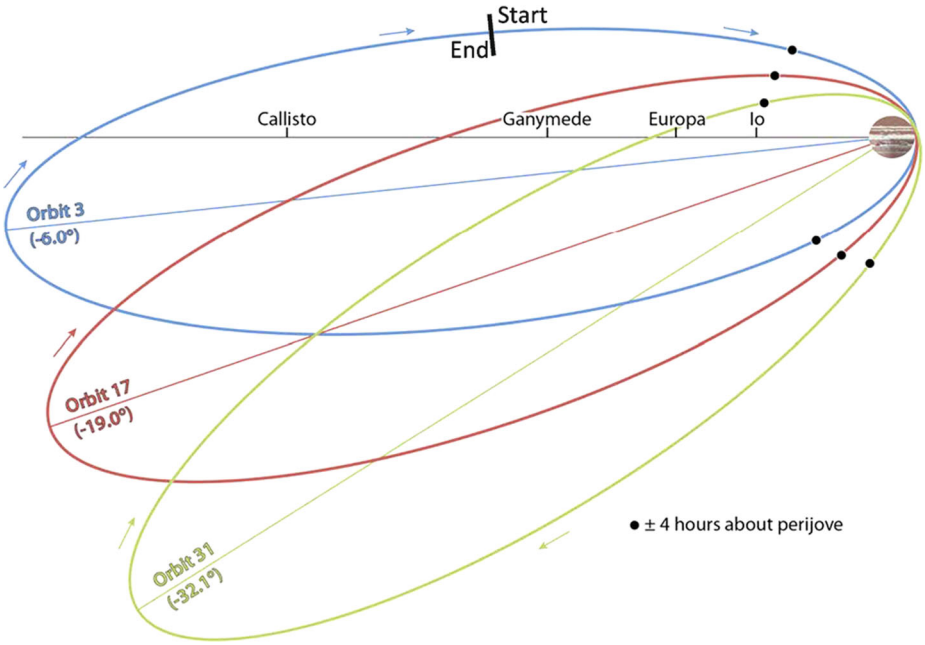

Fig. 7 Three selected *Juno* orbits: early, (PJ3 2016 Nov. 10 16:46), middle (PJ17 2017 Apr. 13 07:27), end (PJ31 2017 Sep. 13 21:49) showing precession of line of apsides relative to Jupiter's geographic equator. The orbits are numbered according to the sequence of perijoves (PJ), where PJ0 is the initial orbit insertion, with the start/end of a numbered orbit about a day before perijove. The full orbit period is about 11 days. The *black dots* indicate ±4 hours of perijove. High-cadence observations are planned for about 12 hours near perijove

map out longitude structures in the atmosphere and interior, as well as gravity and magnetic fields (see Connerney et al. 2014, this issue; Anderson et al. 2014, this issue; Janssen et al. 2014, this issue).

Labeling orbits by perijove (where orbit insertion is PJ0), we show the geometry of science orbits 3, 17 and 31 in Fig. 7 to illustrate typical early, middle and late orbits. A time for the start/stop of a numbered orbit is chosen about a day before perijove. The perijove distance of ∼1.05 R_J is ∼5000 km above Jupiter's cloud deck. The black dots (at ±4 hours of perijove) illustrate how *Juno* passes very quickly from pole-to-pole (moving ∼60 km/s around perijove, ∼20 km/s over the poles), gathering data at high rates. The high-rate data are stored on the spacecraft and then transmitted to Earth over the remaining days of the ∼11-day orbit. The orbit precession driven by Jupiter's oblateness not only produces a ∼1° increased tilt per orbit but also brings the (non-perijove) equatorial crossing distance closer to Jupiter by ∼0.9 R_J per orbit. Figure 8 shows how *Juno*'s northward crossing of Jupiter's geographic equator of (plane of Galilean satellite orbits) moves inwards, crossing each satellite orbital distance only once over the duration of the mission. *Juno* crosses the orbit of Callisto between orbits 11 and 12, the orbit of Ganymede between orbits 23 and 24, and the orbit of Europa at the very end of the nominal mission between orbits 33 and 34. The planned prime mission for *Juno* has the spacecraft entering Jupiter on PJ34 with the result that *Juno* does not come close to the orbit of Io. Hansen et al. (2014, this issue) show when the Galilean satellites can be imaged by *Juno*Cam.

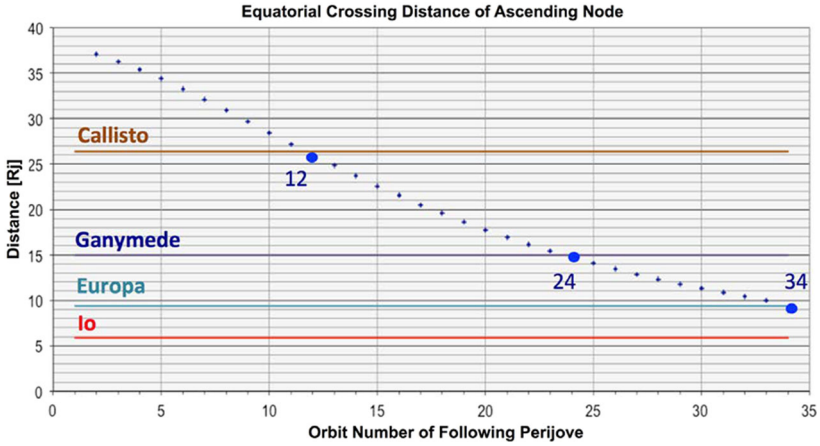

Fig. 8 Distance that the *Juno* orbits cross the equatorial plane with the orbits of Callisto (26.33 R_j), Ganymede (14.97 R_j), Europa (9.38 R_j) being crossed on the orbits before perijoves 12, 24 and 34. The planned prime mission for *Juno* has the spacecraft entering Jupiter on PJ34 with the result that *Juno* does not come close to the orbit of Io (5.89 R_j)

2.2 Boundary Crossings

Figure 6 shows the locations of the magnetopause (MP) and bow shock (BS) derived by Joy et al. (2002) based on combining previous spacecraft measurements and an MHD model. The average MP and BS distances (close to the equator on the dawn flank) are 105 R_J and 165 R_J respectively with the 10th to 90th percentile ranges shaded (85–145 R_J for the MP and 130–230 R_J for the BS). Comparing these distances with *Juno*'s approach to Jupiter and capture orbit, we can expect the spacecraft to spend ~80 days (~20 on approach and ~60 days during capture) in the boundary regions of the magnetosphere and bow shock.

Typical solar wind conditions based on *Ulysses* data obtained near Jupiter's orbit during the declining phase of the solar cycle, appropriate for *Juno*'s arrival at Jupiter in July 2016, are summarized in Table 2 (based on Ebert et al. 2010). Note that because the distributions of solar wind and interplanetary magnetic field (IMF) properties are far from a simple Gaussian distribution, we show the 10 % and 90 % percentiles, and median, as well as the mean (± standard deviation). The presence of a tail at higher values is particularly noticeable for the cases of solar wind speed, density and temperature. Variability in density and flow speed produce more than a factor of 10 variation in the dynamic pressure between 10 % and 90 % percentiles and correspondingly strong variations in the compressible magnetosphere. Joy et al. (2002) derived a bimodal distribution of magnetopause stand-off distance (with peaks at 63 and 92 R_J). McComas et al. (2014a, 2014b) explain this bimodal distribution based on observed solar wind pressure causing the magnetosphere to expand and compress as rarefaction and compression regions move through the heliosphere.

By contrast, the solar wind flow direction is very tightly constrained to within a few degrees of radial. Of importance for the dynamics of Jupiter's magnetosphere is the direction of the IMF. Table 2 shows that the angle of the IMF out of the ecliptic plane (meridional angle) has a standard deviation of only 30° and 10/90 % percentiles of ±40°. Unlike at Earth, there are very rare occasions when the IMF is anti-parallel to the internal (southward-pointing) field, likely contributing to the low rates of steady, large-scale reconnection at Jupiter (Walker and Russell 1985; Desroche et al. 2012). Similarly, by 5.2 AU the Parker

Table 2 Statistical properties of the interplanetary medium around the orbit of Jupiter[a]

	10 %[b]	Mean[c]	Standard Deviation[c]	Median	90 %[b]
Proton speed (km/s)	369	451	±71	438	557
Solar wind azimuthal deflection (deg)	−3.1	−0.3	±2.1	−0.2	2.0
Solar wind meridional deflection (deg)	−2.6	−0.16	±2.1	−0.16	2.1
Proton temperature (eV)	0.55	2.8	±3.8	1.4	6.8
Proton density (cm^{-3})	0.036	0.22	±0.27	0.13	0.50
Alpha particle composition (% by density)	2.6	3.1	±3.3	3.1	3.1
Dynamic pressure (nPa)	0.014	0.084	±0.11	0.045	0.20
B-field strength (nT)	0.18	0.69	±0.63	0.45	1.5
B-field azimuthal angle, Bt > 0 (deg)	46	95	±35	98	137
B-field azimuthal angle, Bt < 0 (deg)	−134	−81	±38	−79	−31
B-field meridional angle (deg)	−40.4	0.37	±31.1	0.49	40.8
Plasma β[d]	0.12	0.66	±1.6	0.38	1.2
Alfvén Mach Number[e]	7.4	17.7	±11.5	16	29

[a]These values are based on 1-hour averages of *Ulysses* data obtained between 2003 (Day Of Year 340) and 2005 (Day Of Year 008) at heliocentric distances of 5.273 to 5.403 AU within 10° of Jupiter's inclination at the time. These data were obtained around the phase of the solar cycle (descending from maximum) that *Juno* is expected to arrive at Jupiter. Based on Ebert et al. (2010)

[b]10th and 90th percentiles of the solar wind distribution

[c]Mean and standard deviation of the distribution

[d]Ratio of proton thermal pressure to magnetic field pressure

[e]Ratio of solar wind speed to Alfvén speed

spiral of the IMF has wound up to nearly azimuthal. That is, fields originally pointed away vs. towards the Sun have become wound up so they are close to ±90° from radial at Jupiter. This means that the field changes direction a few times per solar rotation, but remains within 45° of azimuthal for 80 % of the time. Included in Table 2 are a couple of parameters that are useful for characterizing the solar wind interaction with the magnetosphere as discussed further in Sect. 3.4: the plasma beta (ratio of thermal pressure to magnetic field pressure) and the Alfvén Mach number (ratio of flow speed to Alfvén speed). Note that over the *Juno* capture orbit we expect the polarity of the IMF to change dozens of times during this >3 month period.

Using the Joy et al. (2002) model of how these boundaries vary with solar wind dynamic pressure and 1-hour averages of *Ulysses* SWOOPS solar wind data (Bame et al. 1992), we predict that *Juno* will cross the BS 64 ± 9 times and the MP 42 ± 9 times. To illustrate the frequent crossings of these boundaries that *Juno* might expect, we have plotted the MP and BS distances based on 2500 hours of SWOOPS solar wind pressure data and superimposed a sample trajectory of *Juno* over its capture orbit in Fig. 9. The pattern of recurring compression regions (responsible for sharp decreases in magnetospheric size shown in Fig. 9)

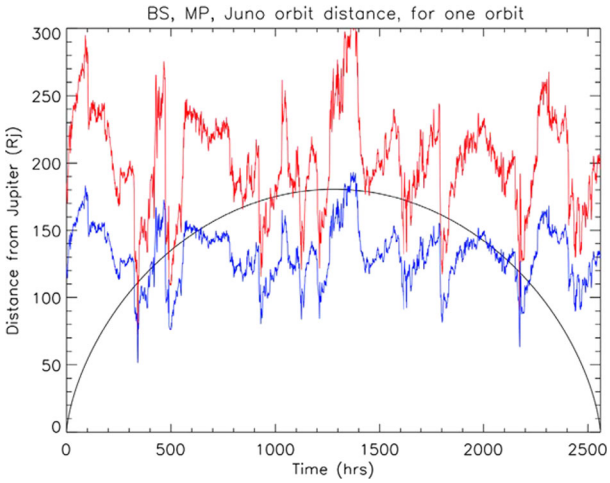

Fig. 9 Illustration of anticipated statistical variations in magnetopause (*blue line*) and bow shock (*red line*) distances on the dawn flank of the magnetosphere based on empirical dependence on solar wind pressure (Joy et al. 2002) and measurements from the *Ulysses* SWOOPS instrument at ∼5 AU (Ebert et al. 2010). A sample *Juno* trajectory (*black line*) shows the frequent crossings Juno is expected to make of these boundaries on its capture orbit

is characteristic of the declining phase of the solar cycle experienced by *Cassini* at Saturn in 2004-8 (Jackman et al. 2004) and by *Juno* a solar cycle later. McComas et al. (2013) point out long-term trends of decreasing solar output from which McComas et al. (2014a, 2014b) conclude that the BS and MP will likely be farther than indicated here. Ebert et al. (in preparation) examine the properties of the solar wind at ∼5 AU in further detail, making quantitative predictions of the statistics of Juno crossings of these boundaries under these weaker solar wind conditions.

Observations of the solar wind, aurora and magnetospheric conditions during this phase of the mission provides an excellent opportunity to explore the nature of the solar wind interaction with Jupiter's dawn magnetosphere (see discussion in Sect. 3.4 below).

2.3 Magnetospheric Models

In order to relate the *Juno* orbits to structures of the magnetosphere we need a magnetic field model. The detailed history of models of Jupiter's magnetic field is reviewed by Connerney (2007) and Connerney et al. (2014, this issue). The VIP4 and VIT4 models of Connerney et al. (1998) and Connerney (2007) combine spacecraft measurements of the in situ field with the location of the localized auroral emission associated with Io (which must map along the magnetic field to the known location of Io's orbit) to constrain up to 24 coefficients of the internal field. Grodent et al. (2008) noted that both the Io and Ganymede auroral footprints required a region of anomalously strong magnetic field. They add a small dipole field (∼1 % of primary field) located about 3/4 of the planet's radius from the planet's center in the northern hemisphere. Hess et al. (2011) modified the VIP4 model to match both the latitude of the Io footprints as well as the longitude, assuming a propagation lead angle from the Alfvén wing model of the Io interaction. Hess et al. (2011)'s VIPAL model produces a good match to the measurements of Io-triggered radio emission such as maximum frequency and arc shape (see discussion in Sect. 3.1).

Figure 10 (from Hess et al. 2011) illustrates the magnetic field at Jupiter's cloud tops (∼1 bar level of the atmosphere) from three magnetic field models (VIP4, Grodent, VIPAL) as well as the predicted and observed location of Io's magnetic footprint on the planet. The differences between these models are important for planning *Juno* observations of the auroral regions (see Sect. 3.1 below). The close passage of *Juno* to the planet and extensive

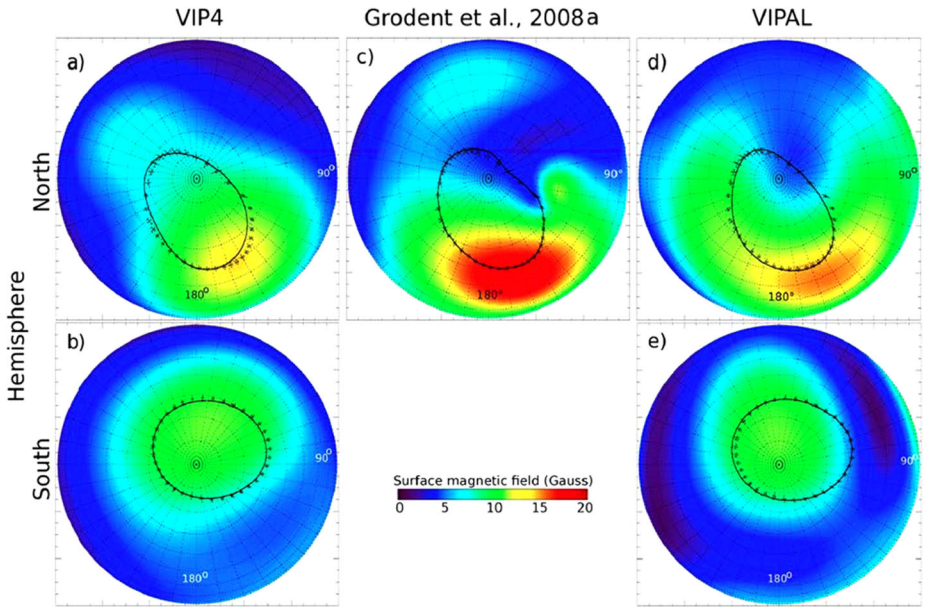

Fig. 10 Surface magnetic field strength, observed Io's UV aurora (*crosses*), and modeled locus of footprints (*continuous line*) of field lines that connect Io to Jupiter. All models include the 1/15.4 oblateness of the planet to define the planetary "surface" (∼1 bar level). *Left:* The VIP4 model of Connerney et al. (1998) for (**a**) the northern hemisphere and (**b**) the southern hemisphere; *Center:* The empirical model of Grodent et al. (2008) for the (**c**) the northern hemisphere; *Right:* The VIPAL model of Hess et al. (2011) for (**d**) the northern hemisphere and (**e**) the southern hemisphere. From Hess et al. (2011)

coverage in both latitude and longitude allows the MAG team to determine the internal magnetic field of Jupiter in greater detail and to much higher accuracy (Connerney et al. 2014, this issue).

Models of magnetospheric structure that include external currents as well as the internal magnetic field, are generally of 3 types: empirical formulations based on matching in situ magnetic field measurements; models that use observed distributions of particle pressure to derive equilibrium solutions for the equatorial plasma sheet; and numerical MHD models. While a global MHD model is desirable, the global models to date have tended to concentrate on the outer magnetosphere, ignoring the dipole tilt and higher order moments. Furthermore, current MHD models do not have the necessary heating of magnetospheric plasma and hence have not managed to match the observed plasma pressures in the plasma sheet (Walker and Ogino 2003; Fukazawa et al. 2005, 2006, 2010; Chané et al. 2013). Hence current global MHD models are not very useful for predictions of what *Juno* measures in the plasma sheet. Models of the plasma sheet that do fold in realistic pressure distributions either assume axisymmetry (Caudal 1986; Caudal and Connerney 1989; Cowley et al. 2005, 2008b; Nichols 2011) or again concentrate on the outer magnetosphere (Belenkaya 2004; Alexeev and Belenkaya 2005; Belenkaya et al. 2005, 2006). A useful model for global magnetic field structure has been that of Khurana (1997) and Khurana and Schwarzl (2005), which combines internal magnetic field components (e.g., VIP4 of Connerney et al. 1998), an equatorial current sheet that varies with local time, plus currents in the magnetotail and on the magnetopause. The parameters of the model have been derived by matching magnetic field data, primarily from *Galileo*.

Figure 11 shows examples of the magnetic field structures in the extended magnetosphere of Jupiter. The top panel shows a sketch of the current and field configurations. The equatorially stretched magnetic flux tubes are associated with the strong azimuthal currents (j_φ) that flow in the plasma sheet. Radial currents through the plasma sheet (j_r) are closed into/out of the ionosphere via field-aligned currents ($j_\parallel$). It is the upward (or outward) currents that are likely carried by the downward-precipitating electrons that excite the main auroral oval (reviewed by Clarke et al. 2004). The true locations of the necessary downward (or inward) currents that close the current system are not known. Some argue that they flow at least partly at the magnetopause (Cowley and Bunce 2001; Bunce et al. 2004; Kivelson et al. 2002; Cowley et al. 2005), while others suggest that the downward currents are interspersed with the upward currents in the interior of the plasma sheet (Mauk and Saur 2007). The middle two panels of Fig. 11 shows the currents and magnetic fields from the axisymmetric model of Cowley et al. (2008b) for the coupling of Jupiter's plasma disk to the ionosphere. The model field is the sum of the planetary dipole and the field from a 5-R_J-thick equatorial current sheet (following Connerney 1981). The magnetic field lines that map to the ionosphere at co-latitudes of 5–25° relative to the northern and southern magnetic poles, are shown at steps of 5°. In both panels the green lines, also magnetic field lines, show the regions of upward-directed field-aligned current, the solid lines show the central field line of the current layer and the dashed lines the approximate boundaries on either side. Specifically, the current regions shown by the outer pair of green solid lines in the northern and southern hemispheres map to the model open-closed field line boundaries at 10.7° with respect to both poles with the dashed green lines showing the ~0.4° expected width of these currents. Similarly the green lines in the equatorial region correspond to the center and range of the upward currents that couple the ionosphere and plasma sheet. The left panel shows positive and negative contours (±2, ±5, ±10, ±20, and ±50 nT) of the azimuthal B field produced by the magnetosphere-ionosphere coupling current system. In the right panel the contours show the tilt angle of the field out of magnetic meridian plane.

Extensive analysis of the *Galileo* magnetometer data show that there are strong asymmetries in the magnetic field with local time (Khurana and Kivelson 1989; Khurana 2001). The effects of local asymmetries in the magnetic field (illustrated in the bottom two plots of Fig. 11) are included in the model of Khurana and Schwarzl (2005). They show that the bend-back (i.e. deviation from the meridian plane) is much stronger on the dawn side than the dusk side. This local time variation in field bend-back must be due to non-axisymmetry of the radial currents, as illustrated in Fig. 11B.

2.4 Science Orbits

To illustrate the effect of Jupiter's tilted magnetic field, Fig. 12 shows orbit 3 at two different phases of Jupiter's rotation ~5 hours apart. Around apojove (when the spacecraft moves slowest), the plasma sheet flaps every 5 hours over the spacecraft. As the spacecraft passes over the poles, the phase of the tilt is critical for predicting when the spacecraft crosses the field-aligned currents that couple the plasma sheet to the planet.

To further illustrate the effect of the tilt, Fig. 13 shows the orbits of perijoves 3, 17 and 31 in a magnetic coordinate system that is aligned with a 9.515° tilt of the dipole approximation to Jupiter's internal field. The magnetic field model, equatorial current sheet and field-aligned current systems are derived from the azimuthally symmetric model of Cowley et al. (2008b) illustrated in the center panel of Fig. 11. Note how these "wiggle plots" illustrate how the spacecraft trajectory crosses the current systems, both in the equator and over the poles. In the early orbits the inbound and outbound trajectories each cross both equatorial and polar regions. But as the orbit precesses the inbound segment crosses the north

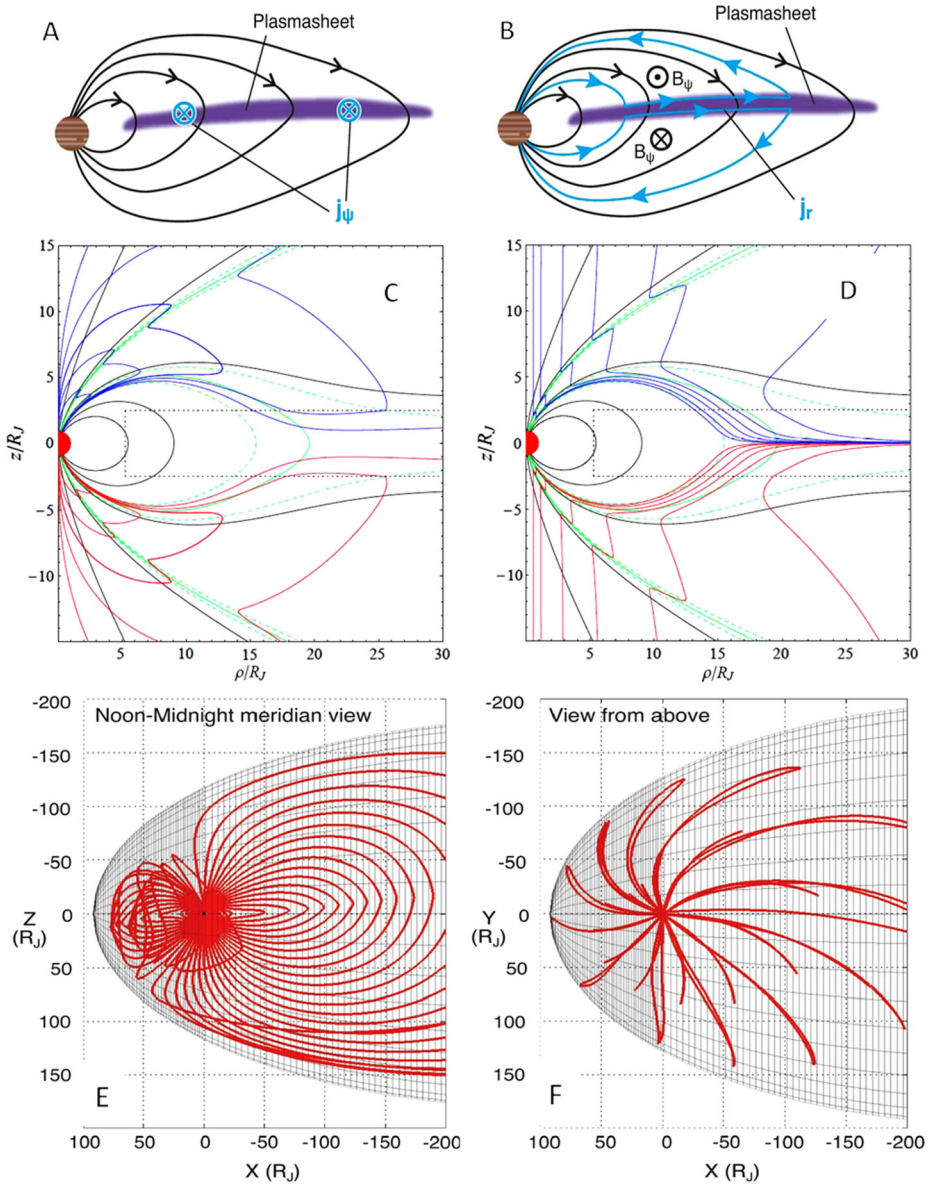

Fig. 11 *Top:* Main plasmadisk currents. *Middle:* Axisymmetric magnetic field model of Cowley et al. (2008a, 2008b). *Bottom:* Three-dimensional magnetic field model of Khurana and Schwarzl (2005) that includes the VIP4 model for the interior field plus external magnetospheric currents. In **C**, **D** *black solid lines* show field lines mapping to the ionosphere at magnetic colatitudes of 5–25° in steps of 5°. The equatorial current sheet is restricted to the *black dotted rectangle*. The *green lines* show the regions of upward-directed field- aligned currents. *Red and blue lines* (**C**) show contours (±2, ±5, ±10, ±20, ±50 nT), of the azimuthal field, and (**D**) show the tilt angle of the field out of magnetic meridian plane (from left to right the contours are for tilt angle magnitudes of 0.1°, 0.2°, 0.5°, 1°, 2°, and 5°)

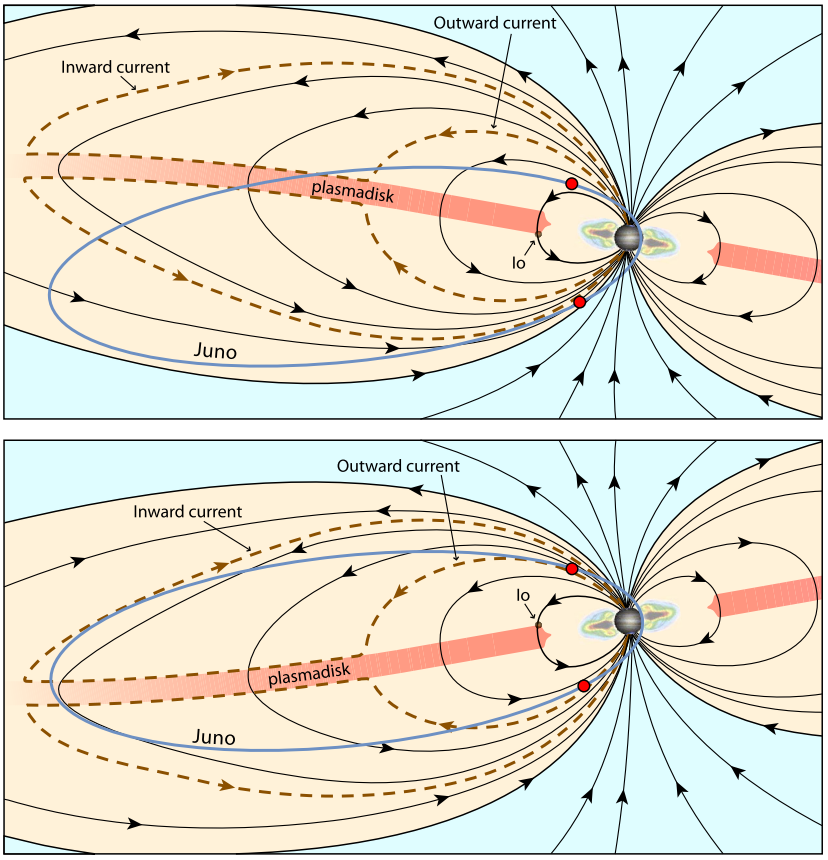

Fig. 12 The ~9.5° tilt of Jupiter's magnetic field from the planet's rotation axis causes Juno to pass many times through the plasmadisk, particularly during apojove of the early orbits. The *blue line* shows orbit of PJ3 (as shown in Fig. 7). The *top and bottom graphics* illustrate the orientation of the field and plasmasheet ~5 hours apart. The *red dots* are located on Juno's trajectory approximately ±4 hours around perijove

polar currents very close to the planet while the outbound segment makes multiple crossings of the southern polar currents. This evolution of the orbit means that *Juno* traverses the important polar regions at a range of heights above Jupiter's atmosphere. Sometimes, the spacecraft seems to move parallel to a magnetic L-shell for several hours which allows *Juno*'s instruments to map structure along the field (e.g. locate potential structures such as double-layers, the radio emission generation region, etc.; see Hess et al. 2007a, 2009, Mottez et al. 2010 and discussion in Sect. 3.1.4). At other times, the spacecraft rapidly crosses a range of magnetic latitudes providing an opportunity to measure latitudinal structures. For example, note that the inbound trajectory on orbit 3 makes multiple crossings of the (upward) current structures that couple the planet to the magnetospheric plasma sheet and the outbound trajectory on orbit 17 makes multiple crossings of the (downward) currents that couple to the outer magnetosphere.

2.5 Polar Region Coverage

In Figs. 7 and 12 the dots on the trajectory illustrate the location of *Juno* ±4 hours of perijove. Considering each of these points as examples, one can see that at any moment in

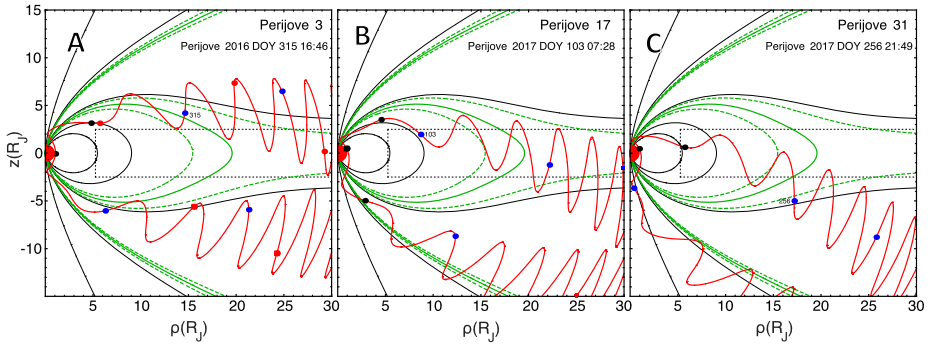

Fig. 13 The current and magnetic field model of Cowley et al. (2008a, 2008b) is azimuthally symmetric and centered in a tilted (*dipole*) frame in which the spacecraft appears to "wiggle" up and down. Model field lines (*black*) are shown in a magnetic meridian plane with the spacecraft trajectory (*red*) superposed. *Blue dots* show the start of each day, with *red dots* at 12 hour intervals between. The *black dot* close to the planet shows perijove, while the *two black dots* either side show perijove ±4 hours. The *black dotted lines* delineate the region of the equatorial azimuthal current sheet. The *green solid and dashed lines*, show field lines that mark the centers and cross-field extent of field-aligned currents in each hemisphere, as in panels C and D of Fig. 11

time (or location) along the *Juno* trajectory, a magnetic field model allows one to extrapolate along the magnetic field (say from the approaching, northern red dot 4 hours out) and project down onto the planet the instantaneous magnetic footprint of the spacecraft. For the same instant, it is possible to calculate, using the same magnetic field model, where the conjugate field line intersects the planet at the opposite hemisphere of the planet. We have carried out this exercise using the VIP4+Khurana magnetic field for each of the orbits and Fig. 14 shows orbits 3, 17 and 31. Since we are not confident in the models beyond 80 R_J we cut off the conjugate mapping if the field line goes beyond 80 R_J. The left projections are the shortest path for the inbound/northern hemisphere (above) and outbound/southern hemisphere (below). On the right we show the footprint path mapped to the corresponding conjugate hemispheres. The fact that the planet rotates (every 9.925 hours) under the spacecraft produces a curled path in the System III coordinate system rotating with Jupiter (see Appendix for description of coordinate systems). This means that *Juno* is likely to make multiple crossings of the region mapping to the main auroral oval during a single orbit. Mapping the magnetic field to the outer magnetosphere becomes increasingly unreliable at larger distances and gaps in the conjugate footprint path reflect times when the field line from the spacecraft maps to distances beyond 80 R_J. Note that as the orbit precesses, the inbound footprint spends increasingly more time outside the main oval (for both north/local and south/conjugate hemispheres) while the outbound footprint spends increasingly more time in tighter curls well inside the main auroral oval (as also illustrated in magnetic coordinates of Fig. 13).

We are not only interested in where a field line being traversed by the *Juno* spacecraft maps to the planet, but also how far the field maps out into the magnetosphere. Figure 15 shows the mapping along the field line from the spacecraft to the point that is farthest from Jupiter. Note that the 10° tilt of the magnetic dipole from the rotation axis means that the farthest crossing point oscillates twice per ∼10 hour rotation period. Also note that because the magnetic field models are not able to reliably map to large distances from Jupiter, we have cut off the plots at 80 R_J from Jupiter. As the orbits precess to greater southern latitudes, an increasing fraction of the orbit maps to such large distances. Since the ratio of magnetic field strength between the poles and equator is very large ($>10^5$), the loss cone for particles

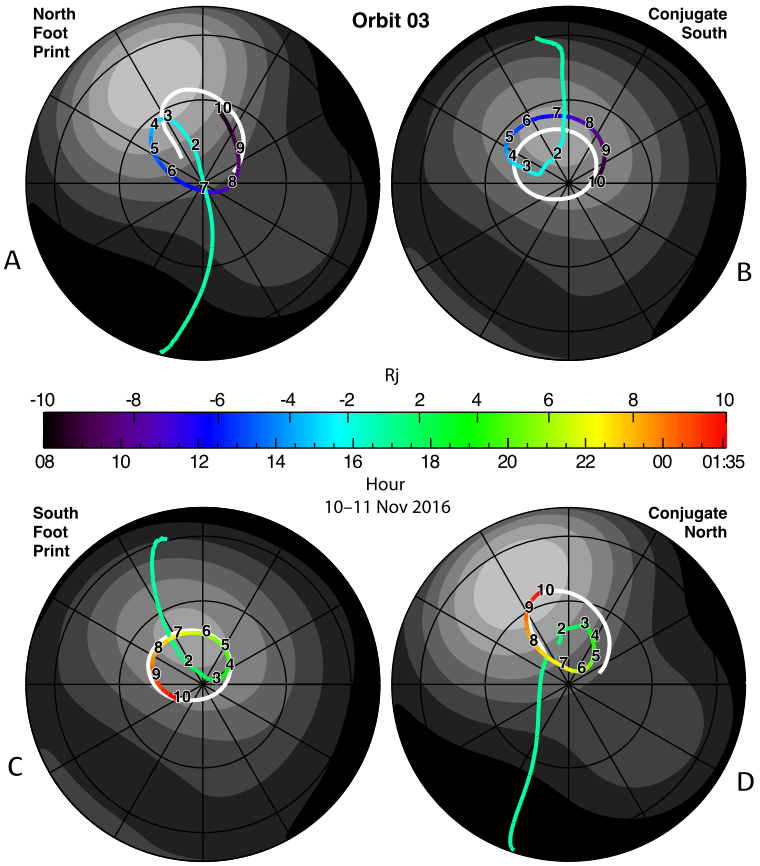

(a)

Fig. 14 (**a**) Perijove 3, (**b**) Perijove 17, (**c**) Perijove 31. Locations of the footprints at each ends of the magnetic field passing through the spacecraft, mapped onto the "surface" of Jupiter using the VIP4+Khurana magnetic field. The north and south polar regions are shown fixed in System III longitude (0° towards the bottom of the page for the north, and towards the top for south). The curled path is due to the planet spinning under the spacecraft. The *gray contours* show the surface magnetic field strength. The *white lines* show the average location of the main aurora. The timescale corresponds to the time when $R < 10\ R_J$ and the trajectory lines are colored corresponding to the timeline. The numbers on the trajectories correspond to the radial distance of the spacecraft at the time of the mapping. *Top*: The inbound trajectory mapping to the closest, north polar region (A) and conjugate, south (B) region. *Bottom*: The outbound trajectory mapping to the closest, south polar region (C) and conjugate, north (D) region

originating at the distant equatorial regions is very small ($<10^{-3}$ degrees). Therefore, the only particles that can reach high latitudes (and the *Juno* spacecraft as it traverses the polar region) must be very closely aligned with the magnetic field at the equator, unless they are accelerated close to the planet by strong electric fields parallel to the local magnetic field.

2.6 Synchrotron Belt Coverage

The first two flyby missions, *Pioneer 10* and *11*, passed relatively close to Jupiter and the energetic particle detectors on board measured intense fluxes of both ions and elec-

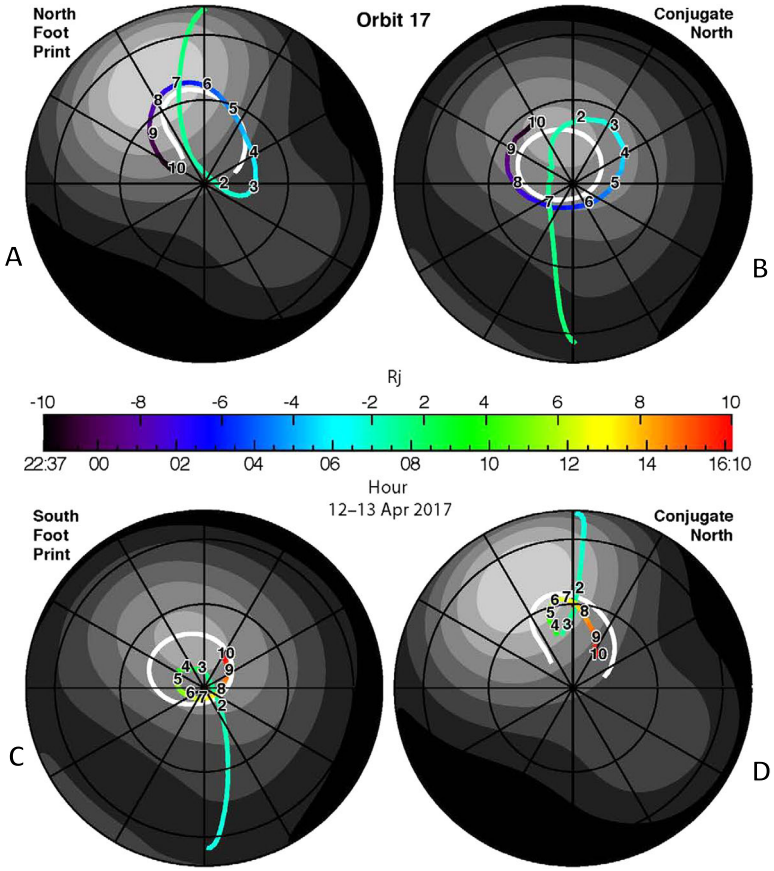

(b)

Fig. 14 (*Continued*)

trons (Fig. 5 and Fig. 16). Ground-based and space-based radio receivers have mapped and monitored the associated synchrotron emission (see reviews by Schardt and Goertz 1983; Bolton et al. 2004). The subsequent *Voyager* flybys and the *Galileo* orbits largely avoided the intense radiation belts close to the planet because of the hazard they pose to instrumentation. Similarly, *Juno*'s orbit is designed to avoid the regions with the most intense fluxes for as much of the mission as possible. The orbit precession, however, eventually brings the spacecraft into the hazardous regions later in the mission (as illustrated by orbit 31 in Fig. 16). Meanwhile, on each of *Juno's* orbits, the MWR instrument detects emissions from these radiation belts at 6 microwave wavelengths, mapping out the radiation belt structure over the duration of the mission (Janssen et al. 2014, this issue).

3 How Juno Addresses the Scientific Issues

In Sect. 1.4 above, we listed the outstanding issues of Jupiter's magnetosphere, particularly of the unexplored polar regions. Having described the *Juno* trajectory, we next delve further into these science issues and discuss how *Juno* addresses them.

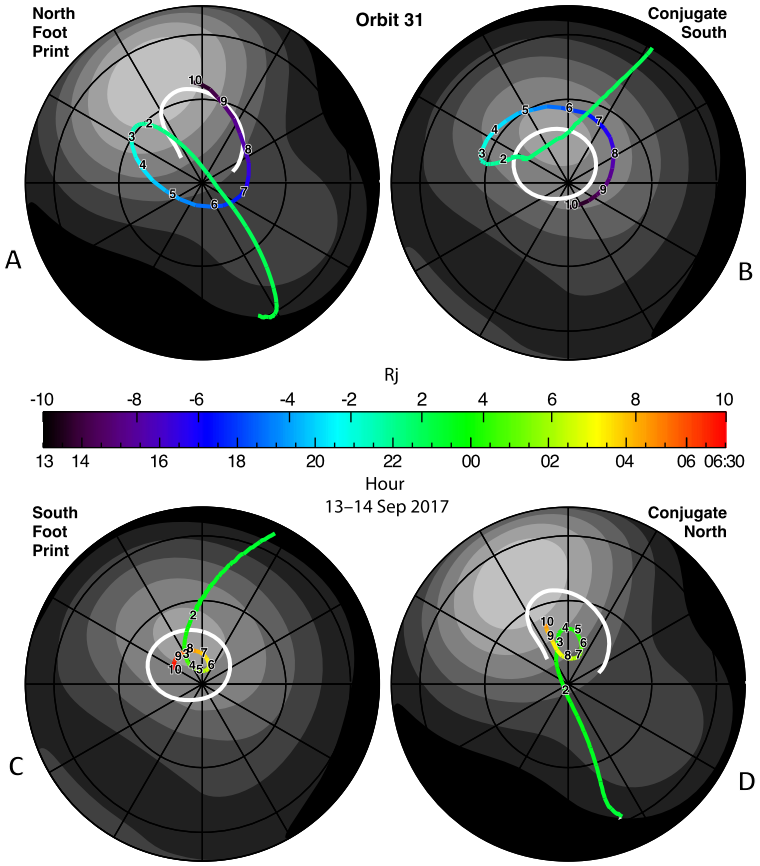

(c)

Fig. 14 (*Continued*)

3.1 Auroral Processes

Auroral processes at Jupiter generate emissions at wavelengths across the spectrum—from radio to x-rays—that are reviewed by Clarke et al. (2004) and in nine chapters of *Auroral Phenomenology and Magnetospheric Processes* edited by Keiling et al. (2012). Remote observations of radio emissions and in situ measurements of plasma waves are indications of the processes that accelerate electrons and, less often, ions (reviewed by Carr et al. 1983; Zarka 1998, 2000). When these accelerated particles bombard the atmosphere they excite the atmospheric constituents (mostly hydrogen) that then re-radiate their energy. While visible auroral emissions were observed by the Galileo spacecraft (Vasavada et al. 1999), and New Horizons (Gladstone et al. 2007), most of the emissions are in the UV (H and H_2 Lyman and Werner bands) or IR (H_3^+ emissions). X-rays have also been observed (see reviews by Elsner et al. 2005a, 2005b; Branduardi-Raymont et al. 2007a, 2007b, 2008; Hui et al. 2010; Cravens and Ozak 2012) and are thought to be excited when very energetic (10 MeV) oxygen and sulfur ions bombard the atmosphere (Ozak et al. 2010). A model based on the intense field-aligned currents expected on Jupiter's dayside cusp has been discussed by Bunce et al. (2004).

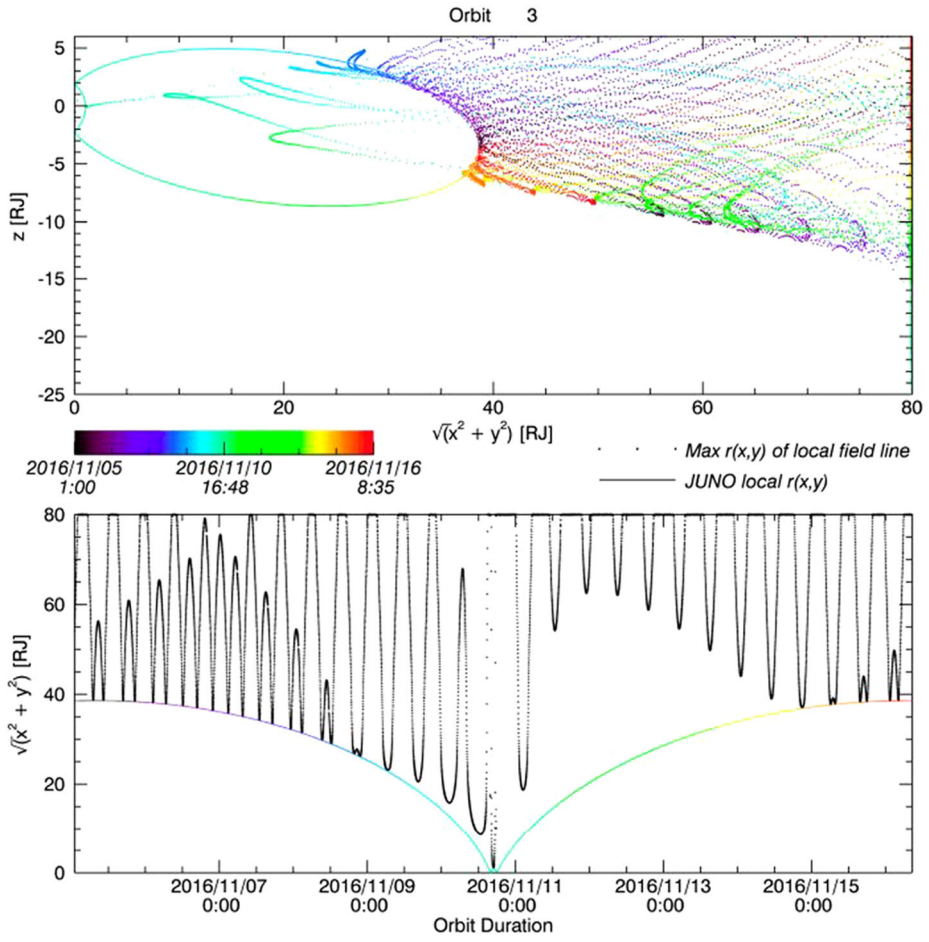

(a)

Fig. 15 (**a**) Perijove 3, (**b**) Perijove 17, (**c**) Perijove 31. Mapping from the spacecraft along the Khurana magnetic field model to the farthest point from Jupiter for the orbit around perijove 3. *Top:* The spacecraft trajectory is shown in the (vertical) meridian plane with dots showing the location of the point farthest from the planet along the flux tube that instantaneously intersects Juno's trajectory. *Below:* the distance of the trajectory (*color*) and farthest crossing points (*black curve*) vs. time

Figure 17 presents an overview of Jupiter's auroral emissions at different wavelengths. Most of the emission remains within ∼15° of the magnetic poles, and while much more powerful than the terrestrial aurora (see Table 1), the main emissions are far less variable in size and strength. The steady, narrow (∼1° or ∼1500 km wide) main aurora comprises ∼70 % of the emission and is a signature of Jupiter trying to spin the magnetospheric plasma up to corotation with the planet's 10-hour rotation period (Cowley and Bunce 2001; Hill 2001). Equatorward of the main auroral emission are three small regions of emissions that are associated with the moons Io, Europa and Ganymede. No emission has been detected associated with Callisto, but this may be because such emission would be hard to separate from the main auroral emissions. Poleward of the main aurora is the remaining ∼30 % of the emission that is highly variable both in time and space.

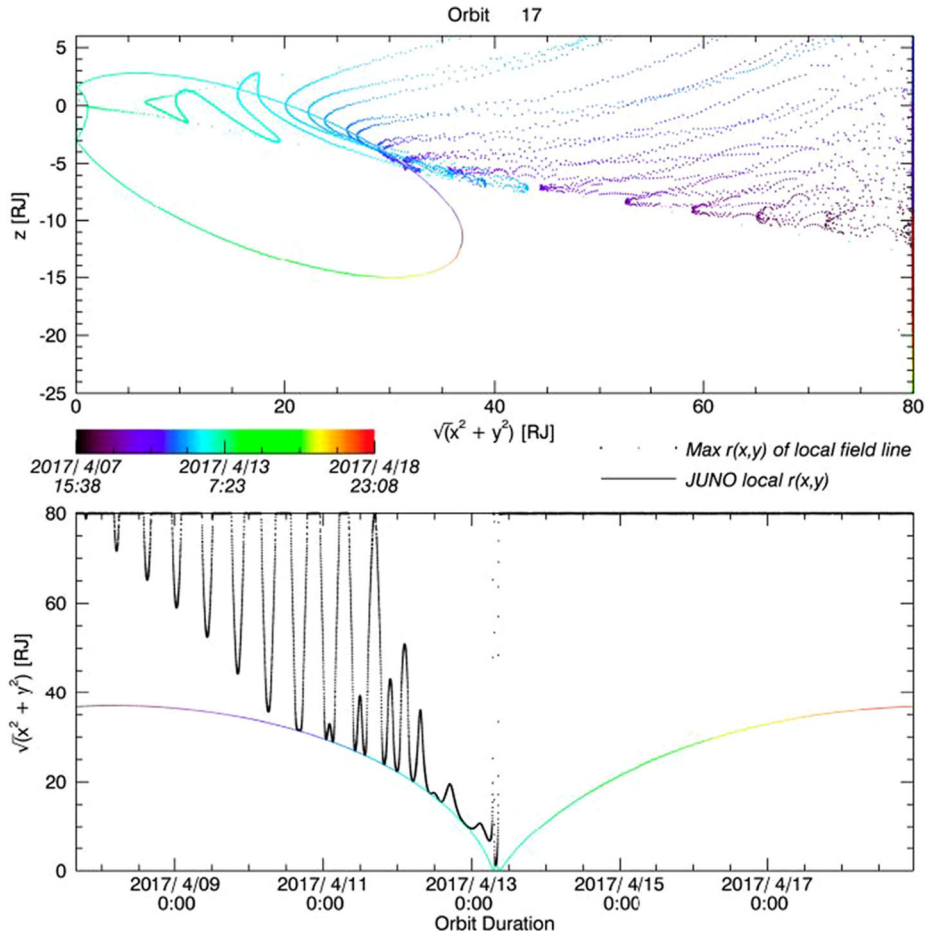

(b)

Fig. 15 (*Continued*)

Auroral emissions are often described as providing the television screen that reveals magnetospheric structures and processes. But, in practice, without in situ measurements at high latitudes it is hard to directly relate what is seen in the aurora to magnetospheric dynamics, especially in the polar regions where the magnetic field mapping from the planet to the (outer) magnetosphere is very uncertain. Spectroscopic studies of emissions, combined with measurements of brightness above the planet's limb have been modeled to diagnose the energy of precipitating particles as well as atmospheric composition and structure (Bonfond et al. 2009; Tao et al. 2011, 2012; Gustin et al. 2013). The mean electron energy is ∼100 keV for the main emissions. However this energy varies both with time and location. For example, the Io footprint occurs at a higher altitude than the main emissions and is generated by electrons with a broad energy distribution and a mean energy of ∼1 keV. On the other hand, during dawn storms, the mean electron energy could reach ∼460 keV (Gustin et al. 2006). Nevertheless, lacking in situ measurements at high latitudes, ideas about processes that generate aurora are largely based on experience at Earth and are untested at Jupiter.

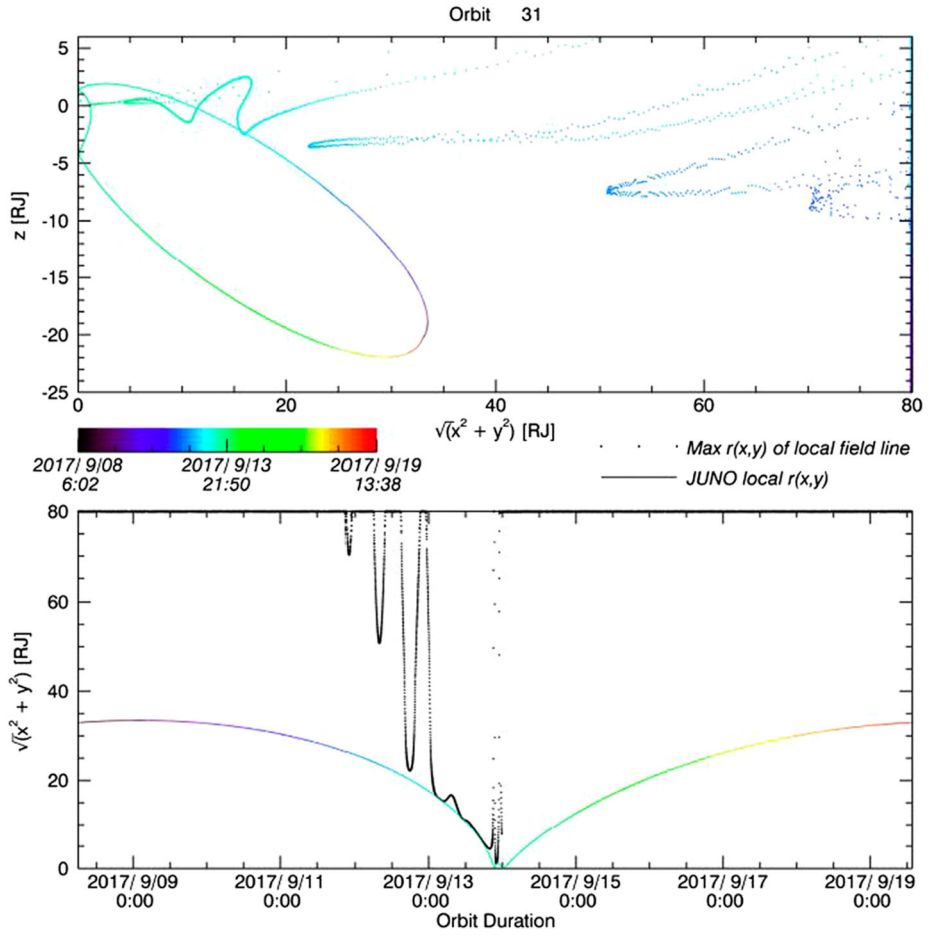

(c)

Fig. 15 (*Continued*)

Figure 18 shows an example of the view of the aurora on a sample *Juno* pass over the north pole. Since the spacecraft is spinning at 2 rpm, the UVS and JIRAM slit-shaped fields-of-view scan swaths over the planet. In this case, the UVS slit passes over the Io footprint wake aurora and roughly half of the main aurora. The location of the spacecraft footprint (S/C FP) for the VIP4 and VIPAL magnetic field models are shown about ∼5° apart. JIRAM will make observations of the aurora on the planet and at its limb. The instrument will be able to map the aurora and take spectral measurements and possibly retrieve the temperatures at which the H_3^+ is emitting as well as provide an estimate of the column density of the H_3^+. For further discussion of the JIRAM observations see Adriani et al. (2014, this issue).

Figure 19 illustrates the morphology of various radio emissions that have been detected coming from Jupiter (reviewed by Zarka 1998, 2000, 2004). The Io decametric emission is Io-DAM, while Io-independent emission (non-Io-DAM) merges with the hectometer component (HOM). The auroral broadband kilometric component (bKOM) is associated with the main aurora while the narrowband kilometric emission (nKOM) is generated by unidentified torus inhomogeneities at the outer regions of Io's torus. The cones

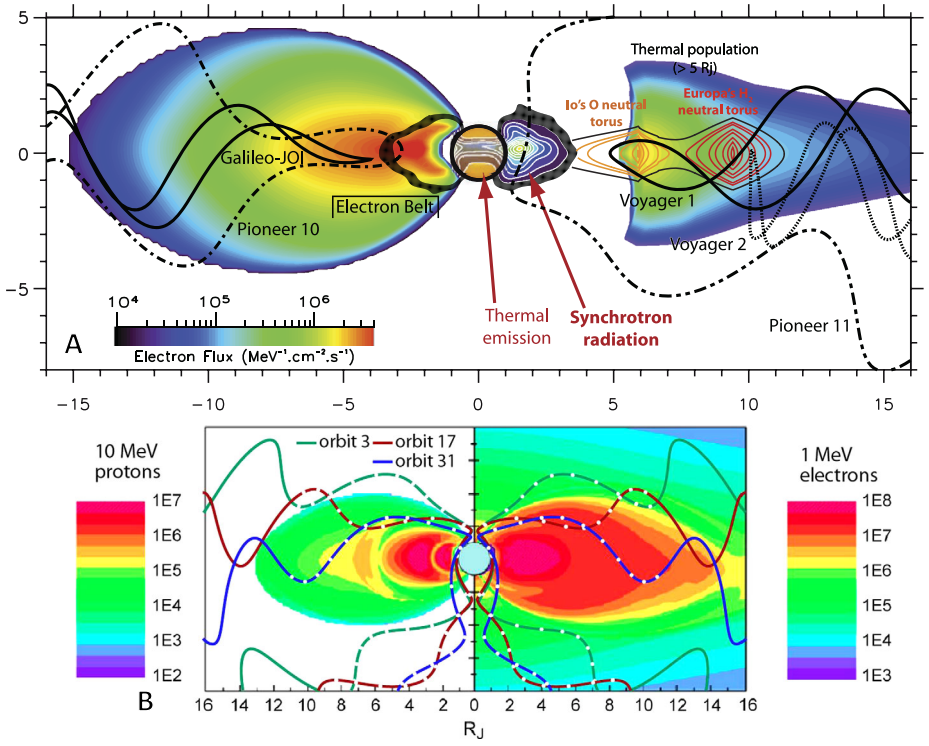

Fig. 16 *Top:* Coverage of the inner magnetosphere by missions previous to Juno. *On the left* the colored contours show fluxes of energetic electrons. *On the right* the innermost contours show the sychrotron emission, neutral cloud (*red lines*) and thermal plasma (*blue-yellow contours*). *Bottom:* Coverage of the proton (*left*) and electron (*right*) inner radiation belts by Juno on orbits of perijoves 3, 17 and 31. The (integral) particle fluxes are calculated from the GIRE model and are in units of $(\mathrm{cm\,s})^{-1}$. The *white dots* on the trajectories are shown with 1-hour tick marks for ± 10 hours around perijove. Note that the spacecraft appear to move in "wiggle" orbits in this coordinate system that is based on the magnetic dipole

emphasize the radiation pattern of the high-latitude emission sources (via the Cyclotron Maser Instability, largely accepted as the generation mechanism of high latitude radio emissions), which exist in both northern and southern hemispheres. Radio emissions labeled bKOM, HOM and DAM are generated near the local electron gyrofrequency f_{ce} and are beamed in widely opened hollow cones aligned on magnetic field lines with $L \sim 6$ (Io-DAM, see e.g; Queinnec and Zarka 1998; Zarka et al. 2001b), $L = 7$–9 (HOM), $L > 10$ (bKOM, Ladreiter et al. 1994), and $L > 7$ (non-Io-DAM) where L refers to the radial distance of the farthest point along the magnetic flux tube that is emitting the radio emission. The inset shows the correspondence of these radio sources with UV emissions: main aurora with non-Io-DAM and bKOM, and Io's spots and trail with Io-DAM. Quasi-periodic emissions (QP) may originate from auroral latitudes (Hospodarsky et al. 2004; Kimura et al. 2010), while non-thermal-continuum (NTC) is thought to be produced at density gradients near the magnetopause (Kurth 1992), or alternately may be the low frequency end of QP bursts having been reflected by magnetospheric density gradients.

At the same time that the remote sensing instruments are making these measurements, the MAG instrument measures the planet's magnetic field and small-scale perturbations due to the auroral currents that couple the planet to the magnetosphere. The JADE instrument suite

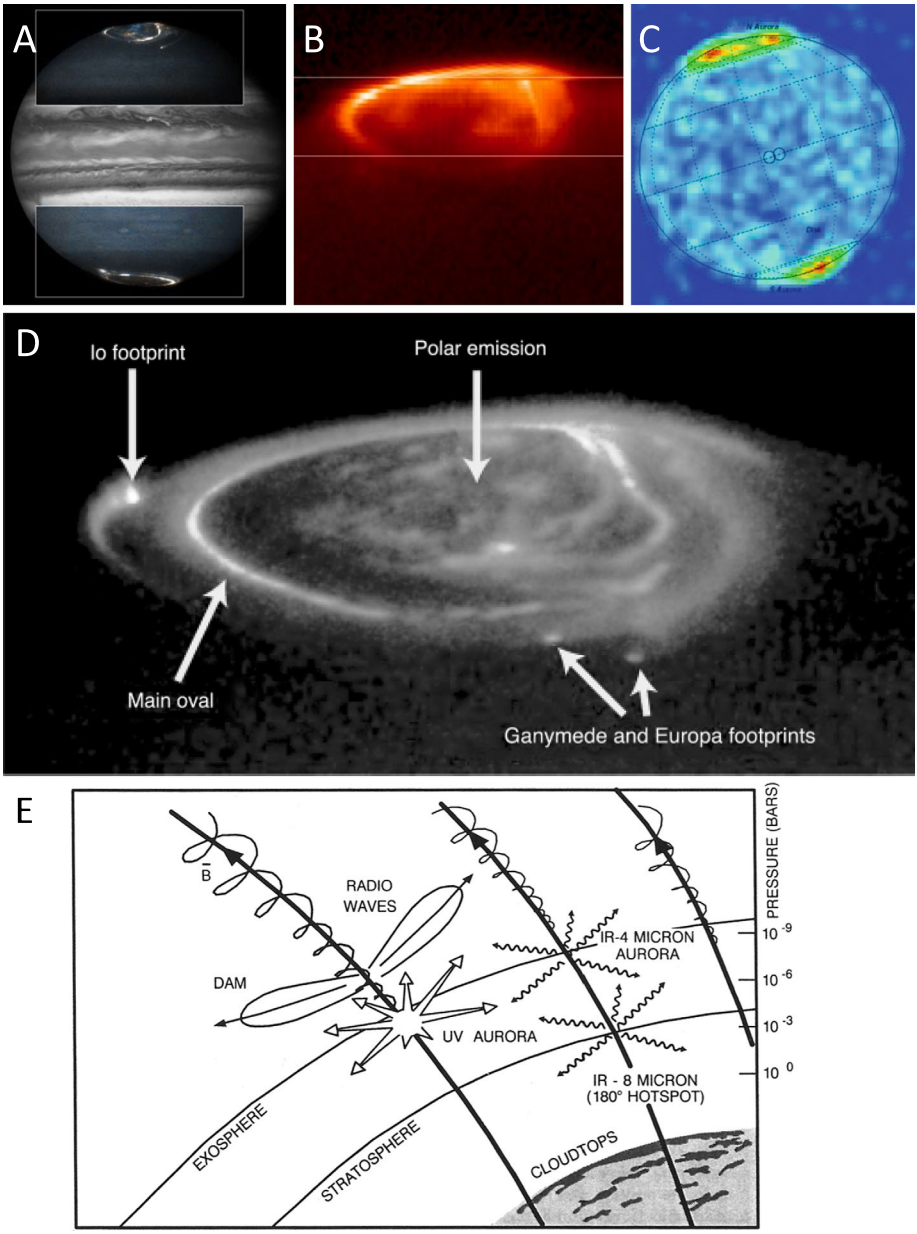

Fig. 17 Auroral emissions at different wavelengths: (**A**) UV from the HST (NASA/John Clarke, BU); (**B**) IR (ESO/Tom Stallard, U. Leicester); and (**C**) X-ray wavelengths from the Chandra Space Telescope (Elsner et al. 2005). (**D**) Morphology of the three main types of Jovian aurora (Clarke et al. 2004). (**E**) Schematic illustration of charged particles sprialling along the magnetic field and the various emissions they generate as they approach the atmosphere in the north polar region (from Connerney 1992)

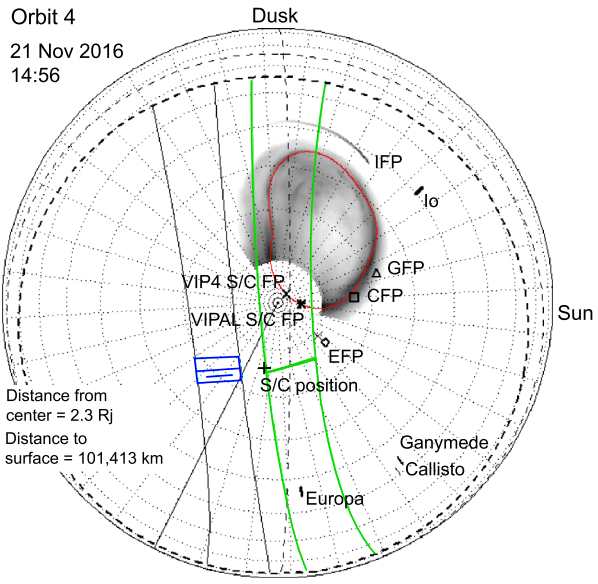

Fig. 18 Polar projection of the predicted northern aurora on Jupiter for orbit 4 on 21 November 2016 at 14:56:00 UT. The 0° meridian is shown as a solid black line. The dashed circles are the *Juno* horizon at the 1 bar level (*thick dashed line*) and 1000 km above the surface (*thin dashed line*). The *grey shape* is the averaged UV aurora for February 2007 from HST. The *red contour* highlights the statistical auroral oval for this month. The swath and the slit of the Juno-UVS instrument are drawn in *green*, assuming a pointing mirror angle of +10°. The field of view of the JIRAM instrument is shown in *blue* along with its swath (*thin black line*). The predicted latitude and longitude of the spacecraft is represented by a cross (+). The tick marks indicate the longitude of the four Galilean satellites, with predicted location of footprints (IFP, EFP, GFP, CFP). The foot of the field line passing through *Juno* has been computed with two magnetic field models: VIP4 (thick X) and VIPAL (∗)

includes three electron sensors (JADE-E) arrayed to instantaneously observe essentially all pitch angles and one ion composition sensor (JADE-I) (McComas et al. 2014a, this issue). JADE-E provides complete electron distribution measurements from ∼0.1 to 100 keV with detailed electron pitch-angle distributions at a 1 s cadence. JADE-I measures ions from ∼0.005 to ∼50 keV over an instantaneous field of view of 270° × 90° each 4 seconds, with observations over all directions in space each 30-second rotation of the *Juno* spacecraft. JADE-I also provides ion composition measurements from 1 to 50 amu with $m/\Delta m \sim 2.5$, which is sufficient to separate the heavy and light ions, as well as oxygen vs. sulfur ions, in the Jovian magnetosphere. The JEDI instruments cover wide fields of view to allow them to measure the electrons and ions moving along the magnetic field. For further discussion of the *Juno* JADE experiment see Mauk et al. (2014, this issue).

Figures 13, 14 illustrate how the ∼9.5° tilt of the magnetic dipole axis and ∼10 hour spin of the planet produces multiple crossings of auroral structures. Figure 7 shows that the altitude at which *Juno* crosses the polar regions varies as the orbit precesses over the mission. This means that *Juno* likely passes directly through the regions where auroral particles are accelerated and allows the MAG and Waves instruments to measure the local magnetic and electric field perturbations. The Waves instrument measures the electric and magnetic components of waves in the frequency range from 50 Hz to 20 kHz and the electric component, only, from 20 kHz to ∼40 MHz. In survey mode, Waves acquires a complete spectrum from both electric and magnetic sensors at a nominal rate of once per second within a few hours

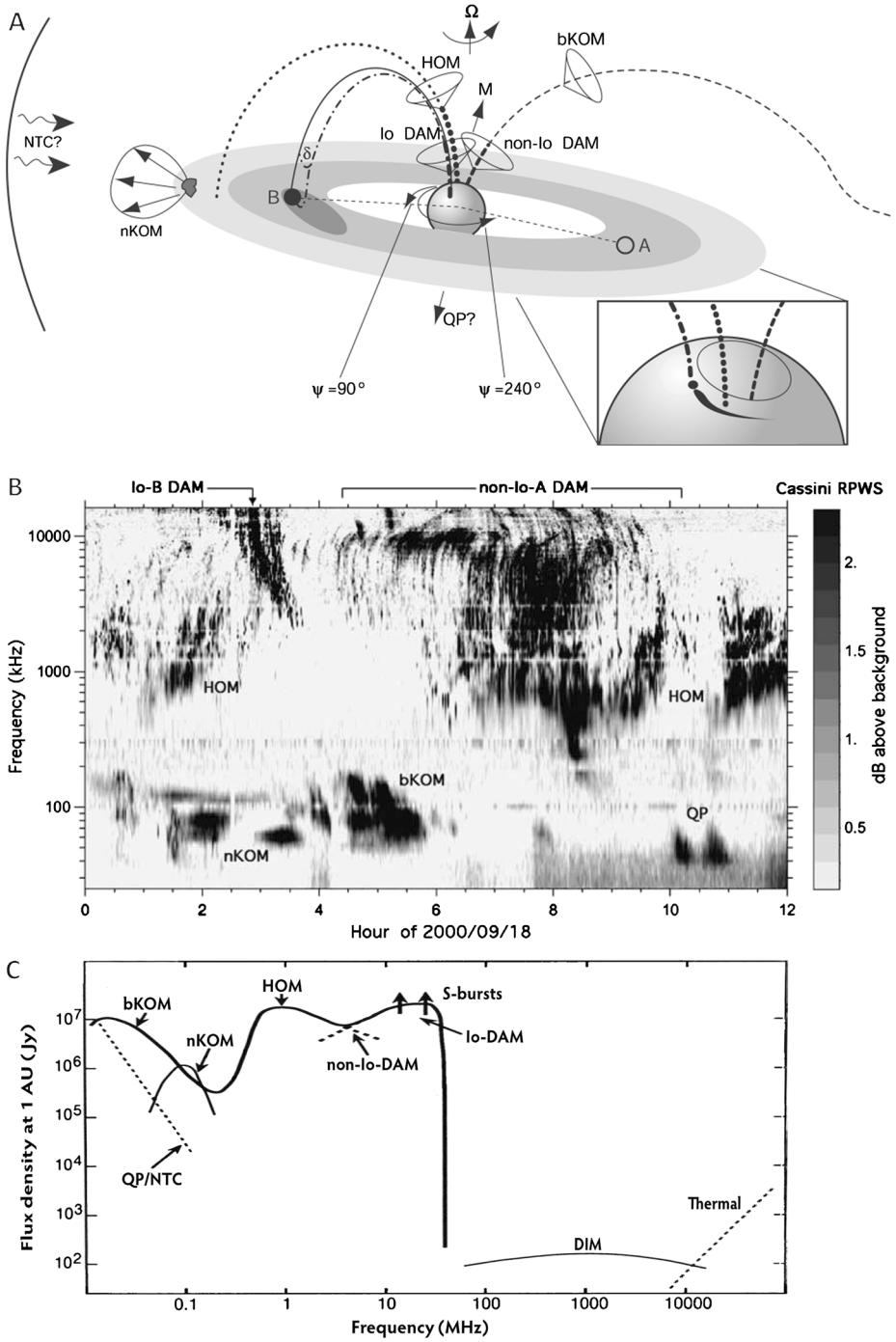

Fig. 19 (**A**) Morphology of the types of Jovian radio emissions from Zarka (2000). (**B**) Frequency-time spectrogram of radio emissions obtained by Cassini when it flew past Jupiter in 2000 (from Zarka et al. 2001a, 2001b). (**C**) Power of emissions (as received at Earth) for Jovian radio emissions versus frequency. Kilometric radiation from Saturn, Earth, Uranus and Neptune are indicated as S-, T-, U-, and NKR. Note that the decimetric synchrotron emission (DIM) is over four orders of magnitude weaker than the high latitude radio bursts. From Zarka (2004)

of perijove. Burst data comprising waveforms from 50 Hz through 150 kHz and a 1 MHz band including the local electron cyclotron frequency are also acquired for a limited number of ~minute-long intervals triggered by large amplitudes in the band below 150 kHz. For further discussion of the *Juno* Waves experiment see Kurth et al. (2014, this issue).

While the locations of the auroral features are relatively well known, the different magnetic field models (as illustrated in Fig. 10) produce slightly different mappings of the instantaneous footprint of the field line passing through the *Juno* spacecraft. Such uncertainties in field have to be considered for planning *Juno* observations but also for analysis of the data returned, at least for the initial orbits, until the magnetic field is updated using *Juno* MAG data. This uncertainty is what drives the need for Waves onboard event detection to retain the most interesting (most intense) time periods.

Below we look at the three source regions of aurora, summarize current understanding of how they are generated and describe the issues that *Juno* addresses.

3.1.1 Main Aurora

Figures 20A, 20B illustrate the location of the main aurora obtained by averaging images from the Hubble Space Telescope and mapping them onto Jupiter's rotating coordinates. The figure shows averages of HST STIS images from Dec. 2000–Jan. 2001 projected to views from above the (A) north and (B) south hemispheres from Grodent et al. (2003a). This main emission remains fairly stable in both location (variations of $<$ few degrees) and intensity (variations of factor ~few) with limited response to variations in the solar wind (Nichols et al. 2009b). Note that because the northern magnetic pole is tilted farther towards the equator than the south, more of the northern auroral region can be imaged than the south. The "kidney-bean" shape of the northern emission (Pallier and Prangé 2001) is thought to be due to a region of weak magnetic field—a magnetic anomaly—that is located at about 75°N and 115° System III longitude that pushes the main aurora poleward and the tail of the Io-related emission equatorward. The possibility that Jupiter's magnetic field has an anomalous region was first proposed by Dessler and Vasyliūnas (1979) to explain longitudinal variations in the Io torus (see review by Hill et al. 1983). Figure 20C compares the dayside UV emissions (observed from Earth orbit by HST, Grodent et al. 2008) with the nightside optical emissions (observed by Galileo, Vasavada et al. 1999). The persistence of the kink shows that it is internal rather than a feature of local time. Figure 10 illustrates different attempts to model this high-order structure in Jupiter's magnetic field (Grodent et al. 2008; Hess et al. 2011). The fact that Ganymede's auroral emission usually lies outside the main auroral oval tells us that these auroral field lines (and the associated currents) map to distances beyond Ganymede's 15 R_J orbit, though an exceptional occasion in 2007 is noted by Bonfond et al. (2012).

The idea that Jupiter's auroral current system is driven by rotational energy combined with the production and outward transport of iogenic plasma was first proposed by Hill (1979) and further developed by many authors (Pontius and Hill 1982; Huang and Hill 1989; Hill 2001; Cowley and Bunce 2001, 2003; Nichols and Cowley 2004; Ray et al. 2010, 2012, 2014; Nichols 2011). A consequence of the current closure is that the rotation of the ionosphere is coupled to the rotation of the equatorial plasmas, and the equatorial plasmas are accelerated to a substantial fraction of the rigid rotation speed. Hill (1979) pointed out that these coupling-currents (and corresponding aurora) are stronger where the plasma begins to slip behind rigid corotation. *Voyager* measurements showed the plasma departing significantly from corotation around ~17–20 R_J (McNutt et al. 1979). Models gained greater sophistication with improved current sheet models but the primary differences between the

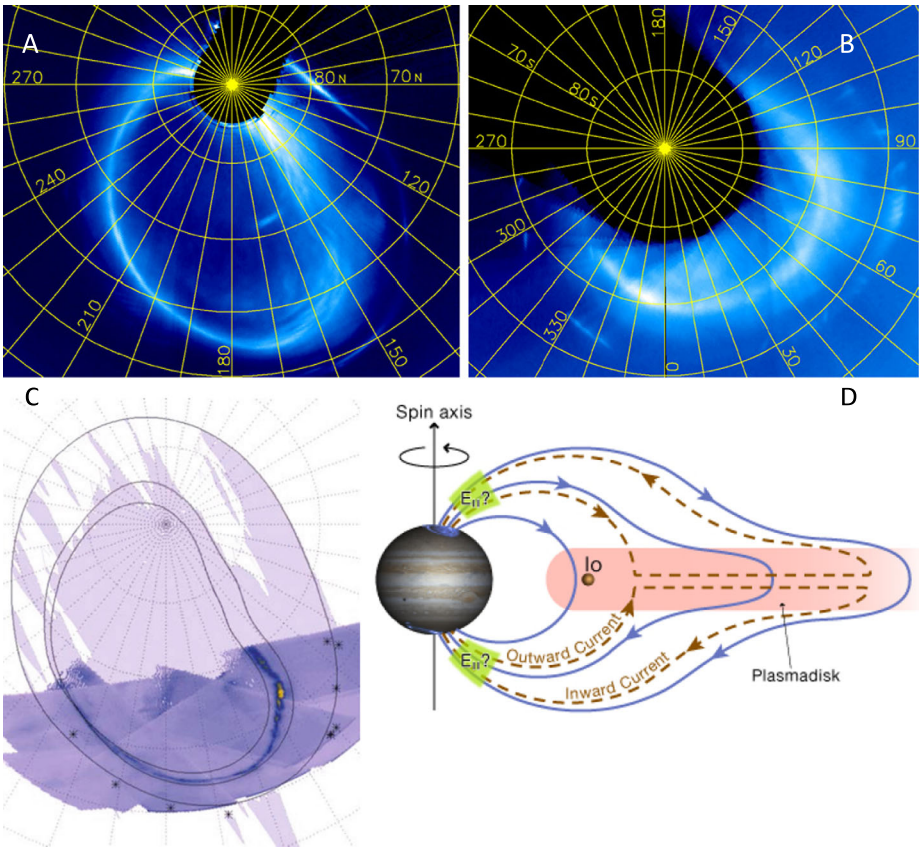

Fig. 20 *Top:* Jupiter's main auroral emission in the (**A**) north and (**B**) south hemispheres (Grodent et al. 2003a, 2003b). Grid lines indicate System III longitude and planetocentric latitude with respect to the spin axis. The arcs at the lowest latitudes are from Io footprint emissions on different days. *Bottom:* (**C**) Optical emissions observed by Galileo (Vasavada et al. 1999) projected onto the same grid as **A**, with lines illustrating locations of the main emissions and the Io footprint. (**D**) The Iogenic magnetospheric plasma is coupled to the rotating planet via electrical currents (*brown dashed lines*) that flow along magnetic field lines (*blue solid lines*) to the auroral regions of Jupiter's atmosphere (adapted from Cowley and Bunce 2001)

various studies cited above are whether the coupling between the planet's rotation and the magnetospheric plasma is limited by the transfer of angular momentum from the deep atmosphere to the ionosphere (e.g. Huang and Hill 1989); the ionospheric conductance (e.g. Nichols and Cowley 2004); or the lack of current-carrying electrons at high latitudes between the ionosphere and plasma sheet, modifying the relation between current and the voltage along the magnetic field (e.g. Ray et al. 2010). Resolving this issue requires measurements of particles and fields at high latitudes.

Experience at Earth, however, cautions us not to take the sketch in Fig. 20D, nor the plots in Figs. 13 and 14, too literally and that auroral currents are likely much more structured and variable than suggested. Mauk and Saur (2007)'s analysis of data in the plasma sheet indicates there are multiple pairs of upward and downward currents. Saur et al. (2003) suggested that the structuring is so pervasive on multiple scales that turbulent processes may be the prime energy conversion mechanism for the generation of Jupiter's aurora and argue that there is sufficient energy in the magnetic turbulence to power Jupiter's main aurora.

This is perhaps similar to Earth's "Alfvénic aurora". *Juno* not only takes field and plasma measurements at high cadence at polar latitudes but also makes multiple passes through the equatorial plasma sheet (illustrated by Figs. 12 and 13 in Sect. 2.4 above) to test such ideas.

Figure 19 illustrates the wide variety of radio wave phenomena (non-Io-DAM, HOM, b-KOM) expected on main auroral field lines based on our understanding of Earth's auroral region. Figure 24 illustrates the range of plasma waves in the auroral region, such as auroral hiss which should highlight the field lines that connect to the main auroral emissions from Jupiter's atmosphere. These are the types of emissions considered when the Waves instrument was designed. For example the electron solitary waves, or phase space holes, were identified in the near-equatorial middle magnetosphere by Barbosa et al. (1981) on field lines directed nearly parallel to the equator. In 1981 this phenomena was known as broadband electrostatic noise as the Fourier-transformed appearance of the solitary waves before the detailed waveforms were identified. Based on the occurrence of broadband electrostatic noise at Earth, Barbosa et al. (1981) used this phenomenon as a connection from the plasmasheet boundary layer to the auroral region. This was the first identification of the mapping of the middle magnetosphere back to the main auroral which was confirmed by the subsequent identification of the H_3^+ Io footprint aurora located well equatorward of the main oval (Connerney et al. 1993). At higher frequencies we expect *Juno* to traverse the DAM and/or HOM source regions, hence, we target the Waves experiment at a 1-MHz band including the local electron cyclotron frequency in order to make high spectral resolutions of the cyclotron maser instability emissions and compare in-situ measurements to detailed predictions on mode and propagation angle by Mottez et al. (2010).

A correlation of the auroral emitted power with the solar wind pressure has been reported by Nichols et al. (2007), Clarke et al. (2009), Nichols et al. (2009a). Southwood and Kivelson (2001) predicted that solar wind compressions would increase the angular velocity of the equatorial plasma, decrease the currents related to the corotation lag, and thus result in a dimmer aurora. Contrary to these expectations, Nichols et al. (2007) reported a brightening of the main emission corresponding to a period when the magnetosphere first modestly shrunk and then expanded, based on images acquired in 2000 while Cassini was upstream of Jupiter. Clarke et al. (2009) compared the brightness of the whole Jovian aurora with the solar wind conditions during the large 2007 HST campaign and came to a similar conclusion, i.e. a correlation of the auroral brightness with the solar wind pressure. Using the same 2007 data set, Nichols et al. (2009a) separated the aurora into distinct regions: the low latitude emissions, the main emissions, and the high latitude emissions, in order to identify the component of the aurora which responded the most to the solar wind input. The outer region does not appear to be correlated with the solar wind condition, but enhancements of the main emissions and, to a lesser extent, of parts of the polar emissions were associated with solar wind compressions, as in Nichols et al. (2007). It should be noted that estimates of the solar wind conditions at Jupiter relying on Earth-based measurements have always been challenging, the trickiest part being the accurate prediction of the arrival time of the shocks. The delay between the arrival of a compression region at the sub-solar magnetopause and the auroral response is thus unclear with the current dataset. The emission region of the main aurora is buried deep in the magnetosphere and is generally agreed to be primarily associated with field-aligned currents that couple the 20–30 R_J plasma disk to the ionosphere. On the other hand, there is evidence for a solar wind connection in non-thermal radio emissions (Prange et al. 1993; Zarka 1998; Echer et al. 2010; Hess et al. 2012) and energetic particle events couple variations in auroral, Io torus, and the distant magnetosphere, despite their widely disparate locations (Louarn et al. 2000).

As illustrated in Figs. 13 and 14, *Juno* crosses regions of these main auroral currents many times and at a range of altitudes. The MAG, Waves, JEDI and JADE instruments

make in situ measurements of fields and particles (measuring currents, electric fields, particle fluxes, etc.) at the same time that UVS, JIRAM and *Juno*CAM instruments measure auroral emissions on the planet (characterizing the location, altitude profile and spectra of the auroral emissions). Moving at ~20 km/s over the poles of Jupiter, *Juno* takes only a

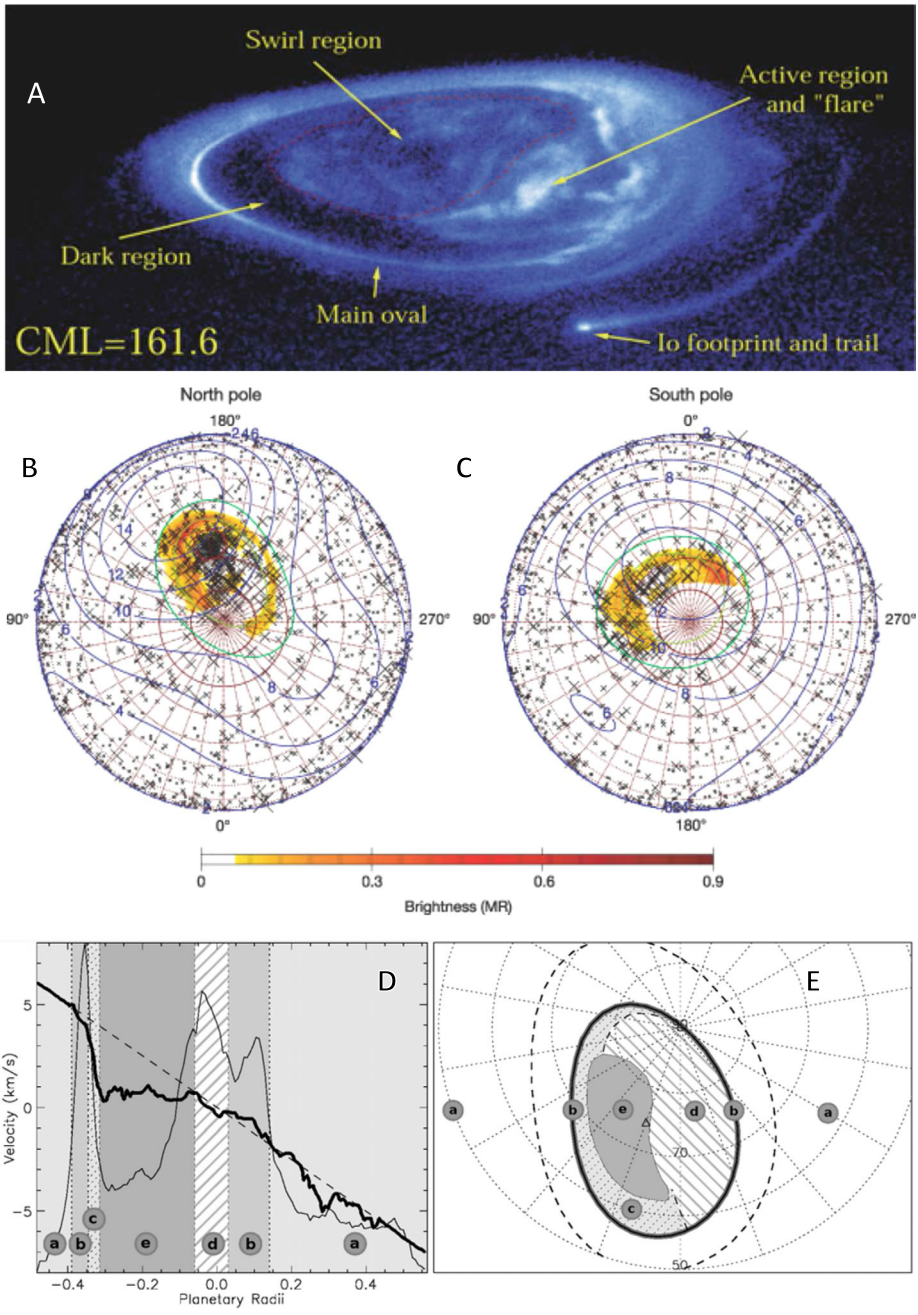

few minutes to cross the narrow width of the main aurora. The opportunity to observe the whole aurora for various orientations of the dipole will help disentangle local time effects from System III longitude effects, in term of brightness and location of the main emissions. *Juno* will also reveal the relative importance of the internal parameters, such as variations of plasma sheet density, versus the external parameters, such as the solar wind dynamic pressure, in determining the morphology and brightness of the main aurora.

Without an upstream monitor of the solar wind, *Juno* will have to rely on extrapolation from Earth of solar wind properties to Jupiter. Nevertheless, Waves, UVS, JIRAM and *Juno*Cam will measure the auroral emissions as MAG, JEDI and JADE measure particle fluxes as the *Juno* spacecraft makes multiple traversals through magnetic flux tubes connected to the main auroral regions (e.g. see Figs. 14 and 18).

3.1.2 Polar Aurora

Figure 21 shows observations of UV, x-ray and IR emissions from the polar regions of Jupiter. The major issues with interpreting the polar data include (a) variations in space and time on a range of scales, and (b) difficulties in mapping to regions of the magnetosphere. Moreover, these polar regions map to the outer magnetosphere where there is debate about the magnetospheric dynamics (discussed in Sect. 3.4 below).

Perhaps the most comprehensive study of the polar aurora was completed by Grodent et al. (2003b) who showed that the polar emissions contribute ∼30 % of the total auroral brightness and show bursts lasting ∼100 seconds. Combining these UV images with IR spectroscopy of H_3^+ emissions (Stallard et al. 2001, 2003), defines three main regions: a dark region on the dawn side, polarward of the main aurora that may be connected to regions of magnetospheric flow in the middle to outer magnetosphere where plasma is moving inward and sunward; an active region around noon and into the dusk side where there are bright flares and arc-like structures (Nichols et al. 2009a) and a "swirl" region of variable emission with slow/stagnant flows which may be the region of magnetic flux that connects to the solar wind. Mapping observed magnetic flux at the equator to the polar regions supports the idea that the swirl region contains flux tubes that are connected to the planet at one end and are open to the solar wind at the other (Vogt et al. 2011). Deep in the magnetotail (50–100 R_J), blobs of plasma—plasmoids—have been observed to disconnect from the plasma sheet and leave down the magnetotail (Woch et al. 2002; Kronberg et al. 2007; Vogt et al. 2010; Kasahara et al. 2013). Grodent et al. (2003b, 2004) and Radioti et al. (2008, 2010, 2011) have associated small bursts of polar emission on the dusk and nightside with these plasma

◀ **Fig. 21** *Top:* (**A**) HST image (14 Dec. 2000) illustrates the auroral features poleward of the main oval—the polar aurora. Arrows point to the dark region and the active region where "flares" and "arcs" are often observed. From Grodent et al. (2003a, 2003b). *Middle:* Polar projections of X-rays seen by Chandra and simultaneous HST UV images. The mapped locations of individual X-ray photons (*crosses*) are overlaid on averages of several northern (**B**) and southern (**C**) auroral images made with HST-STIS during 10–20 UT on 18 December 2000. Contours show the surface VIP4 model magnetic field strength, the Io footprint path (*green*) and $L = 30$ (*yellow*). The size of each cross gives an approximate indication of the uncertainty in location of the corresponding X-ray photon. The HST-STIS images made with the 25MAMA filter are displayed in false colour with auroral H_2 emission brightnesses in mega-rayleighs (MR) as indicated by the colour bar. From Gladstone et al. (2002). *Bottom:* (**D**) Spectroscopic IR diagnostics of Jupiter's polar region. The typical H_3^+ line-of-sight velocity (*bold line*) and normalized intensity (*thin line*) plotted against the corotation rate (*dashed line*). The velocity profile is divided into regions with patterned backgrounds and letters, directly relating to the lettered sections in the (**E**) map of ion flow in the northern auroral regions of Jupiter (at a CML of 160°): ***a*** is low latitude emission; ***b*** is the main auroral region; ***c*** is the dark region; ***d*** is the active, variable region; ***e*** is the stagnant/low speed region. From Stallard et al. (2012)

ejections. On the dayside, a bright auroral spot has often been seen around noon in a region that may map to the magnetospheric cusp (Pallier and Prangé 2001, 2004; Waite et al. 2001; Bonfond et al. 2011).

X-ray emissions from Jupiter have been observed since 1979. Most recent observations are by the Chandra and XMM-Newton telescopes in Earth orbit (reviewed by Elsner et al. 2005a, 2005b; Branduardi-Raymont et al. 2010). Careful modeling of the interaction of energetic (10 MeV) oxygen and sulfur ions with Jupiter's atmosphere suggest that these x-rays are produced by high-charge-state ions—such as O^{6+} and O^{7+}—that are stripped of electrons as they bombard the atmosphere (Hui et al. 2010; Ozak et al. 2010). This begs the question of where the 10 MeV ions come from. Cravens et al. (2003) suggest high voltage (million volt) potential drops in regions of downward currents. Bunce et al. (2004) suggest such accelerations could be produced via reconnection at the dayside magnetopause in regions of intense downward field-aligned current.

Juno's MAG, Waves, JEDI and JADE instruments make in situ measurements of fields and particles, measuring currents, electric fields, particle fluxes, etc., at the same time that UVS, JIRAM and *Juno*CAM instruments measure the rapidly varying locations and spectra of polar auroral emissions on the planet. But the transient and small-scale nature of these polar emissions likely makes such structures harder to resolve. However, the unique point of view offered by *Juno* will allow observations of the whole polar region, including midnight emissions poorly visible from Earth, for a complete range of sub-solar longitudes. The Waves instrument covers the polar auroral region with 1-s cadence full spectra coupled with burst mode observations as described above for the main auroral oval.

3.1.3 Satellite Aurora

The interaction of magnetospheric plasma with Io, Europa and Ganymede all excite Alfvén waves that travel along Jupiter's magnetic field towards the planet (see reviews by Kivelson et al. 2004; Saur et al. 2004; Jia et al. 2009). Because of the dense plasma between the moons and Jupiter, the travel time between these moons and the planet is longer than the time it takes the corotating plasma to flow past the moon. This means that there is not a fixed current system connecting the moon to the planet (sometimes described as a "unipolar inductor") but rather there is a stream of Alfvén waves that are reflected at the edges of the Io plasma torus or Jupiter's ionosphere. The possible exception might be Io where Hill and Pontius (1998) argue that the stagnated flow close to the moon might allow a closed current system. We have known for many decades that moons, particularly Io, trigger radio emissions (see Io-DAM in Fig. 19). There are theories proposed for how disturbances generated by the moons accelerate radio-emitting electrons (reviewed by Hess et al. 2010a, 2010b). Furthermore, the bright auroral spots (Fig. 17) tell us that fluxes of these electrons bombard the atmosphere. Specifically, Hess et al. (2007a) calculated a typical energy of ~4 keV for electrons producing Io-induced fast radio bursts, whereas Bonfond et al. (2008, 2009) showed that the vertical distribution of aurora above Jupiter's limb suggests a mean energy of the electrons of ~1 keV and that the spacing of multiple auroral spots indicates that electron beams reflect between hemispheres, which is also consistent with the time-frequency drift of radio bursts.

Figure 22 shows the characteristic frequency-time arcs of Io-triggered radio emissions that have been observed with Earth-based radio telescopes since 1964. Such shapes are well-matched by the recent model of Hess et al. (2008a) that uses current magnetic field models and assumes that electrons with unstable loss-cone distributions generate the emission via the cyclotron maser instability. Figure 23 illustrates some of the auroral process

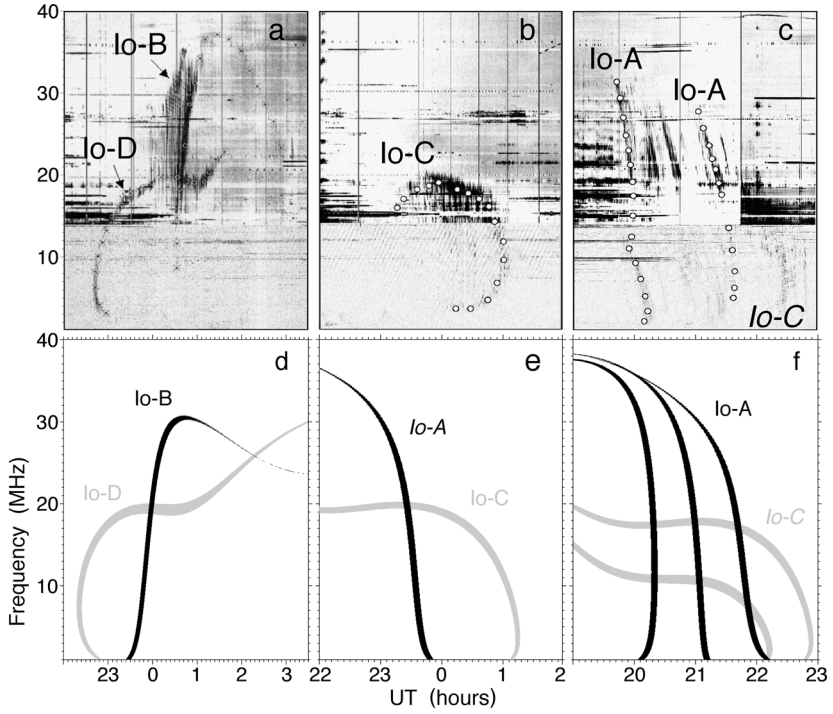

Fig. 22 *Top* (**a**, **b**, **c**) Dynamic spectra of typical Io-Jupiter arcs observed by Wind/Waves and the Nancay decameter array (adapted from Queinnec and Zarka 1998). The various symbols superimposed along the arcs were used to identify their line of maximum intensity in the frequency-time plane. *Bottom* (**d**, **e**, **f**) Dynamic spectra of Io-Jupiter emission for the same time intervals as above simulated using loss-cone cyclotron maser instability where the *black arcs* are generated in the northern hemisphere and *grey arcs* are in the south. From Hess et al. (2008a, 2008b)

associated with Io, but similar processes are expected to be responsible for auroral spots produced by Europa and Ganymede. There may be a weak interaction at Callisto but any auroral emission is probably swamped by the main aurora. Bonfond et al. (2008) used combinations of electron beams and Alfvén waves to explain the spacing of Iogenic auroral spots. While the Io spots and associated radio bursts are associated with electrons accelerated by Alfvén waves (such as modelled by Su et al. 2003; Hess et al. 2007b; Jones and Su 2008), Ergun et al. (2009) argues that the auroral emission produced downstream of Io (an auroral "wake" sometimes stretching half the way around the planet) is produced by a steady system of upward and downward currents. Hill and Vasyliūnas (2002) argue that the Pedersen conductivity of the ionosphere limits the currents and dictates the length of the wake. Ergun et al. (2009) suggest that the wake extends far behind Io because the lack of current-carrying electrons at high latitudes limits the currents that can flow between the mass-loaded plasma behind Io and Jupiter's ionosphere, implying that potential structures develop at high latitudes (as sketched in Fig. 20). Parallel potential drops of $\sim$ keV energy were nevertheless detected in radio above the Io flux tube footprints (Hess et al. 2007a). Bonfond et al. (2009) questions these two hypotheses since the altitude profile of the main Io spot and the tail are very similar, suggesting that a similar process (Alfvén wave acceleration of electrons) generates both features.

The *Juno* orbits have been designed to systematically map the planet, so it is unlikely that the spacecraft passes directly through the flux tubes connected to the satellites (e.g.

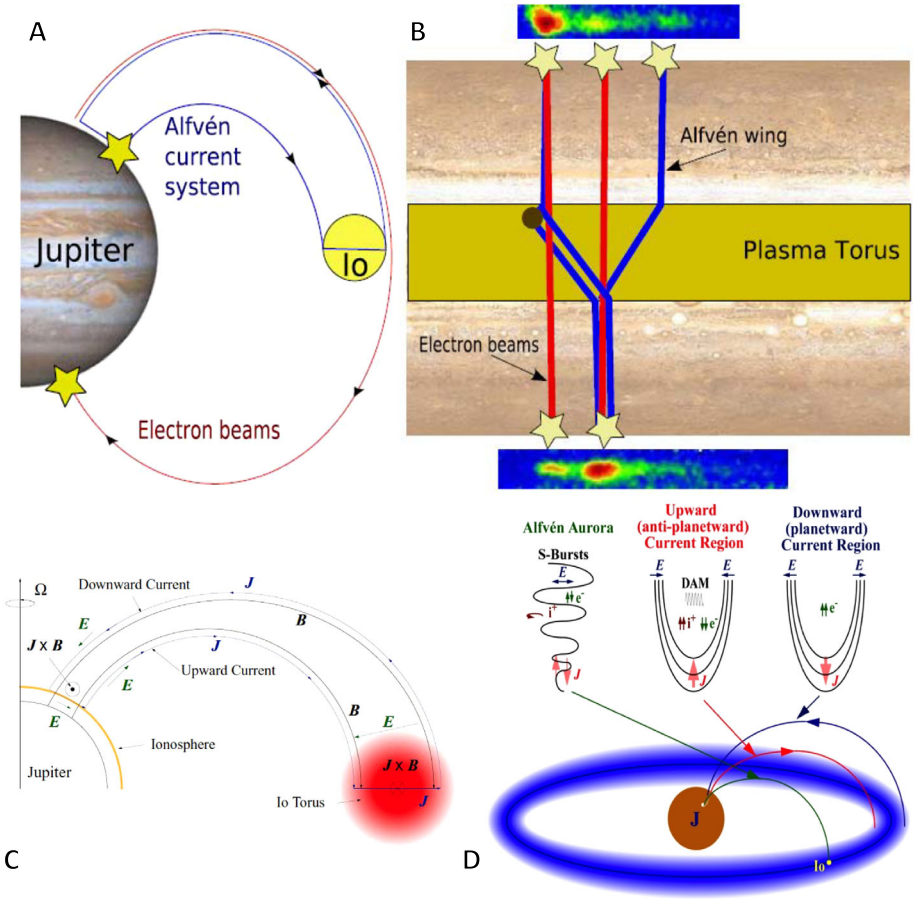

Fig. 23 Satellite aurora, shown here for Io, but similar processes are expected to be responsible for auroral spots produced by Europa and Ganymede. *Top:* The Alfvén waves generated by the Io-plasma interaction accelerate electrons. Some of these electrons bombard the atmosphere of Jupiter and excite aurora. But some of the electrons are reflected between the hemispheres. Bonfond et al. (2008) used combinations of electron beams and Alfvén waves to explain the spacing of Iogenic auroral spots. *Bottom:* The disturbance at Io is coupled to the planet via Alfvén waves that propagate along the magnetic field. It takes some time for the additional material added to the torus to be brought up to corotation with the surrounding plasma resulting in a quasi-steady upward and downward current system in the "wake" downstream of Io (Hill and Vasyliūnas 2002). From Ergun et al. (2009)

Fig. 18). But *Juno* likely crosses at least the wake of the Io auroral emission. We expect that the UVS and JIRAM instruments will make multiple observations of the satellite auroral emissions. The location of the different spots, their relative distance as well as the altitudinal profiles will be observed. Moreover, spectral measurements will provide further information about the energy of the precipitating electrons and the atmospheric response to this localized energy input.

As with the main aurora and polar aurora, Waves will use 1-s spectral cadence and its burst mode to collect detailed waveforms to acquire information on plasma waves contributing to the presumably Alfvénic-driven aurora and how they compare to the other types of auroras. The variety of phenomena summarized in Fig. 24 represents the differences one

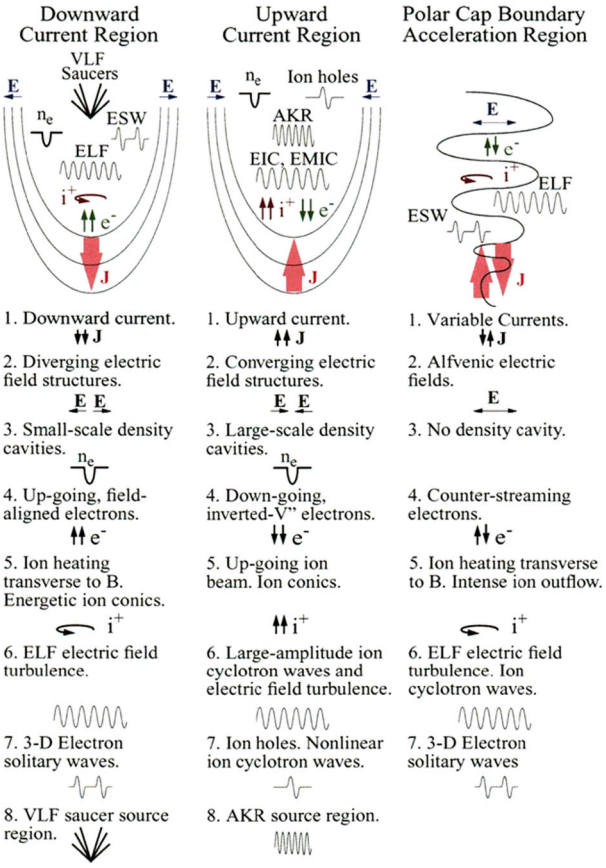

Fig. 24 The three types of auroral zones based on experience from Earth: upward currents, downward currents and Alfvénic regions. Adapted from Carlson et al. (1998)

would expect from our understanding of Earth's auroras, hence, we will have an opportunity to see if a similar menu of phenomena can be attributed to the various Jovian auroras.

3.1.4 Auroral Physics

The obvious advantage of studying auroral processes at Earth comes from both the long and extensive coverage of observations from the ground, from several decades of spacecraft observations from a range of altitudes, including inside the Earth's AKR sources (Viking, FAST). As in many areas of science, detailed knowledge tends to change basic questions into more complex questions. Studies of aurorae at other planets, such as Jupiter, requires us to return to the more basic issues (what are the driving forces, how do the processes work, what factors modulate auroral behaviors, etc.) and test our understanding of the underlying physics under rather different conditions. In their introductory chapter to Keiling et al. (2012)'s recent monograph of auroral studies, Mauk and Bagenal (2012) note that "A central question of planetary space science in general and auroral physics in particular is: What aspects are universal and what aspects are specific to the conditions that prevail at any one planet?" The current understanding of auroral processes at Earth is summarized in Paschmann et al. (2002) as well as in Keiling et al. (2012) where several chapters compare Earth with other planets.

A traditional view of the generation of auroral phenomena consists of (1) the generation of electrical currents and voltages within the magnetized plasma of the magnetosphere, (2) the diversion of those electrical currents along magnetic field lines toward the polar auroral regions, (3) the generation of parallel electric fields along the magnetic field lines close to the planet as a result of the low density of charge carriers in the regions just above the ionosphere, (4) the acceleration of charged particles out of the regions of parallel electric fields onto the upper atmosphere as well as out into the distant magnetosphere, (5) the excitation and ionization of atoms and molecules within the upper atmosphere by the accelerated electrons resulting in strong auroral emissions and enhancements in the electrical conductivity of the ionosphere, (6) the closure of the up-going and down-going electric current through the partially conducting ionosphere, and (7) the associated heating through ohmic dissipation in the upper atmosphere through the collision of current-carrying ions and neutral atmospheric constituents. These are all general processes that Earth and Jupiter probably share. The differences are likely found in the relative importance of each process and in the local properties of the plasma where these processes are operating.

Based on experience at Earth, Fig. 24 (from Carlson et al. 1998) outlines the electric current structures for different types of auroral zones: upward current regions, downward current regions and regions of time-varying current. The goal of the FAST satellite was to gather particles and fields data at a rate fast enough to be able to resolve these auroral structures as it flew through them (Carlson et al. 1998). Figure 25 (from Paschmann et al. 2002) shows example data obtained by the FAST satellite. At the bottom of Fig. 23 there is an image from the Polar satellite that shows ultraviolet aurora (measured by the UVI instrument) and the projected trajectory footprint of the FAST satellite (similar measurements were obtained by Viking, see Bahnsen et al. 1989). While FAST took the data in Fig. 25, it was moving poleward across the nightside auroral oval. The top panel of data shows the magnetic field perturbation relative to Earth's reference field, with the inferred field-aligned currents indicated in green (downward), blue (upward) and the Alfvénic currents in red. The DC electric field fluctuations in the second panel show the electrostatic shock structures associated with the auroral acceleration region. The next four panels show ion and electron spectrograms versus energy and pitch-angle. The bottom three panels show integrated ion outflow, and wave activity ranging from near-DC to MHz frequencies.

Note that the whole of Fig. 25 covers a duration of only seven minutes during which the spacecraft traverses at least five different regions. Terrestrial auroral structures are observed from $\sim$1000 km in scale down to $<$1 km and probably extend to smaller scales, below current observational limits. To observe small scale structures, the FAST mission included instruments that operated at very high cadence for short-durations—in burst mode. Specifically, ion and electron spectra were sampled every 78 ms while electron fluxes could be sampled as fast as once every 1.6 ms (Carlson et al. 2001). The FAST spacecraft, over its $>$50,000 orbits of Earth, could gather data at rates of 8 Mbits/sec, store and process data onboard and deliver data to the ground at rates of 2 Mbits/sec (few Gbits/day).

At Jupiter, pre-*Juno* observations of the auroral structures are limited to remote sensing either from Earth or from distant spacecraft. In radio at decameter wavelengths the very high temporal and spectral resolutions achieved from the ground allow to study the source microphysics (see e.g. Hess et al. 2007a, 2008a, 2008b; Ryabov et al. 2007), but this is not the case for other waves and particles measurements. Typical width-scales of auroral structures are on the order of 1° or 1500 km in Jupiter's atmosphere. To scale such widths to the location of *Juno* at distance R from the center of Jupiter we use a relationship of $R^{3/2}$ corresponding to a dipole field. For example, we find that when *Juno* is 2 R_J from the center of Jupiter, it crosses a distance of $\sim$4000 km corresponding to the width of the main

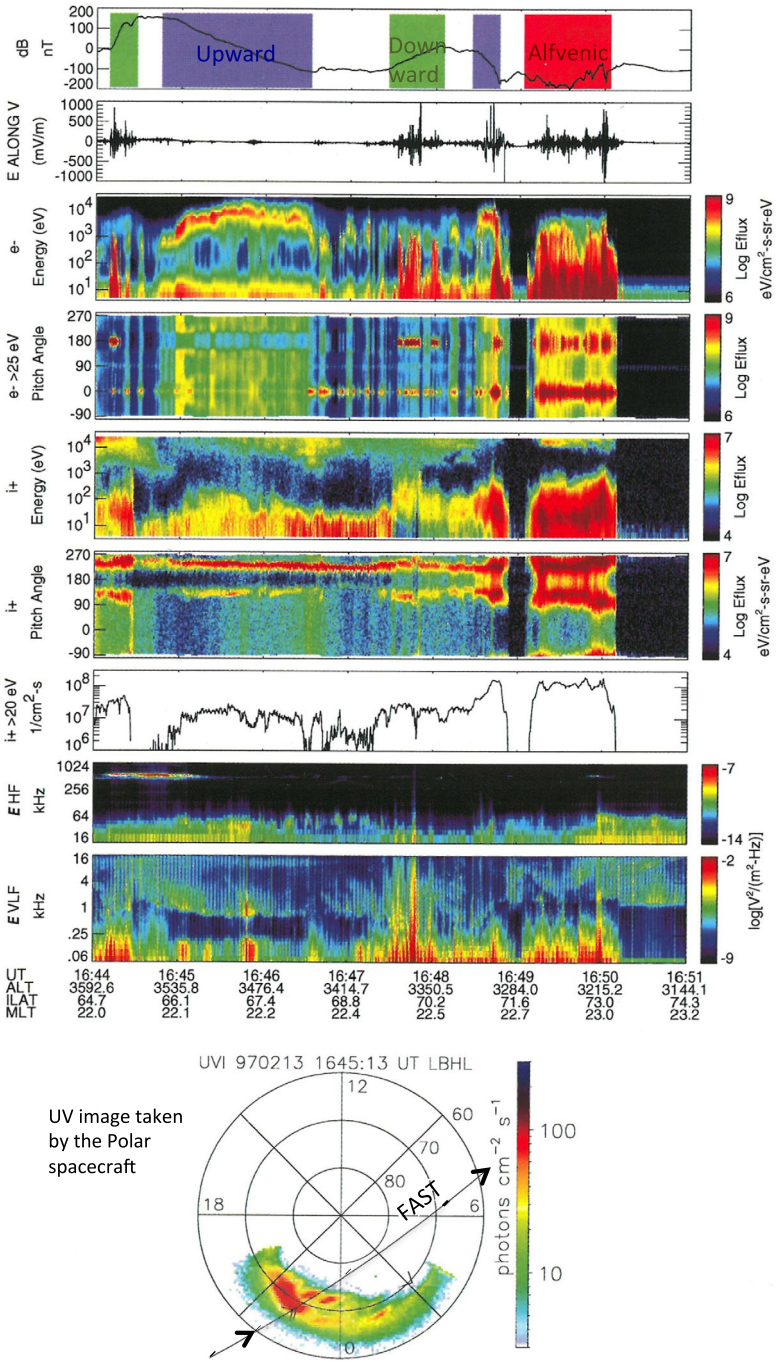

Fig. 25 FAST data obtained as the spacecraft passed through the 3 types of coupling regions illustrated in Fig. 24. *Below:* UV image of the aurora taken by the Polar satellite. The projection of the FAST trajectory shows the spacecraft crossing the night side auroral region. From Paschmann et al. (2002)

aurora. Since *Juno* is moving at ~20 km/s over the poles and ~60 km/s around perijove, this distance is covered in a few minutes, a couple of *Juno* spin periods. Thus, the JADE highest resolution (burst-mode data rate) of 1 sec for electrons and 4 sec for ions (further detailed in McComas et al. 2014a, this issue) resolves the main auroral and possible sub-structures that are to be expected if Jupiter's aurora follows our experience at Earth.

At 10 s keV to MeV energies the JEDI instrument (further detailed in Mauk et al. 2014, this issue) resolves these structures with ~second sampling. JEDI detects energetic electrons (above 40 keV to over 500 keV) and energetic ions (about 20 keV to >1 MeV for protons, and 50 keV to >1 MeV for oxygen) with high energy, time, and angular resolution. It comprises three nearly identical sensors, two fans covering $12° \times 160°$ and one that covers $12 \times 148°$. They are mounted on the spinning spacecraft with no moving parts. Two of the sensors view almost entirely in the plane perpendicular to the high-gain antenna. The third fan is perpendicular to this plane so that, with the spacecraft spin rate of about 2 RPM, nearly the whole sky is sampled every 30 s. Within each sensor there are six look directions to provide angular coverage. At high enough energies, ions and electrons will pass into the collimator, through a series of foils, and into solid-state detectors. Secondary electrons liberated in the foils by the passage of the ions also provide a time-of-flight measurement. Together with the energy detection in the SSD, the ion energy and species can be calculated.

In the polar regions, JEDI has excellent coverage of precipitating and upwardly moving energetic particles. Dense, heavy ion plasma is centrifugally confined at Jupiter, but particles at the JEDI energies can mirror at high latitudes and even reach the planetary atmosphere. It is expected that fluxes of particles that generate the planetary aurora and heat and ionize Jupiter's upper atmosphere will be obtained with very high time and spatial resolution. Outside the polar regions, JEDI will detect the electron and ion radiation belts of Jupiter. Furthermore, by shielding some detectors on one of the sensors, JEDI measures the flux of >1 MeV electrons hitting the detector.

At high latitudes along the *Juno* orbit, JEDI makes very coarse measurements of energetic neutral atoms (ENAs) emitted from the inner regions. These are neutrals created when energetic ions undergo charge-exchange collisions with neutral populations. The resulting ENA has approximately the same energy as its parent ion. ENAs in Saturn's magnetosphere have been invaluable in understanding some polar processes and magnetospheric activity in general. They are a tool for inferring the presence of neutral distributions and also for illuminating temporal magnetospheric processes.

The MAG investigation measures the vector magnetic field throughout periapsis at a rate of 64 vector samples per second, with a vector accuracy of 100 parts per million in magnitude and direction referenced in inertial space (via the ASC star cameras co-located with the MAG sensors) to some tens of arcseconds. This should allow us to resolve auroral current sheets with a characteristic dimension of about a km (further detailed in Connerney et al. 2014, this issue).

Associated with the main aurora are broadband kilometric (bKOM), and hectometric (HOM), and decameteric (DAM) radio emissions (Fig. 19, Zarka 2000). The *Juno* Waves experiment measures AC electric fields between frequencies of 50 Hz and >40 MHz, not only detecting radio emissions along much of the orbit but also directly measuring the electric fields in high latitude regions where these emissions are thought to be generated (further detailed in Kurth et al. 2014, this issue). These measurements allow us to study the microphysics of the radio sources in situ, as done at Saturn with Cassini (Lamy et al. 2010; Mutel et al. 2010). But the Waves experiment will also detect the Jovian radio emissions along much of the orbit. Modeling the time-frequency morphology of these emissions has proved to provide efficient remote sensing of their source region (Hess et al. 2008a,

2008b, 2010a, 2010b). Although DAM emissions are not detected above 40 MHz by a near-equatorial observer, today's magnetic field models permit an emission at slightly higher frequencies, that could be beamed only toward high latitudes. *Juno* will settle this question.

Just as Fig. 25 shows an Earth auroral image taken by Polar while FAST gathered in situ data, the *Juno* UVS, JIRAM and *Juno*Cam instruments image the Jovian aurora in UV, IR and visible wavelengths while *Juno*'s in situ detectors measure the local particles and fields. The cadence of the remote sensing data is largely dictated by the 30 second spin period of the spacecraft. As with FAST, it is key to arrange the *Juno* data sets together to allow identification of the types of auroral regions from combined plots such as shown in Fig. 25.

3.2 Synchrotron/Radiation Belts

The radio emissions at decimeter wavelengths (DIM, see Fig. 19) are known to be synchrotron emission from energetic (∼MeV) electrons that are trapped in Jupiter's strong magnetic field within a few Jovian radii (see reviews by Carr et al. 1983; Bolton et al. 2004). Spacecraft traversals of the Jovian magnetosphere have also measured strong fluxes of energetic particles much farther from Jupiter in an outer radiation region (6–20 R_J) is be discussed in Sect. 3.3 below.

Figure 26 presents synthetic images of Jupiter's inner radiation belts obtained via remote sensing of electromagnetic radiation via high frequency (DIM) radio emission and models of electron fluxes based on these emissions plus a few in situ measurements obtained when Pioneer 11 and Galileo passed through this region. Note that Fig. 26A shows a ground-based observations intensity at 1400 MHz made at the Very Large Array (VLA) and shows emission from particles at both the magnetic equator as well as at high latitudes. Figure 26B shows linear polarization recorded by the *Cassini* spacecraft (when it flew past Jupiter in 2000), and only shows emission from the particles concentrated at the equator. Santos-Costa et al. (2008) show less than factor of ∼2 variation in total radio flux between 1962 and 2002. The bottom of Fig. 26 shows a sketch of the processes that affect the radiation belt particles as they diffuse inwards toward Jupiter, interact with moons and dust, and lose energy via radiating synchrotron emission (Santos-Costa and Bourdarie 2001; Santos-Costa and Bolton 2008).

Synchrotron emission from Jupiter's inner radiation belt is a foreground "noise" source for microwave observations of the atmosphere, but also provides valuable information about the distribution of high-energy electrons trapped in Jupiter's inner magnetosphere. Ground-based measurements have been used to adjust models of the radiation belts (Garrett et al. 2005), but the spatial resolution is limited. Furthermore, synchrotron emission is beamed in the direction of electron motion, which is inextricably linked to the Jovian magnetic field, and the strength of synchrotron emission is dependent on both the energy of the electrons and the strength of the magnetic field. From Earth, we can only observe Jupiter from a limited range of angles, all within ∼10 degrees of the magnetic equator. As an electron spirals up and down the magnetic field, it spends most of its time near the "mirror point", where it reverses direction with a pitch angle of 90 degrees. The synchrotron emission taps the perpendicular energy of the electrons and the bulk of the Jovian synchrotron emission seen from Earth comes from electrons mirroring on magnetic field lines that are perpendicular to the line of sight. Thus, information about the energy distribution of the electrons is entangled with information about their pitch-angle distribution, and complicated by the structure of Jupiter's magnetic field. The MWR on *Juno* (Janssen et al. 2014, this issue) does not suffer from this limitation.

With each spin of the spacecraft, MWR observes the synchrotron emission at each of six frequencies, over a wide range of angles, from a unique vantage point. Furthermore,

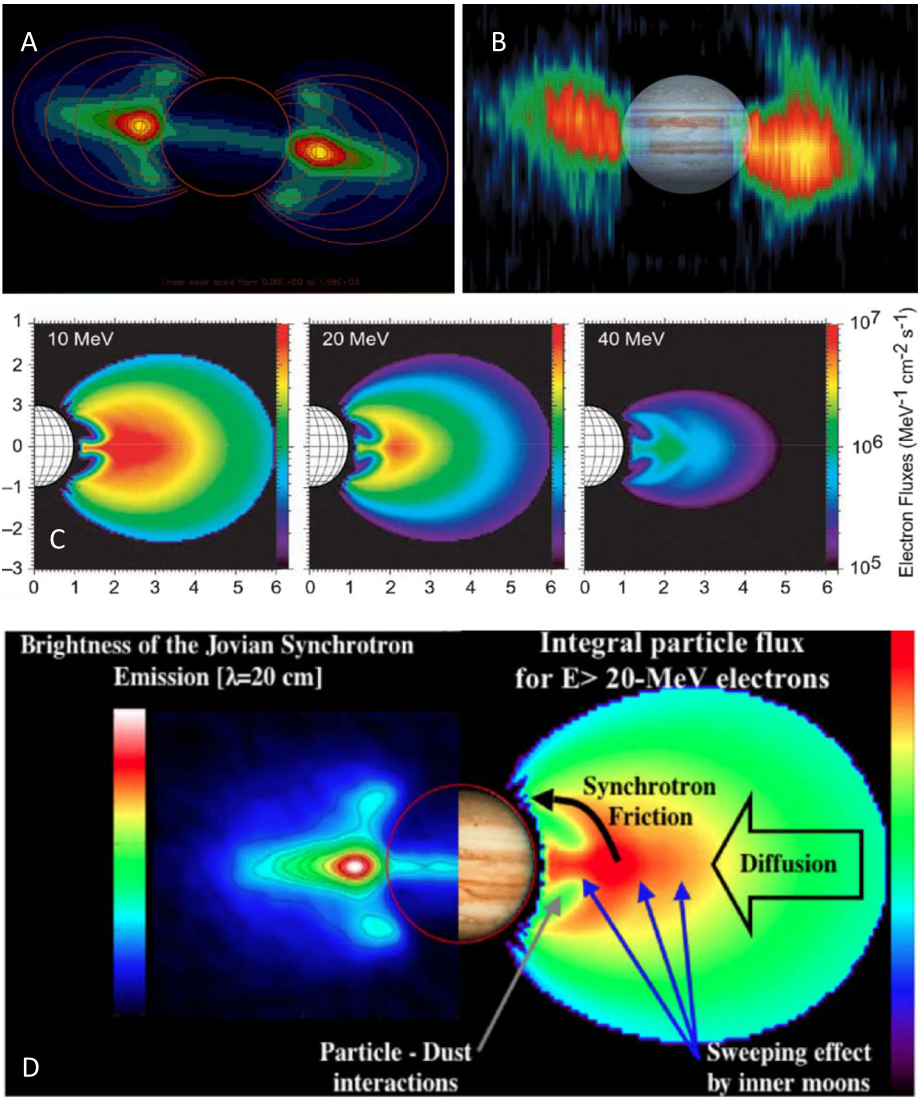

Fig. 26 Jupiter's synchrotron/radiation belts. *Top:* Images of radio emission at (**A**) 1400 MHz obtained by the VLA (total intensity); (**B**) 2.2 cm obtained by the *Cassini* spacecraft (horizontal linear polarization). From Bolton et al. (2004). *Middle:* Models of omni-directional differential electron fluxes in a meridian plane for three energies (from Bolton et al. 2004). *Bottom:* Schematic of electron transport, energization, and loss processes at Jupiter that contribute to the spatial and spectral characteristics of the synchrotron emissions from Jupiter's inner magnetosphere. From Santos-Costa and Bolton (2008)

the magnetometer experiment on *Juno* will be making a greatly improved map of the Jovian magnetic field (B). The different frequencies pick out different electron energies (ε) because the peak frequency of the synchrotron spectrum is proportional to $\varepsilon^2 B$. As shown in Fig. 26A, observations with the Very Large Array (VLA) show strong emission near the equator, implying a "pancake" distribution of electrons with equatorial pitch angle close to 90 degrees, plus high-latitude lobes which require a component with a more isotropic distri-

bution of pitch angles near $L = 2$. The relative absence of emission at intermediate latitudes adds complexity, requiring either a more complicated pitch-angle distribution or an energy distribution that depends on both pitch angle and L-shell. *Juno*'s trajectory takes it over the poles, and close to the planet at the equator, allowing both the high latitude and the equatorial regions to be observed at a wide range of angles with respect to the magnetic field, including both parallel and perpendicular to the field lines. Observations at multiple frequencies from this wide range of vantage points, combined with a precise map of the magnetic field, allows us to disentangle the energy and pitch angle distributions from the line-of-sight effects. This is because the source is optically thin, allowing tomographic reconstruction.

The JEDI instrument (Mauk et al. 2014, this issue) makes in situ measurements of the radiation belts, characterizing electron spectra up to 0.5 MeV. However, there is information about electron intensities at higher energies that is provided in two different forms. (1) JEDI includes "witness detectors" that reside within the FOV of JEDI that are covered with enough shielding to prevent <1 MeV electrons from hitting them. By comparing the response of these witness detectors to the identical detectors within the JEDI FOV that do not have the shielding, JEDI measures the integrated flux of >1 MeV electrons. (2) The overall shielding to the JEDI SSD detectors is sufficient to keep penetrating electrons with energies greater than a threshold value ($\sim$12 MeV) of electrons from reaching the detectors. This means that all of the solid-state detectors could be impacted by electrons with energy >12 MeV. Since both the >1 MeV and the >12 MeV electrons that reach the detectors also penetrate the detectors, modeling these responses should be able to provide a measure of the in situ fluxes of electrons in this energy range.

In addition to the inner electron radiation belts mentioned above, there is also an inner radiation belt of energetic protons. The source of these ions is likely the CRAND process (cosmic ray albedo neutron decay). Here cosmic rays impact Jupiter or its ring; the cosmic rays are able to liberate neutrons from material and these decay in a very short time. If this decay occurs close enough to the planet, the proton becomes trapped by the magnetic field. From studying the proton radiation belts of Saturn, *Cassini* has clarified the pathway from cosmic rays to the intense proton belts. Roussos et al. (2011) correlated the protons in the Saturn belts with the solar cycle phase and suggest that during times of high solar activity, the cosmic rays are impeded from entering the solar system and the proton belts are weaker.

3.3 Plasma Sheet

The magnetosphere of Jupiter extends well beyond the orbits of the Galilean satellite system. These moons provide most of the plasma that forms a disk around the planet (see list of properties in Table 3 and reviews by Thomas et al. 2004; Khurana et al. 2004; Krupp et al. 2004). In particular, Io loses about one ton per second of atmospheric material (mostly SO_2 and dissociation products), which, when ionized to sulfur and oxygen ions, becomes trapped in Jupiter's magnetic field (Fig. 1D). Compared with the local plasma, which is nearly corotating with Jupiter at 74 km/s, the neutral atoms are moving slowly, close to Io's orbital speed of 17 km/s. When a neutral atom becomes ionized (largely via electron impact) it experiences an electric field, resulting in a gyromotion of 57 km/s. Thus, new S^+ and O^+ ions gain 540 eV and 270 eV in gyro-energy, respectively. The new "pick-up" ion is also accelerated up to the bulk speed of the surrounding plasma. The necessary momentum comes from the torus plasma, which is in turn coupled, via field-aligned currents, to Jupiter—the Jovian rotation being the ultimate source of momentum and energy for most processes in the magnetosphere. About one-third to one-half of the neutral atoms are ionized to produce additional fresh plasma while the rest are lost via reactions in which a neutral

Table 3 Flow of mass and energy through the magnetosphere of Jupiter[a]

	Magnetosphere of Jupiter
Mass of neutrals	~70 kton
Mass of plasma	1.5 Mton
Plasma production	260–1400 kg/s
Neutral production	600–2600 kg/s
Fast neutral loss	320–1740 kg/s
Plasmoid loss[b]	~30 kg/s
Solar wind flux[c]	230 ton/s
Total Kinetic Energy[d]	7.5×10^{18} J
Power: Kinetic Energy[d]	1.4–7.8 TW
Total Thermal Energy[e]	1×10^{18} J
Power: Plasma Thermal Energy[e]	0.3–1.4 TW
Total Energetic Ion Energy[f]	1.4×10^{19} J
Power: Energetic Ion Energy[f]	2.7–15 TW
Net Heating of Plasma Disk	3–16 TW
Power: Atmosphere/ionosphere[g]	~200–300 TW
Power: Solar Wind[h]	~200 TW
Power: UV Torus Emission	1.2–2.5 TW
Power: Aurora	200–800 GW
Power: Magnetotail Flows	1 TW
Power: Satellite Interaction	1 TW
Power: Satellite Aurora	6 GW

[a]From Bagenal and Delamere (2011)

[b]Based on estimate of one plasmoid per day, from Bagenal (2007)

[c]Flux of solar wind onto area of πR_T^2 where R_T is magnetopause distance at terminator (~150 R_J)

[d]Rotational kinetic energy of plasma. Power estimate assumes a range in time scales of 11–60 days

[e]Total thermal energy of the plasma in plasma disk. Power estimate assumes a range in time scales of 11–60 days

[f]Total energy of the supra-thermal component of plasma in the plasma disk, from Mauk et al. (2004). Power estimate assumes a range in time scales of 11–60 days

[g]Power transferred from the thermosphere/ionosphere to the magnetosphere for models of Cowley et al. (2005) and of Yates et al. (2012)

[h]About 1 % of the kinetic energy flux of solar wind onto area of πR_T^2 where R_T is the magnetopause distance at terminator (~150 R_J)

atom exchanges an electron with a torus ion. When neutralized, the previously charged, corotating particle is no longer confined by the magnetic field and, since the corotation speed is well above the gravitational escape speed from Jupiter, flies off as an energetic neutral atom. This charge-exchange process adds gyro-energy to the ions and extracts momentum from the surrounding plasma, but it does not add more plasma to the system.

Strong centrifugal forces confine the plasma near the equator. Thus, the densest plasma forms a torus around Jupiter near the orbit of Io. A lighter population of H^+ ions (with a relative concentration of a few % and a temperature of a few 10 s eV), less confined near the equator, has been inferred from radio (DAM) measurements (Zarka et al. 2001b). The

Io plasma torus has a total mass of ∼2 megaton, which would be replenished by a source of ∼1 ton/s in ∼40 days. Multiplying by a typical energy ($T_i \approx 60$ eV, $T_e \approx 5$ eV) we obtain $\sim 6 \times 10^{17}$ J for the total thermal energy of the torus. The observed UV power is about 1.5 TW, emitted via more than 50 ion spectral lines, most of which are in the EUV. This emission would drain all the energy of the torus electrons in ∼7 hours. Ion pickup replenishes the energy, and Coulomb collisions feed the energy from ions to electrons, but not at a sufficient rate to maintain the observed emissions. A source of additional energy, perhaps mediated via plasma waves and/or Birkeland currents, seems to be supplying hot electrons and a comparable amount of energy as ion pickup. The ∼40 day time scale (equivalent to ∼100 rotations) for the replacement of the torus indicates surprisingly slow radial transport that maintains a relatively strong radial density gradient. Flux tubes laden with denser, cooler, plasma move outwards while relatively empty flux tubes containing hotter plasma from the outer magnetosphere move inwards—a process called flux tube interchange (reviewed in Thomas et al. 2004).

Voyager, *Galileo*, and, particularly, *Cassini* observations of UV emissions from the torus show temporal variability (by about a factor of a few) in torus properties (see review by Thomas et al. 2004 for earlier papers and more recent work with *Cassini* data by Steffl et al. 2004a, 2004b, 2006). Models of the physical chemistry of the torus match the observed properties in regard to the production of neutral O and S atoms, radial transport time, and source of hot electrons (Delamere and Bagenal 2003). A population of supra-thermal electrons is essential for producing both ionization states (the average ionization state of ions in the torus is between 1.6 and 1.9) and the terrawatts of UV emissions. Steffl et al. (2008) showed that a small (<1 %) hot electron population that varies with longitude and drifts by a few percent with respect to corotation could explain modulations in ionization state and emissions. This is supported by the subcorotating nKOM sources identified as plasma inhomogeneities in Io's torus (Reiner et al. 1993; Zarka 1998). Rotation dominates the plasma flows observed in the Jovian magnetosphere out to distances of ∼70 R_J. Yet, the presence of sulfur and oxygen ions in the middle magnetosphere, far from Io, indicates that plasma is transported outwards, transverse to the magnetic field. The net radial transport is thought to be slowest near Io's orbit (∼15 m/s) and to speed up farther out (∼50 m/s beyond 10 R_J). Plasma from the Io torus spreads out from Jupiter as a ∼5 R_J-thick plasma sheet throughout the magnetosphere.

Figure 27 shows an overview of conditions in the Jovian plasma sheet and Table 3 lists estimates of the mass, energy and flows of these quantities through the Jovian system. The distribution of plasma is based on *Voyager* and *Galileo* data, combined with simple models for the distribution of plasma along magnetic field lines (see discussion in Bagenal and Delamere 2011). The total plasma density (Fig. 27A) is fairly well measured in the Jovian plasma sheet by different instruments and has a profile that seems fairly constant (to a factor of ∼2) with time. On the other hand, the measurement of the temperature of the ions (Fig. 27B) is complicated by (a) the mixture of ions of O and S in a range of ionization states, dominated at the ∼80 % level by O^+ and S^{++} ions which both have a mass/charge ratio of 16 amu/e; (b) ion distributions with non-Maxwellian supra-thermal tails; and (c) plasma instruments with different upper limits to their measurement range in E/q (∼6 keV for *Voyager*, ∼50 keV for *Galileo*). For example, as illustrated in Fig. 27B, there are clearly times when the *Voyager* PLS instrument (data shown in black) measured pockets of plasma containing a cold population of ∼10 eV ions in the plasma sheet out to >40 R_J (Belcher 1983). At the same time, the *Galileo* PLS instrument (green data points) showed that, because of the high energy tail of the ion distribution, typical ion energies average from ∼200 eV at 10 R_J, up to 1000 eV beyond 20 R_J. The smooth curve of temperature in Fig. 27B is consistent with the latitudinal distribution of density measured as the plasma sheet flapped over

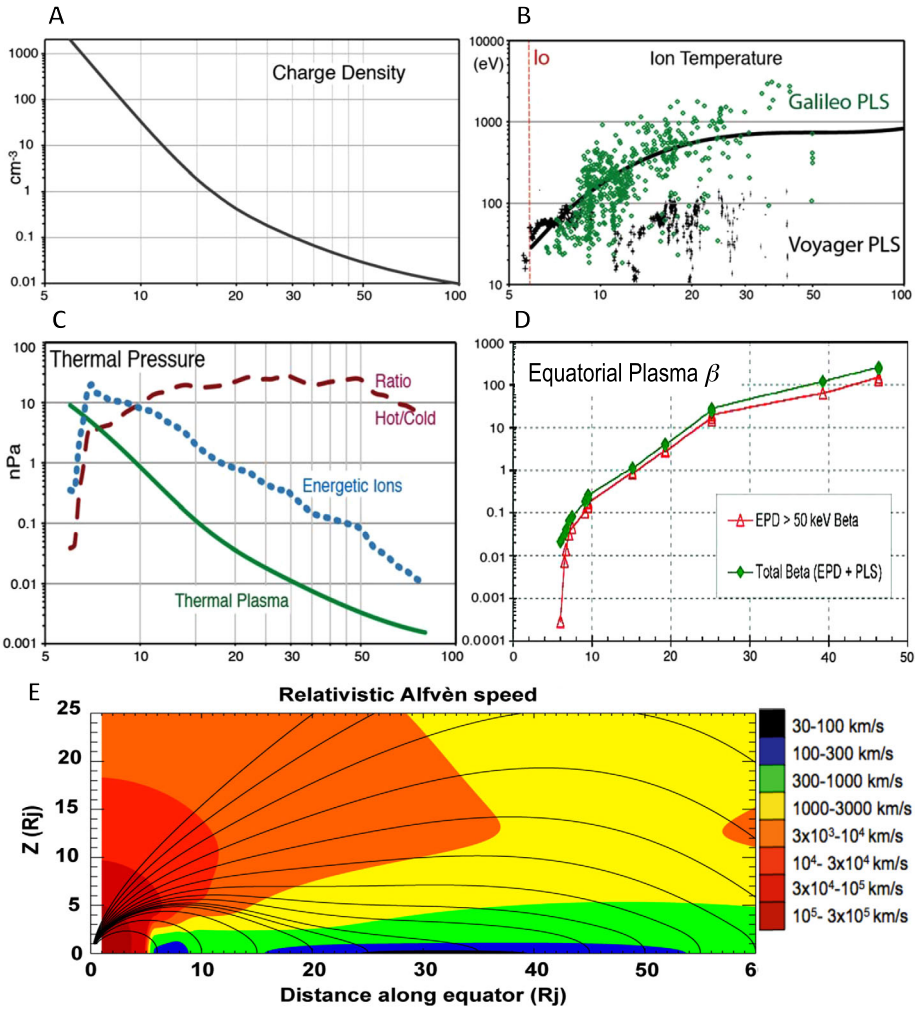

Fig. 27 Radial profiles along the equator of electron density (**A**), ion temperature (**B**), and particle pressure (**C**), based on *Galileo* and *Voyager* data (Bagenal and Delamere 2011). (**D**) shows the ratio of particle pressure to magnetic field pressure (plasma beta) from Mauk et al. (2004). (**E**) By combining mass density and the Connerney (1992) O_4^+-current sheet magnetic field model, a local Alfvén speed can be estimated

the spacecraft (see discussion in Bagenal and Delamere 2011). Considering the *Voyager* and *Galileo* plasma measurements together provides a picture of a dense central plasma sheet with ~100 eV heavy ions plus a less-confined supra-thermal >1 keV population (perhaps combining both protons and heavy ions) that increasingly dominates the plasma pressure at larger radial distances.

The important conclusion, however, is that as the plasma moves radially outwards through the plasma sheet, it heats up. This is contrary to expectations that the plasma would cool on expansion into a larger volume. The nature of the heating mechanism has remained a puzzle since the first *Pioneer* flybys of Jupiter in the 1970s (Dessler 1983). Figure 27C shows plasma pressure (directly proportional to energy density) as a function of distance

from Jupiter in the plasma sheet. The green line shows the thermal pressure of the bulk of the plasma (the thermal core of the ion distribution), the blue dotted curve shows the suprathermal population of ions (10s keV energies), while the dark red long-dashed line shows the ratio of these pressures. The pressure of the energetic ions dominates over the torus plasma except very close to the orbit of Io where the profile drops precipitously. This drop is due to the inward-diffusing energetic ions charge exchanging with the cloud of neutral particles that surround the orbit of Io and, to some extent, Europa. Apart from the region close to Io, the energetic particles not only dominate over the pressure of the thermal plasma but beyond about 15 R_J the ratio of particle pressure to the pressure of the magnetic field (characterized by the parameter β) is greater than unity, rising to over a hundred beyond 40 R_J. The consequence of this high-β plasma is the stretching of the plasma sheet (Sect. 2.3) and compressibility of the magnetosphere, as discussed in Sect. 2.2 above.

As noted by Northrop and Birmingham (1982), there is plenty of rotational energy in the atmosphere of Jupiter. Estimates of the power transferred from the thermosphere/ionosphere to the magnetosphere are on the order of 200–300 TW (Hill et al. 1983; Cowley et al. 2005; Yates et al. 2012). The issue is how to transfer the bulk motion of rotation into heating the plasma. Kivelson and Southwood (2005) proposed that the expansion of fluxtubes on the dusk side of Jupiter's magnetosphere could be sufficiently rapid to violate the second adiabatic invariant, leading to ion heating. Preliminary studies by Vogt et al. (2013) suggest this could be a viable mechanism.

Combining the plasma mass density with a magnetic field model, in this case the Connerney (1992) O6-plus-current sheet model, we get an estimate of the local Alfvén speed (Fig. 27E). Note that the speeds are quite slow in the plasma sheet (<300 km/s) but approach the speed of light off the magnetic equator, closer to the planet where the magnetic field is very strong and the density very low. Since Alfvén waves are how stresses are conveyed between the magnetospheric plasma and Jupiter's ionosphere, it is these high Alfvén speeds that make numerical models of the Jovian magnetosphere so demanding. At the same time, the very large scales of the Jovian magnetosphere produce large timescales for Alfvén waves to travel between the equator and ionosphere. For example, at 100 R_J the one-way Alfvén travel time is about 100 minutes, during which time Jupiter's ionosphere has rotated 60° and the plasma sheet has rotated about 30°. The Alfvén speed would be further decreased if, as Vogt et al. (2013) suggest, the ions develop high thermal anisotropy. Thus, as the plasma moves radially away from the planet we expect it to be increasingly de-coupled from the rotating ionosphere.

Table 3 lists quantities that illustrate the flow of mass and energy through the system. The distribution of mass for typical conditions in the plasma sheet is shown in Fig. 28. Variation in torus emissions observed over several months by *Cassini* reflect the observed changes in the output of Io's volcanic plumes of about a factor of 5 (between 600 kg/s and 2600 kg/s of neutral material). Note that these are sources of neutral material. Physical chemistry models matching the *Voyager* and *Cassini* data suggest that between 1/2 to 2/3 of this material is lost through charge exchange reactions as neutrals that escape the Jovian system. This means that only 1/3 to 1/2 of the neutral production rate (260 to 1400 kg/s) becomes plasma that is transported radially outwards through the plasma disk. Taking these values of plasma production/transport (≅) and the observed density profile, gives radial transport speeds of ∼50 to ∼200 km/s (Fig. 28B). The corresponding range in torus residence time varies inversely with the source strength, from 14 to 64 days (Delamere et al. 2004; Bagenal and Delamere 2011). This produces relatively minor (factor ∼2) variations in density with time.

The status of understanding of the structure and dynamics of the Jovian magnetosphere at the end of the *Galileo* mission are summarized by Khurana et al. (2004) and Krupp et al.

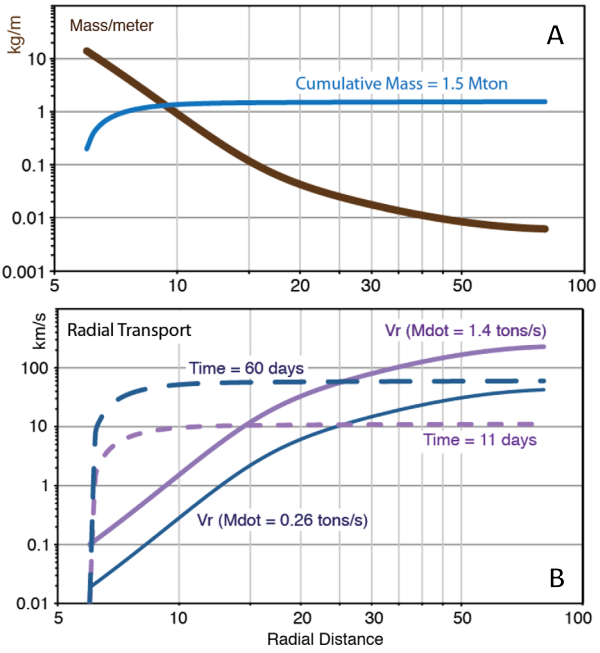

Fig. 28 Radial properties of the Jovian plasma disk. (**A**) Mass per unit radial distance outwards through the disk and cumulative mass of the disk, based on the density and temperature profiles in Fig. 27. (**B**) Radial transport speed and cumulative time for radial transport assuming high (1.4 tons/s) and low (0.26 tons/s) rates of mass production and transport (From Bagenal and Delamere 2011)

(2004) respectively. More recent studies can be categorized as those which concentrate on the structure of the magnetodisk with simplified assumptions about the coupling to the thermosphere/ionosphere (Nichols and Cowley 2004, 2005; Cowley et al. 2005, 2007; Nichols 2011), vs. models which simplify the magnetospheric structure and concentrate on the thermosphere-ionosphere structure and dynamics (Smith and Aylward 2009; Tao et al. 2009; Yates et al. 2012). Figure 29 provides an example, from Nichols (2011), of the magnetic field and current sheet structures for a steady-state axisymmetric model. They assume the plasma sheet content has a constant value of 8×10^{21} ions per Weber for three values of the quantity $(\Sigma_P^*/\cong)$ where Σ_P^* is the effective conductivity of the ionosphere and $\cong$ is the mass flux through the plasma sheet.

Estimates of the potential power supply from the thermosphere/ionosphere to the magnetosphere for the model of Cowley et al. (2005) are about 200 to 300 TW (Table 3). Yates et al. (2012) find similar numbers with a similar model with more sophisticated treatment of the atmosphere/ionosphere. Studies by Ergun et al. (2009) and Ray et al. (2010, 2012, 2014) point out that the lack of plasma between the plasma sheet and the ionosphere leads to small-scale regions of parallel electric fields ("double-layers") a few R_J above the ionosphere. They argue that the linear approximation to Knight's current-voltage relation (Knight 1973), commonly assumed for ionosphere-magnetosphere coupling, breaks down and that the currents flowing between the two regions become saturated, modifying the coupling between the magnetosphere and ionosphere. There is clearly plenty of energy in the atmosphere/ionosphere to both accelerate and heat the Jovian plasma sheet (see power estimates in Table 3). The outstanding questions of the dynamics of the Jovian plasma sheet are (a) what specific processes control the momentum transfer from the planet to the magnetosphere—as well as how/when these processes fail to transfer momentum—and (b) how processes convert rotational momentum into heat in the plasma sheet. Vasyliūnas (1994) developed a general description of how the magnetospheric plasma will decouple

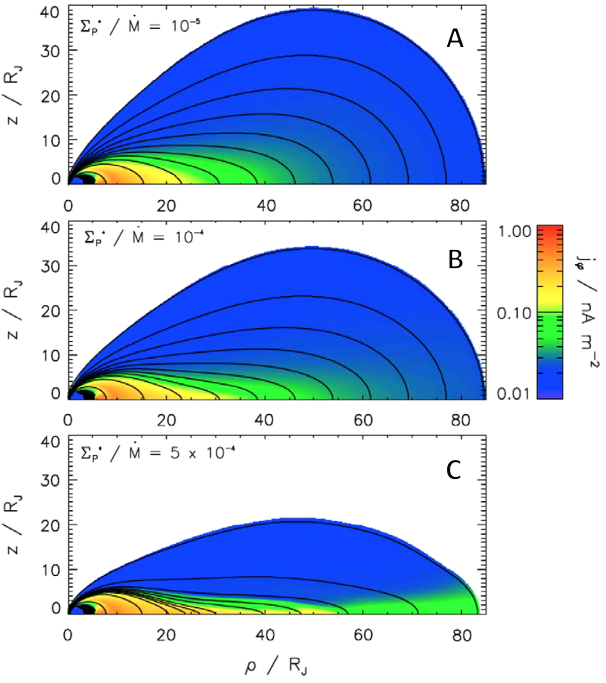

Fig. 29 Magnetic field and current sheet structures computed using three values of the quantity (Σ_P^*/M), (**A**) 10^{-5}, (**B**) 10^{-4}, and (**C**) 5×10^{-4} mho s kg^{-1}. The *black lines* indicate magnetic field lines, and the *colors* indicate the density j_ψ (in nA m^{-2}). From Nichols (2011)

from the ionosphere where the acceleration time (in its simplest form proportional to the ionospheric Pedersen conductivity times the magnetic field divided by the flux tube content) becomes comparable to or exceeds the radial out flow time scale. This is a generalization of Hill (1979)'s inertial limit to corotation. But, as we have mentioned above, the complicating factors of finite Alfvén travel time between the plasma disk and the ionosphere, plus the possibility of double-layers and current saturation, leaves the question of what controls the de-coupling of the magnetosphere from the ionosphere poorly determined.

A major scientific goal of the *Juno* mission is to explore the key high latitude regions for the first time as well as make multiple traversals of the plasma sheet to quantify the conditions and discriminate between different theories of how the magnetosphere couples the planet's angular momentum to the plasma sheet. The trajectories shown in Figs. 12 and 13 illustrate that *Juno* traverses the plasma sheet many times during the outer sections of the science orbits, making many passes through the region on the left-hand half of the plots in Fig. 27. The JADE instrument makes extensive measurements (density, temperature, flows, composition) in the energy range of ~0.1 to 100 keV for electrons and ~0.005 to ~50 keV for ions; electron pitch angle distributions can be returned as rapidly as a 1 s cadence and complete ion measurements are made over the 30s spacecraft rotation (for details see McComas et al. 2014a, this issue). At the same time, the JEDI detectors measure the 10 s–100 s keV ions and electrons (for details see Mauk et al. 2014, this issue). The MAG instrument provides measurements of the magnetic field, both the internal field and perturbations due to currents flowing in the plasma sheet, and also derive an estimate of the coupling currents between the planet and the magnetosphere. The Waves instrument provides measurements of plasma waves that could be heating the plasma as well as an estimate of the total electron density. For specific plasma sheet crossings selected by the MWG, Waves will increase its cadence from the nominal 1 spectrum per 30 seconds

to one per 10 seconds. Presently, no burst data are planned for these, but such observations are possible if deemed to be important. These combined particles and fields measurements allows us to characterize the plasma properties and their variations with radial distance, latitude and longitude. Over the ~12 months that *Juno* is in the Jupiter system we will improve the estimates of mass and energy flow through the system (e.g. the quantities in Table 3) as well as describe any variations with time due to either volcanic output of Io or solar wind disturbances passing the Jovian magnetosphere. We will also monitor the location of the main emissions and the Ganymede footprint, since they also vary as a function of the mass outflow rate and the plasma sheet density (Grodent et al. 2008; Bonfond et al. 2012).

Furthermore, key for our understanding of atmosphere-ionosphere-magnetosphere coupling is the region of low plasma density between the plasma sheet and ionosphere (Fig. 13). *Juno* makes in situ measurements of the thermal plasma (JADE) and energetic particle populations (JEDI) as well as detect perturbations in the electric (Waves) and magnetic (MAG) fields in these regions where, if experience at Earth applies, we expect to see potential structures—transient or steady-state—as illustrated in Figs. 20, 23 and 24.

3.4 Outer Magnetospheric Dynamics

As plasma moves radially outwards in the plasma sheet, the coupling to the rotating ionosphere weakens, and the influence of the solar wind increases. Beyond about 50 R_J the radial outflow becomes comparable to the azimuthal (rotational) speed and the plasma spirals outwards (see Fig. 2). The high-beta plasma sheet (Fig. 27D) is very compressible as manifested by the observed weaker power law dependence of the magnetopause standoff distance on solar wind ram pressure (nominally, $R_{MP} \propto (\rho V^2)_{sw}^{-1/4.5}$) than the $-1/6$ power law that one expects for a magnetic dipole alone (discussed in Sect. 1.2 above). On the dayside of the magnetosphere the ram pressure of the solar wind compresses the magnetosphere. Inward motion on the dawn side reduces the load on the ionosphere, producing a correspondingly dark region in the dawn polar aurora (Fig. 21A). On the dusk side the plasma expands outwards and strong currents try to keep the magnetospheric plasma corotating. These strong currents produce the active dusk polar aurora. Kivelson and Southwood (2005) argued that the rapid expansion of flux tubes in the afternoon to dusk sector means that the second adiabatic invariant is not conserved, which results in the heating and thickening of the plasma sheet (Vogt et al. 2013).

As pointed out in his seminal article (in which the dynamics of the outer magnetosphere was first addressed in a substantial fashion) Vasyliūnas (1983) argued that at some point centrifugal forces take over from rotational coupling to the planet, stretching out the plasma sheet and magnetic field to the point where the plasma disconnects from the planet as blobs of plasma—plasmoids—that are ejected down the tail. Vasyliūnas (1983) presented a sketch of magnetospheric structure that looks similar to the left hand of Fig. 2 except that the line of plasmoid disconnections—the x-line—is tilted away from the Sun on the dawn side rather than sunward. Analysis of plasma and magnetic field data led several authors to conclude that the x-line is sporadic and is tilted sunward on the dawnside (Woch et al. 2002; Kronberg et al. 2005, 2008; Vogt et al. 2010; Ge et al. 2010; Kasahara et al. 2013). The flow lines in the outer magnetosphere shown in Fig. 2A were calculated by combining an empirically-derived azimuthally symmetric spiral (roughly equal rotation and outward transport), with anti-solar stresses associated with coupling of the solar wind (via small-scale, intermittent reconnection at the magnetopause boundary layer) to the magnetosphere (Delamere and Bagenal 2010, 2013). Alternative views (e.g. Cowley et al.

2007; Kivelson and Southwood 2005; Badman and Cowley 2007) combine the Vasyliūnas rotationally-driven ejection of plasmoids with a cycle of large-scale opening reconnection on the dayside and closing reconnection (entraining flux from the lobes) in the tail driving magnetospheric convection, as first proposed for the Earth by Dungey (1961). One problem with invoking a substantial role for a Dungey-style reconnection-driven convection system is that there is very little evidence of much dayside reconnection, making the Dungey reconnection potential small compared with the planetary corotation potential (Walker and Russell 1985; Badman and Cowley 2007). While the involvement of lobe reconnection remains debated, the presence in the post-midnight local time sector of an x-line (likely variable in both time and space) is generally accepted, with plasmoids ejected tailward and sun-ward, depolarizing flows on the Jupiter side of the x-line. For the foreseeable future the dusk side of the Jovian magnetotail remains terra incognita and, unfortunately, will not be explored by Juno.

Pursuing evidence for Vasyliūnas' argument that plasmoids are ejected down the Jovian magnetotail, Grodent et al. (2003b, 2004) found spots of auroral emission poleward of the main aurora connected to the nightside magnetosphere that lasted for a few 10s of minutes. Such events appear to recur every 2 to 3 days (Radioti et al. 2008). These flashes seemed to occur from the dusk sector to the dawn sector, and they are probably coupled to a region of the magnetotail that was about 5 R_J to 50 R_J across and located further than 100 R_J down the tail (Grodent et al. 2004, Radioti et al. 2010, 2011). Studies of in situ measurements (Russell et al. 2000; Woch et al. 2002; Kronberg et al. 2005; Vogt et al. 2010; Ge et al. 2010; Kasahara et al. 2013) led to the conclusion that plasmoids on the order of $\sim$25 R_J in scale were being ejected every 4 hours to 3 days, with a predominance for the post-midnight sector at distances of 70 R_J to 120 R_J. Using radio signatures, it was shown that global perturbations affect the whole disk, from Io torus to 100–120 R_J, on time scale of a few hours and quasi-periodic variations of 3–10 days (Louarn et al. 1998). Interestingly, these major disturbances are closely related to phases of thickening/thinning of the disk and, thus, likely to sequence of plasma loading/unloading of the disk (Louarn et al. 2000, 2001).

Could such plasmoids account for most of the plasma loss down the magnetotail? Bagenal (2007) approximated a plasmoid as a disk of plasma sheet 2 R_J thick having diameter 25 R_J and density of 0.01 cm^{-3}, so that each plasmoid has a mass of about 500 ton. Ejecting one such plasmoid per day is equivalent to losing 0.006 ton/s. Increasing the frequency to once per hour raises the loss rate to 0.15 ton/s. Thus, on the one hand, even with optimistic numbers the loss of plasma from the magnetosphere due to such plasmoid ejections cannot match the canonical plasma production rate of 0.5 ton/s. On the other hand, a steady flow of plasma of density 0.01 cm^{-3}, in a conduit that is 5 R_J thick and 100 R_J wide, moving at a speed of 200 km/s would provide a loss of 0.5 ton/s. Such numbers suggest that a quasi-steady loss rate is feasible. The question of the mechanism remains unanswered. Bagenal (2007) proposes a diffusive "drizzle" across weak, highly stretched, magnetotail fields, or perhaps a quasi-steady reconnection of small plasmoids, below the scale detectable via auroral emissions and limited spacecraft measurements.

In the spring of 2007 the *New Horizons* spacecraft flew past Jupiter, getting a gravitational boost on its way to Pluto, and made an unprecedented passage down the core of the Jovian magnetotail, exiting on the northern dusk flank. For over three months, while covering a distance of 2000 R_J, the spacecraft measured a combination of iogenic ions and ionospheric plasma (indicated by H^+ and H^{3+} ions) flowing down the tail (McComas et al. 2007; McNutt et al. 2007). The fluxes of both thermal and energetic particles were highly variable on time scales of minutes to days. The tailward fluxes of internally generated plasma led McComas and Bagenal (2007) to argue that perhaps Jupiter does not have a complete Dungey cycle but that the large time scale for any reconnection flow suggests that magnetic flux

that is opened near the sub-solar magnetopause re-closes on the magnetopause before it has traveled very far down the tail. They suggested that the magnetotail comprises a pipe of internally generated plasma that disconnects from the planetary field and flows away from Jupiter in intermittent surges or bubbles, with little or no planetward Dungey return flow. Cowley et al. (2008a) argue otherwise (see also McComas and Bagenal (2008) response). At issue is not so much "Vasyliūnas vs. Dungey" cycles (Cowley et al. (2003) showed they are not incompatible), but rather how much steady-state reconnection opens flux on the dayside, how much open (lobe) flux is closed within the magnetotail, and whether there is significant sunward flow driven by this flux closure.

While the magnetosphere of Saturn is much smaller than that of Jupiter and there is stronger evidence of the solar wind influencing magnetospheric dynamics (see reviews by Zarka 1998; Gombosi et al. 2009; Mitchell et al. 2009; Kurth et al. 2009; Mauk et al. 2009), the substantial data gathered by the *Cassini* spacecraft in the Saturn system have stimulated ideas about processes at Jupiter. Specifically, observations as the *Cassini* spacecraft traversed the boundary regions of the dayside magnetopause suggest that velocity shears drive Kelvin-Helmholtz instabilities (KHI), as first proposed based on *Voyager* data by Goertz (1983), substantiated by Galopeau et al. (1995) and further pursued with *Cassini* data by Masters et al. (2009, 2010, 2011a, 2011b, 2012), and Delamere et al. (2011, 2013). Such observations are consistent with large-scale reconnection being suppressed due to higher Alfvén Mach number of the incoming solar wind in the outer heliosphere compared with Earth at 1 AU (though see also Grocott et al. 2009), and a large change in plasma beta across the magnetopauses of Jupiter and Saturn (Masters et al. 2012; Desroche et al. 2012, 2013).

Delamere and Bagenal (2010) argue that, due to such KHI—effectively viscous processes—on the magnetopause boundary, there is a substantial mixing of solar wind plasma and magnetospheric plasmas. Simple estimates (Table 3) show that it is possible to lose much of the iogenic ∼ton/sec of plasma across the magnetopause on the flanks of the magnetosphere and that an equivalent amount of wind plasma (primarily protons with a few percent alpha particles) could enter and mix with the iogenic plasma (primarily sulfur and oxygen ions). The transfer of momentum from the solar wind to the magnetospheric plasma through such viscous processes would slow down the magnetosheath plasma, draping the interplanetary magnetic field (IMF) around the magnetotail. Desroche et al. (2012) shows that if the magnetosphere of Jupiter is flattened due to the extended equatorial plasma disk, then the IMF is carried over the polar regions and draped vertically on the sides, enhancing KHI activity on the flanks. Note that with the exchange of plasma across the magnetopause boundary layer there will also be concomitant exchange of magnetic flux. It is this penetration of the IMF that allows the transfer of stresses, mass-loading the solar wind and accelerating magnetospheric plasma down the tail (Delamere and Bagenal 2013).

In reality, we have very little information about the polar regions of Jupiter's magnetosphere and the sketch on the right of Fig. 2 is guesswork. In particular, a primary issue is how large, if at all, is the polar cap region where magnetic flux tubes are connected to the planet on one end and extend out into the solar wind. Some argue that the magnetosphere is nearly closed (McComas and Bagenal 2007) while others suggest there is a substantial and changing polar cap (Vogt et al. 2010). Studies of the aurora plus conditions in the upstream solar wind suggest a relatively modest (∼15–20 GWb/day or 17–23 kV) rate of flux opening and closing (Nichols et al. 2006).

While *Juno*'s orbits are limited in their coverage of local time (largely confined to dusk at perijove and dawn at apojove), they take the spacecraft over the polar regions where the particles and fields instruments are gathering a wide range of data that will be tested against

the ideas discussed above for the dynamics of the outer magnetosphere. Since this is the first time measurements are made in these regions, the approach is to keep the operations simple for observation of any eventuality. A major opportunity for *Juno* to explore the dynamics of the outer magnetosphere is on approach to Jupiter and during the capture orbit (Fig. 6) when the spacecraft spends several months in the dawn flank of the magnetosphere and is expected to make many crossings of the magnetopause and bow shock as the fluctuating solar wind buffets the compressible magnetosphere (Sect. 2.2, Fig. 9). During the science orbits, while remaining within 38 R_J of Jupiter, the spacecraft crosses magnetic field lines that connect to the outer magnetosphere (Fig. 15). The absence of energetic electrons has often been used as an indicator of whether such field lines have recently been—or continue to be—open to the solar wind (Goertz et al. 1976; Krimigis et al. 1979; Krupp et al. 2004; Delamere and Bagenal 2010). Finally, as *Juno* flies over the poles it looks down on the polar aurora (Figs. 14, 18) and observes polar emissions in UV, IR and optical wavelengths. While Fig. 18 illustrates that *Juno* will probably rarely be connected to the very magnetic field lines in the locations of these small-scale, transient polar emissions, the chances are reasonable that over the whole mission *Juno* will pass several times through a few such polar auroral structures and may be able to map out, in a statistical sense at least, the environment above the planet that maps to the distant, dynamic regions of the outer magnetosphere.

4 Earth Flyby

The original launch by an Atlas V rocket on August 5, 2011 was not able to carry the *Juno* spacecraft directly out to Jupiter. Consequently, on October 9, 2013 *Juno* returned to the Earth and made a close flyby in order to gain sufficient additional velocity to carry the spacecraft to the orbit of Jupiter. Several of the science instruments operated during the flyby, and the *Juno* mission took advantage of this flyby to simulate operations on the spacecraft. For example, *Juno* was programed to make similar changes in the instrument data rate as those that are used during subsequent perijove passes once *Juno* is inserted into orbit around Jupiter. Other Earth-orbiting spacecraft operated during the time of the flyby, and coordinated measurements made, which will enable calibration of the *Juno* instruments.

The orbit of *Juno* mapped onto the surface of the Earth is shown in panel A Fig. 30. Closest approach occured on the nightside around 19:22 UT at an altitude of 559 km. The orbit of *Juno* through the Earth's magnetosphere, shown in panels B and C, approached the Earth in the early afternoon local time sector and passed through the nominal magnetopause just before 18:00 UT. *Juno* only spent about 4 hours within the Earth's magnetosphere before exiting on the dawn side on its way to Jupiter.

During the flyby *Juno* passed directly through the most intense regions of the Earth's radiation belts, offering a unique opportunity to test the sensitivity of some of the *Juno* instruments (especially UVS, JIRAM, the star trackers cameras) to energetic penetrating particles. The passage through the energetic electron belts is illustrated in Fig. 31, based on the AE8 statistical model for electrons with $E > 3$ MeV. The most intense relativistic electron flux is found in the outer radiation belts near $L \sim 4$. *Juno* passed through the outer belt on both the inbound and outbound orbits. However, the flux of energetic electrons in the outer radiation belt can vary by up to three orders of magnitude over timescales less than a day, so the model distributions shown in Fig. 29 are substantially larger than those present at the time of the flyby. Two Earth-orbiting *Van Allen Probes* (Fig. 32) made observations of the radiation environment during the time of the *Juno* flyby and we coordinated the measurements made with the Relativistic Electron and Proton Telescope (REPT) with simultaneous observations

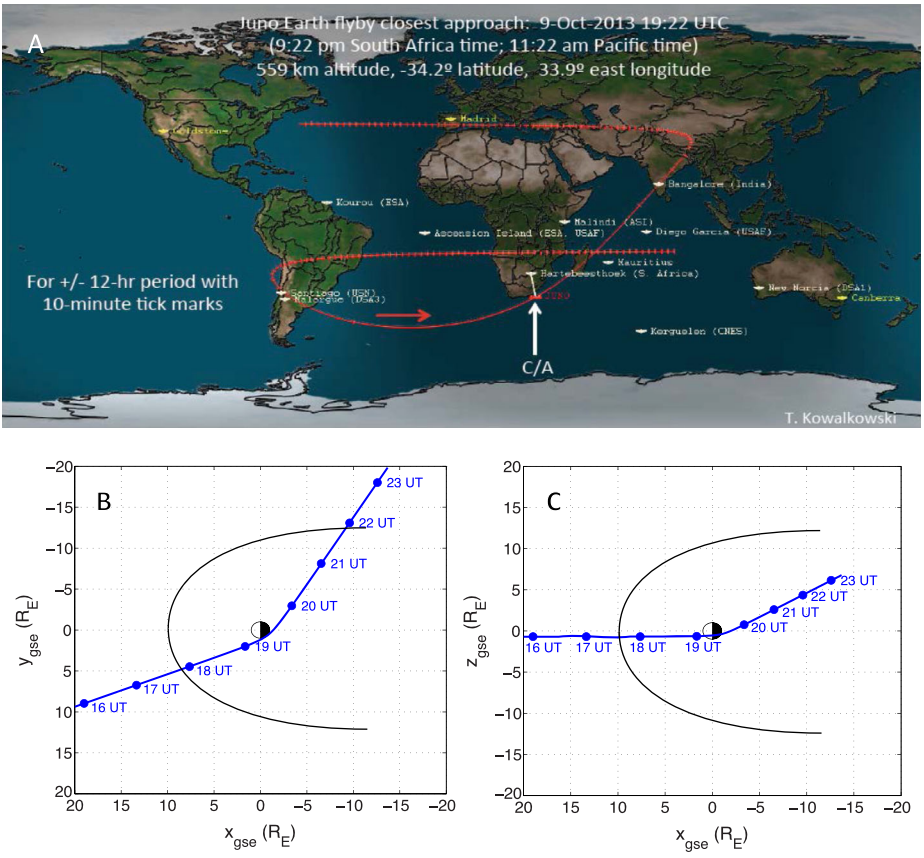

Fig. 30 Juno flyby of Earth on October 9, 2013. *Top:* The orbit of *Juno* projected onto the Earth within plus or minus 12 hours of closest approach. Bottom: The orbit of *Juno* with markers each hour in Earth solar-ecliptic (GSE) coordinates during passage through the Earth's magnetosphere, in (**B**) the $X-Y$ plane and (**C**) the $X-Z$ plane. A nominal average magnetopause boundary with a sub-solar distance of 10 R_E is shownto illustrate the brief time spent within the magnetosphere

of penetrating particles on *Juno*. The lower energy MagEIS instrument on each of the Van Allen Probes covers a similar range as the JEDI instrument on *Juno*, so we intend to use the coordinated observations to calibrate JEDI. *Juno* also passed through the inner electron radiation belt and the more intense energetic (>30 MeV) ion belt near $L \sim 1.5$ soon after closest approach. This offered an opportunity to test the sensitivity of various *Juno* instrument to energetic penetrating ions, which are simultaneously measured by the REPT and RPS instruments on the *Van Allen Probes*.

In addition to coordinated observations on the two *Van Allen Probes*, there are several other spacecraft that were operational during the time of the flyby, including three *THEMIS* spacecraft and the four *Cluster* spacecraft. These spacecraft are all equipped with instruments similar to the particles and fields instruments on *Juno*, and *Juno* makes measurements and performs additional instrument cross-calibration during the flyby. During October 2013 the main science targets of these missions are related to the magnetotail (*THEMIS*) and both the magnetotail and the auroral acceleration regions (*Cluster*) due to the respective spacecraft geometries during this epoch. In addition to the spacecraft measurements discussed

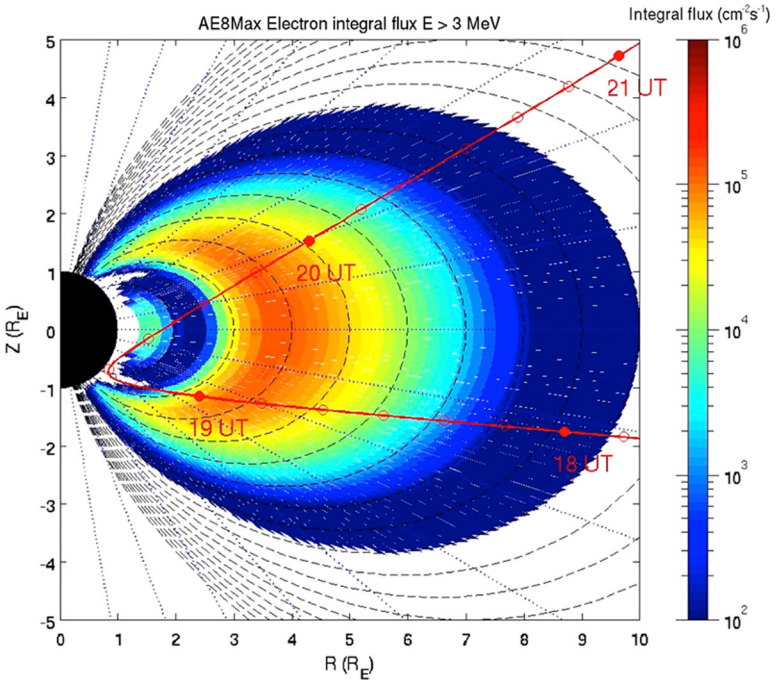

Fig. 31 The orbit of Juno through the Earth's energetic electron radiation belts (with time markers every 10 minutes) shown in Earth magnetic (GSM) coordinates using the AE8 radiation model

above, ground-based facilities such as EISCAT/Millstone Hill and the SuperDARN global network of high latitude HF radars (located in both the northern and southern hemisphere) were also operating. This radar network provides global-scale observations across the polar ionosphere, and as such offers a global picture of magnetospheric dynamics.

Once in the magnetosphere, *Juno* was on magnetic field lines that map into the SuperDARN network's field of view in both hemispheres, while the *THEMIS* and *Cluster* spacecraft were situated in the magnetotail/inner magnetosphere. Science opportunities on the inbound portion of the *Juno* trajectory include observations of dayside processes e.g. reconnection/flux transfer events. The SuperDARN observations of the ionospheric flows during this interval determine the global electric field and global reconnection rate.

5 Conclusions

Juno is the first spacecraft to fly over the polar regions of Jupiter's magnetosphere. The spacecraft trajectory and instrument complement make *Juno* an excellent mission to tackle the key issues of the Jovian aurora (spatial and temporal structure, generation processes, relationship to magnetospheric processes), the synchrotron radiation belt (spatial and temporal structure, source and loss processes) and plasma sheet (spatial and temporal structure, relationship to aurora, particle acceleration processes). Moreover, the approach and capture orbit provide valuable opportunities for *Juno* to quantify the solar wind interaction with boundary layers on the dawn side. Finally, the gravity assist flyby of Earth in October 2013 provided an opportunity to test some of the *Juno* instruments in the Earth's magnetosphere

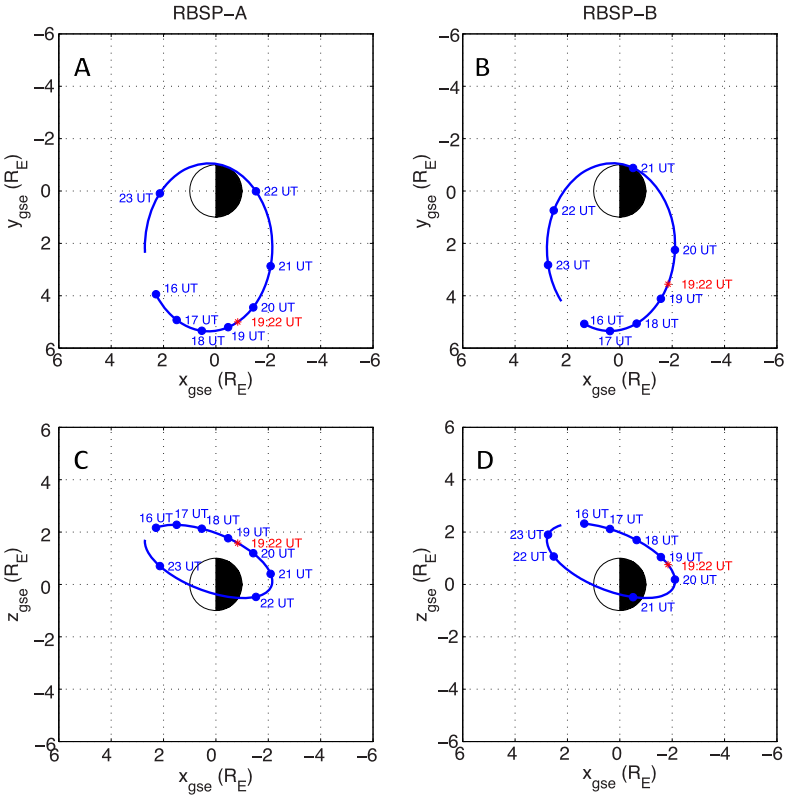

Fig. 32 The orbits of the two *Van Allen Probes* within ±3 hours of closest approach of the *Juno* spacecraft to the Earth (at the time shown in *red*). (**A**) and (**B**) are looking down on the ecliptic plane. (**C**) and (**D**) are looking from the dusk terminator

as well as compare *Juno* observations with those taken from the ground and many spacecraft in Earth orbit.

Acknowledgements We acknowledge all the outstanding contributions from the many people who made the *Juno* mission a reality. We thank Philippe Louarn (IRAP, Toulouse, France) for assistance and Tom Stallard (University of Leicester) for the IR image in Fig. 17. FB would like to thank Steve Bartlett for making several of the graphics, Sarah Vines (SWRI) for proofing, plus others at the University of Colorado for their help with producing materials: Laura Brower, Emma Bunnell, Dinesh Costlow, Frank Crary, Adam Shinn, Christopher Fowler, Drake Ranquist, Andrew Sturner and Rob Wilson. Further information and plots for *Juno* orbits can be found at http://lasp.colorado.edu/mop/resources/juno/.

Appendix: Jovian Magnetospheric Coordinate Systems

Below we describe the five main coordinate systems of potential use by the *Juno* MWG. But first we need to clarify the fiducial value of the radius of Jupiter. Dessler (1983) declared use of the value $R_J = 71400$ km in the appendix of *Physics of the Jovian Magnetosphere*. A full description of the planetary parameters and coordinate systems is provided in Appendix 2 of *Jupiter: Planet, Satellites, Magnetosphere* (Bagenal et al. 2004) where the equatorial radius at the 1-bar level is given as $R_J = 71492 \pm 4$ km (Lindal et al. 1981). The JPL navigation

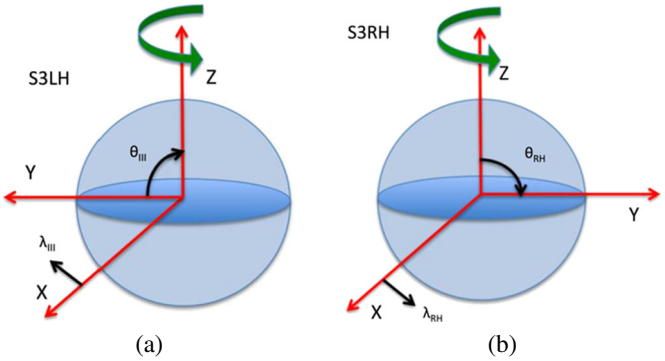

Fig. 33 (**a**) Jupiter System III (1965) coordinates (S3LH). The Z-axis is defined by the spin axis of Jupiter. The X-axis is defined by 0° latitude on the System III longitude $\lambda_{III} = 0°$ (prime meridian). The Y-axis completes the orthogonal left handed system. Latitude (θ_{III}) is defined from the equator. $\mathbf{X} = 0°$ latitude, Prime Meridian, $\mathbf{Y} = \mathbf{X} \times \mathbf{Z}$, $\mathbf{Z}$ = Jupiter spin axis. (**b**) Right-handed System III. This coordinate system has the same basis as the left-handed System III except that longitude is (λ_{RH}) decreases with time and co-latitude (θ_{RH}) is used. $\mathbf{X} = 90°$ colatitude, Prime Meridian, $\mathbf{Y} = \mathbf{Z} \times \mathbf{X}$, $\mathbf{Z}$ = Jupiter spin axis

team that provides *Juno* trajectory information uses $R_J = 71492$ km, the value we propose for all Juno MWG activities throughout the mission. Note that because of the rapid rotation of the planet, the polar radius of Jupiter is much less (66854 km).

A.1 Jupiter System III (S3LH, S3RH)

This system rotates with the planet at the sidereal System III (1965) spin period of 9h 55m 29.711s = 9.92492 hours (or angular velocity of 1.76×10^{-4} rad/s = 870.536°/day). This spin period was originally based on ground-based radio observations and the longitude (λ_{III}) was defined to increase with time, as observed from Earth. The problem with this system is that it is a left-handed coordinate system (which we label S3LH). Since many prefer right-hand coordinate systems, we also define a RH system (S3RH) where the longitude ($\lambda_{RH} = 360° - \lambda_{III}$) decreases with time as viewed from Earth. These two variations on Jovian System III are shown in Fig. 33. The location of the Prime Meridian (the meridian plane in both systems and where both longitudes are zero) is defined in terms of the Central Meridian Longitude (i.e. Earth-Jupiter vector) on a specific date in 1965. S3LH uses latitude (θ_{III}) while S3RH uses colatitude (θ_{RH}).

Note that Higgins et al. (1996, 1997) proposed, based on 35 years of radio observations of Jupiter, that the rotation rate of the planet interior maybe ~25 ms shorter than the System III (1965) rotation rate (see also discussion in relation to magnetic field models by Russell et al. 2001; Yu and Russell 2009; Hess et al. 2011). A 25 ms shorter spin period amounts to just 0.2°/yr which is negligible over the duration of the *Juno* mission but is significant for comparing *Voyager* and *Juno* epochs. Since this is a minimal change in the rotation rate the IAU and the *Juno* project have decided not to change the official System III rotation rate to limit confusion between systems and to allow easy comparison of data sets from different epochs.

Please also note that the rotation rate stated in appendix of the Bagenal et al. (2004) Jupiter book is incorrect.

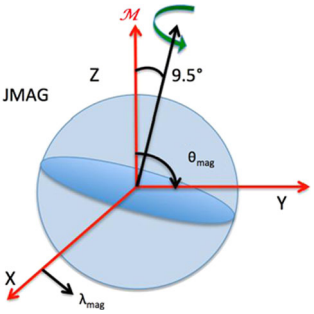

Fig. 34 Jupiter magnetic coordinates. This system rotates with Jupiter but has the Z-axis aligned with the magnetic dipole, M. The X-axis is aligned with the intersection of the magnetic and geographic equators at $\lambda_{III} = 290.8°$ or $\lambda_{RH} = 69.2°$. $\mathbf{X} = 69.2°$ from Prime Meridian (where $\lambda_{III} = \lambda_{RH} = 0$), $\mathbf{Y} = \mathbf{Z} \times \mathbf{X}$, $\mathbf{Z}$ = Jupiter dipole axis

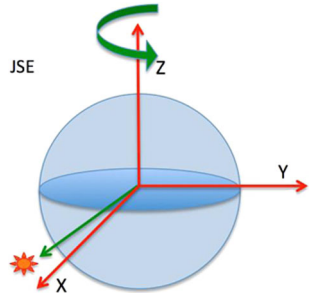

Fig. 35 This system has the Z-axis aligned with Jupiter's spin axis but does not spin with the planet. Instead the X-axis is fixed in the plane containing the spin axis and the Jupiter-Sun vector ($\mathbf{S}$). $\mathbf{X} = \mathbf{Y} \times \mathbf{Z}$, $\mathbf{Y} = \mathbf{S} \times \mathbf{Z}$ (i.e. in the equator), $\mathbf{Z}$ = Jupiter's spin axis

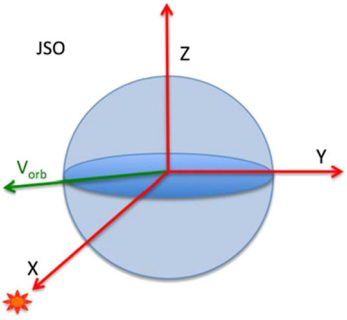

Fig. 36 This system has the X-axis towards the Sun ($\mathbf{S}$) and the Z-axis perpendicular to Jupiter's orbital vector ($\mathbf{V}_{orb}$). This puts $\mathbf{Z}$ normal to Jupiter's orbital plane. $\mathbf{X} = \mathbf{S}$, $\mathbf{Y} = \mathbf{Z} \times \mathbf{X}$, $\mathbf{Z} = \mathbf{V}_{orb} \times \mathbf{X}$

A.2 Jupiter Magnetic (JMAG)

This system is the System III (RH) but is tilted by the 9.5° of the dipole approximation to the magnetic field of Jupiter, tilted towards $\lambda_{III} = 200.8°$ or $\lambda_{RH} = 159.2°$ (Fig. 34). This tilt is based on the VIP4 model (Connerney et al. 1998, 2014, this issue). The magnetic longitude is defined with respect to the meridian where the magnetic and geographic equators cross (where $\theta_{III} = 0°$ and $\theta_{RH} = \theta_{MAG} = 90°$) at $\lambda_{III} = 290.8°$ or $\lambda_{RH} = 69.2°$. Since most models tend to work in right-handed coordinates, we only have a right-handed magnetic system.

A.3 Jupiter-Sun-Equator (JSE)

This system is Jupiter-centered, with the Z-axis aligned with the planet's spin axis but does not spin with the planet (Fig. 35). The X-axis is in the half-plane containing the spin axis and the Jupiter-Sun vector.

A.4 Jupiter-Sun-Orbit (JSO)

This system aligns the X-axis with the Jupiter-Sun vector. The Y-axis is in the plane containing the Jupiter-Sun vector and the orbital vector of Jupiter (Fig. 36).

A.5 Jupiter Heliospheric (JH)

Since *Juno* measures solar wind conditions surrounding Jupiter's magnetosphere we need a coordinate system that is based on heliospheric properties. This system is Jupiter-centered and the X-axis is the Jupiter-Sun vector, the Y-axis is the solar equator, and the Z-axis completes the system. This is the heliocentric system centered on Jupiter.

References

Adriani et al., Space Sci. Rev. (2014, this issue)

I.I. Alexeev, E.S. Belenkaya, Modeling of the Jovian magnetosphere. Ann. Geophys. **23**, 809–826 (2005)

Anderson et al., Space Sci. Rev. (2014, this issue)

S.V. Badman, S.W.H. Cowley, Significance of Dungey-cycle flows in Jupiter's and Saturn's magnetospheres, and their identification on closed equatorial field lines. Ann. Geophys. **25**, 941–951 (2007)

F. Bagenal, Giant planet magnetospheres. Annu. Rev. Earth Planet. Sci. **20**, 289–328 (1992)

F. Bagenal, The magnetosphere of Jupiter: coupling the equator to the poles. J. Atmos. Sol.-Terr. Phys. **69**, 387–402 (2007)

F. Bagenal, Comparative planetary environments, in *Heliophysics: Plasma Physics of the Local Cosmos*, ed. by C.J. Schrijver, G.L. Siscoe (Cambridge University Press, Cambridge, 2009)

F. Bagenal, P.A. Delamere, Flow of mass and energy in the magnetospheres of Jupiter and Saturn. J. Geophys. Res. **116**, 5209 (2011)

F. Bagenal, T.E. Dowling, W.B. McKinnon (eds.), *Jupiter: Planet, Satellites, Magnetosphere* (Cambridge University Press, Cambridge, 2004)

A. Bahnsen, M. Jespersen, E. Ungstrup, B.M. Pedersen, L. Eliasson, Viking observations at the source region of auroral kilometric radiation. J. Geophys. Res. **94**, 6643–6654 (1989)

S.J. Bame, B.L. Barraclough, W.C. Feldman, G.R. Gisler, J.T. Gosling, D.J. McComas, J.L. Phillips, M.F. Thomsen, B.E. Goldstein, M. Neugebauer, Jupiter's magnetosphere: plasma description from the Ulysses flyby. Science **257**, 1539–1543 (1992)

D.D. Barbosa, F.L. Scarf, W.S. Kurth, D.A. Gurnett, Broadband electrostatic noise and field-aligned currents in Jupiter's middle magnetosphere. J. Geophys. Res. **86**, 8357–8369 (1981)

J.W. Belcher, The low-energy plasma in the Jovian magnetosphere, in *Physics of the Jovian Magnetosphere*, ed. by A.J. Dessler (Cambridge Univ. Press, Cambridge, 1983)

E.S. Belenkaya, The Jovian magnetospheric magnetic and electric fields: effects of the interplanetary magnetic field. Planet. Space Sci. **52**, 499–511 (2004)

E.S. Belenkaya, S.Y. Bobrovnikov, I.I. Alexeev, V.V. Kalegaev, S.W.H. Cowley, A model of Jupiter's magnetospheric magnetic field with variable magnetopause flaring. Planet. Space Sci. **53**, 863–872 (2005)

E.S. Belenkaya, P.A. Bespalov, S.S. Davydenko, V.V. Kalegaev, Magnetic field influence on aurorae and the Jovian plasma disk radial structure. Ann. Geophys. **24**, 973–988 (2006)

E.K. Bigg, Influence of the satellite Io on Jupiter's decametric emission. Nature **203**, 1008–1010 (1964)

S. Bolton, R. Thorne, S. Bourdarie, I. DePater, B. Mauk, Jupiter's inner radiation belts, in *Jupiter: Planet, Satellites, Magnetosphere*, ed. by F. Bagenal, T.E. Dowling, W.B. McKinnon (Cambridge University Press, Cambridge, 2004)

Bolton et al., Space Sci. Rev. (2014, this issue)

B. Bonfond, D. Grodent, J.-C. Gérard, A. Radioti, J. Saur, S. Jacobsen, UV Io footprint leading spot: a key feature for understanding the UV Io footprint multiplicity? Geophys. Res. Lett. **35**, 5107 (2008)

B. Bonfond, D. Grodent, J.-C. Gérard, A. Radioti, V. Dols, P.A. Delamere, J.T. Clarke, The Io UV footprint: location, inter-spot distances and tail vertical extent. J. Geophys. Res. **114**, 7224 (2009)

B.D. Bonfond, M.F. Vogt, J.-C. Gérard, D. Grodent, A. Radioti, V. Coumans, Quasiperiodic polar flares at Jupiter: a signature of pulsed dayside reconnections? Geophys. Res. Lett. **380**, L02104 (2011)

B. Bonfond, D. Grodent, J.-C. Gérard, T. Stallard, J.T. Clarke, M. Yoneda, A. Radioti, J. Gustin, Auroral evidence of Io's control over the magnetosphere of Jupiter. Geophys. Res. Lett. **39**, 1105 (2012)

G. Branduardi-Raymont, A. Bhardwaj, R.F. Elsner, G.R. Gladstone, G. Ramsay, P. Rodriguez, R. Soria, J.H. Waite, T.E. Cravens, Latest results on Jovian disk X-rays from XMM-Newton. Planet. Space Sci. **55**, 1126–1134 (2007a)

G. Branduardi-Raymont, A. Bhardwaj, R.F. Elsner, G.R. Gladstone, G. Ramsay, P. Rodriguez, R. Soria, J.H. Waite Jr., T.E. Cravens, A study of Jupiter's aurorae with XMM-Newton. Astron. Astrophys. **463**, 761–774 (2007b)

G. Branduardi-Raymont, R.F. Elsner, M. Galand, D. Grodent, T.E. Cravens, P. Ford, G.R. Gladstone, J.H. Waite, Spectral morphology of the X-ray emission from Jupiter's aurorae. J. Geophys. Res. **109**, 2202 (2008)

G. Branduardi-Raymont, A. Bhardwaj, R.F. Elsner, P. Rodriguez, X-rays from Saturn: a study with XMM-Newton and Chandra over the years 2002-05. Astron. Astrophys. **510**, A74 (2010)

E.J. Bunce, S.W.H. Cowley, T.K. Yeoman, Jovian cusp processes: implications for the polar aurora. J. Geophys. Res. **109**, A09513 (2004)

B.F. Burke, K.L. Franklin, Observations of a variable radio source associated with the planet Jupiter. J. Geophys. Res. **60**, 213–217 (1955)

C.W. Carlson, R.F. Pfaff, J.G. Watzin, The Fast Auroral SnapshoT (FAST) mission. Geophys. Res. Lett. **25**, 2013–2016 (1998)

C.W. Carlson, J.P. McFadden, P. Turin, D.W. Curtis, A. Magoncelli, The electron and ion plasma experiment for Fast. Space Sci. Rev. **98**, 33–66 (2001)

T. Carr, M. Desch, J. Alexander, Phenomenology of magnetospheric radio emissions, in *Physics of the Jovian Magnetosphere*, ed. by A.J. Dessler (Cambridge University Press, Cambridge, 1983)

G. Caudal, A self-consistent model of Jupiter's magnetodisc including the effects of centrifugal force and pressure. J. Geophys. Res. **91**, 4201–4221 (1986)

G. Caudal, J.E.P. Connerney, Plasma pressure in the environment of Jupiter, inferred from Voyager 1 magnetometer observations. J. Geophys. Res. **94**, 15,055–15,061 (1989)

E. Chané, J. Saur, S. Poedts, Modeling Jupiter's magnetosphere: influence of the internal sources. J. Geophys. Res. **118**, 2157–2172 (2013)

S. Chapman, V.C.A. Ferraro, A new theory of magnetic storms. Nature **126**, 129–130 (1930)

J. Clarke, D. Grodent, S. Cowley, E. Bunce, P. Zarka, J. Connerney, T. Satoh, Jupiter's aurora, in *Jupiter: Planet, Satellites, Magnetosphere*, ed. by F. Bagenal, T.E. Dowling, W.B. McKinnon (Cambridge University Press, Cambridge, 2004)

J.T. Clarke, J. Nichols, J.-C. Gérard, D. Grodent, K.C. Hansen, W. Kurth, G.R. Gladstone, J. Duval, S. Wannawichian, E. Bunce, S.W.H. Cowley, F. Crary, M. Dougherty, L. Lamy, D. Mitchell, W. Pryor, K. Retherford, T. Stallard, B. Zieger, P. Zarka, B. Cecconi, Response of Jupiter's and Saturn's auroral activity to the solar wind. J. Geophys. Res. **114**, 5210 (2009)

J.E.P. Connerney, The magnetic field of Jupiter: a generalized inverse approach. J. Geophys. Res. **86**, 7679–7693 (1981)

J.E.P. Connerney, Doing more with Jupiter's magnetic field, in *Planetary Radio Emissions III*, ed. by H.O. Rucker, S.J. Bauer, M.L. Kaiser (1992)

J.E.P. Connerney, Planetary magnetism, in *Planets and Satellites*, ed. by G. Schubert, T. Spohn. Treatise in Geophysics, vol. 10 (Elsevier, Oxford, 2007)

J.E.P. Connerney, R. Baron, T. Satoh, T. Owen, Images of excited H^{3+} at the foot of the Io flux tube in Jupiter's atmosphere. Science **262**, 1035–1038 (1993)

J.E.P. Connerney, M.H. Acuna, N.F. Ness, T. Satoh, New models of Jupiter's magnetic field constrained by the Io flux tube footprint. J. Geophys. Res. **103**, 11929–11940 (1998)

Connerney et al., Space Sci. Rev. (2014, this issue)

S.W.H. Cowley, E.J. Bunce, Origin of the main auroral oval in Jupiter's coupled magnetosphere-ionosphere system. Planet. Space Sci. **49**, 1067–1088 (2001)

S.W.H. Cowley, E.J. Bunce, Corotation-driven magnetosphere-ionosphere coupling currents in Saturn's magnetosphere and their relation to the auroras. Ann. Geophys. **21**, 1691–1707 (2003)

S.W.H. Cowley, E.J. Bunce, T.S. Stallard, S. Miller, Jupiter's polar ionospheric flows: theoretical interpretation. Geophys. Res. Lett. **30**, 1220 (2003)

S.W.H. Cowley, I.I. Alexeev, E.S. Belenkaya, E.J. Bunce, C.E. Cottis, V.V. Kalegaev, J.D. Nichols, R. Prange, F.J. Wilson, A simple axisymmetric model of magnetosphere-ionosphere coupling currents in Jupiter's polar ionosphere. J. Geophys. Res. **110**, 11209 (2005)

S.W.H. Cowley, J.D. Nichols, D.J. Andrews, Modulation of Jupiter's plasma flow, polar currents, and auroral precipitation by solar wind-induced compressions and expansions of the magnetosphere: a simple theoretical model. Ann. Geophys. **25**, 1433–1463 (2007)

S.W.H. Cowley, S.V. Badman, S.M. Imber, S.E. Milan, Comment on "Jupiter: a fundamentally different magnetospheric interaction with the solar wind" by D.J. McComas and F. Bagenal. Geophys. Res. Lett. **35**, 10101 (2008a)

S.W.H. Cowley, A.J. Deason, E.J. Bunce, Axi-symmetric models of auroral current systems in Jupiter's magnetosphere with predictions for the Juno mission. Ann. Geophys. **26**, 4051–4074 (2008b)
T.E. Cravens, N. Ozak, Auroral ion precipitation and acceleration at the outer planets, in *Auroral Phenomenology and Magnetospheric Processes*, ed. by A. Keiling, E. Donovan, F. Bagenal, T. Karlsson. AGU Monograph Series (AGU, Washington, 2012)
T.E. Cravens, J.H. Waite, T.I. Gombosi, N. Lugaz, G.R. Gladstone, B.H. Mauk, R.J. MacDowall, Implications of Jovian X-ray emission for magnetosphere-ionosphere coupling. J. Geophys. Res. **108**, 1465 (2003)
P.A. Delamere, F. Bagenal, Modeling variability of plasma conditions in the Io torus. J. Geophys. Res. **108**, 1276 (2003)
P.A. Delamere, F. Bagenal, Solar wind interaction with Jupiter's magnetosphere. J. Geophys. Res. **115**, 10201 (2010)
P.A. Delamere, F. Bagenal, Magnetotail structure of the giant magnetospheres: implications of the viscous interaction with the solar wind. J. Geophys. Res. **118**, 1–9 (2013)
P.A. Delamere, A. Steffl, F. Bagenal, Modeling temporal variability of plasma conditions in the Io torus during the Cassini era. J. Geophys. Res. **109**, 10216 (2004)
P.A. Delamere, R.J. Wilson, A. Masters, Kelvin-Helmholtz instability at Saturn's magnetopause: hybrid simulations. J. Geophys. Res. **116**, 10222 (2011)
P.A. Delamere, R.J. Wilson, S. Eriksson, F. Bagenal, Magnetic signatures of Kelvin-Helmholtz vortices on Saturn's magnetopause: global survey. J. Geophys. Res. **118**, 393–404 (2013)
M. Desroche, F. Bagenal, P.A. Delamere, N. Erkaev, Conditions at the expanded Jovian magnetopause and implications for the solar wind interaction. J. Geophys. Res. **117**, 7202 (2012)
M. Desroche, F. Bagenal, P.A. Delamere, N. Erkaev, Conditions at the magnetopause of Saturn and implications for the solar wind interaction. J. Geophys. Res. **118** (2013)
A. Dessler (ed.), *Physics of the Jovian Magnetosphere* (Cambridge University Press, Cambridge, 1983)
A. Dessler, V.M. Vasyliūnas, The magnetic anomaly model of the Jovian magnetosphere: predictions for Voyager. Geophys. Res. Lett. **6**, 37–40 (1979)
M.K. Dougherty, L.W. Esposito, S.M. Krimigis (eds.), *Saturn from Cassini-Huygens* (Springer, Berlin, 2009)
F.D. Drake, S. Hvatum, Non-thermal microwave radiation from Jupiter. Astrophys. J. **64**, 329–330 (1959)
J.W. Dungey, Interplanetary magnetic field and the auroral zones. Phys. Rev. Lett. **6**, 47–48 (1961)
R.W. Ebert, D.J. McComas, F. Bagenal, H.A. Elliott, Location, structure, and motion of Jupiter's dusk magnetospheric boundary from 1625 to 2550 R_J. J. Geophys. Res. **115**, 12223 (2010)
E. Echer, P. Zarka, W.D. Gonzalez, A. Morioka, L. Denis, Solar wind effects on Jupiter non-Io DAM emissions during Ulysses distant encounter (2003–2004). Astron. Astrophys. **519**, A84 (2010)
R.F. Elsner, N. Lugaz, J.H. Waite, T.E. Cravens, G.R. Gladstone, P. Ford, D. Grodent, A. Bhardwaj, R.J. MacDowall, M.D. Desch, T. Majeed, Simultaneous Chandra X ray, Hubble Space Telescope ultraviolet, and Ulysses radio observations of Jupiter's aurora. J. Geophys. Res. **110**, 1207 (2005a)
R.F. Elsner, B.D. Ramsey, J.H. Waite, P. Rehak, R.E. Johnson, J.F. Cooper, D.A. Swartz, X-ray probes of magnetospheric interactions with Jupiter's auroral zones, the Galilean satellites, and the Io plasma torus. Icarus **178**, 417–428 (2005b)
R.E. Ergun, L. Ray, P.A. Delamere, F. Bagenal, V. Dols, Y.-J. Su, Generation of parallel electric fields in the Jupiter-Io torus wake region. J. Geophys. Res. **114**, 5201 (2009)
G.B. Field, The source of radiation from Jupiter at decimeter wavelengths. J. Geophys. Res. **64**, 1169–1177 (1959)
K. Fukazawa, T. Ogino, R.J. Walker, Dynamics of the Jovian magnetosphere for northward interplanetary magnetic field (IMF). Geophys. Res. Lett. **32**, 3202 (2005)
K. Fukazawa, T. Ogino, R.J. Walker, Configuration and dynamics of the Jovian magnetosphere. J. Geophys. Res. **111**, 10207 (2006)
K. Fukazawa, T. Ogino, R.J. Walker, A simulation study of dynamics in the distant Jovian magnetotail. J. Geophys. Res. **115**, 9219 (2010)
P.H.M. Galopeau, P. Zarka, D. Le Queau, Source location of Saturn's kilometric radiation: the Kelvin-Helmholtz instability hypothesis. J. Geophys. Res. **100**, 26397–26410 (1995)
H.B. Garrett, S.M. Levin, S.J. Bolton, R.W. Evans, B. Bhattacharya, A revised model of Jupiter's inner electron belts: updating the Divine radiation model. Geophys. Res. Lett. **32**, 4104 (2005)
Y.S. Ge, C.T. Russell, K.K. Khurana, Reconnection sites in Jupiter's magnetotail and relation to Jovian auroras. Planet. Space Sci. **58**, 1455–1469 (2010)
G.R. Gladstone, J.H. Waite, D. Grodent, W.S. Lewis, F.J. Crary, R.F. Elsner, M.C. Weisskopf, T. Majeed, J.-M. Jahn, A. Bhardwaj, J.T. Clarkek, D.T. Young, M.K. Dougherty, S.A. Espinosa, T.E. Cravens, A pulsating auroral X-ray hot spot on Jupiter. Science **415**, 1000–1003 (2002)
G.R. Gladstone, S.A. Stern, S. Alan, D.C.S. Slater, M. Versteeg, M.W. Davis, K.D. Retherford, L.A. Young, A.J. Steffl, H. Throop, J.W. Parker, H.A. Weaver, A.F. Cheng, G.S. Orton, J.T. Clarke, J.D. Nichols, Jupiter's nightside airglow and aurora. Science **318**, 229 (2007)

Gladstone et al., Space Sci. Rev. (2014, this issue)
C.K. Goertz, Detached plasma in Saturn's front side magnetosphere. Geophys. Res. Lett. **10**, 455–458 (1983)
C.K. Goertz, B.A. Randall, M.F. Thomsen, D.E. Jones, E.J. Smith, Evidence for open field lines in Jupiter's magnetosphere. J. Geophys. Res. **81**, 3393–3397 (1976)
T.I. Gombosi, T.P. Armstrong, C.S. Arridge, K.K. Khurana, S.M. Krimigis, N. Krupp, A.M. Persoon, M.F. Thomsen, Saturn's magnetospheric configuration, in *Saturn from Cassini-Huygens*, ed. by M.K. Dougherty, L.W. Esposito, S.M. Krimigis (Springer, Berlin, 2009)
A. Grocott, S.V. Badman, S.W.H. Cowley, S.E. Milan, J.D. Nichols, T.K. Yeoman, Magnetosonic Mach number dependence of the efficiency of reconnection between planetary and interplanetary magnetic fields. J. Geophys. Res. **114**, 7219 (2009)
D. Grodent, J.T. Clarke, J. Kim, J.H. Waite Jr., S.W.H. Cowley, Jupiter's main auroral oval observed with HST-STIS. J. Geophys. Res. **108**, 1389 (2003a)
D. Grodent, J.T. Clarke, J.H. Waite, S.W.H. Cowley, J.-C. Gerard, J. Kim, Jupiter's polar auroral emissions. J. Geophys. Res. **108**, 1366 (2003b)
D. Grodent, J.-C. Gerard, J.T. Clarke, G.R. Gladstone, J.H. Waite, A possible auroral signature of a magnetotail reconnection process on Jupiter. J. Geophys. Res. **109**, 5201 (2004)
D. Grodent, B. Bonfond, J.-C. Gerard, A. Radioti, J. Gustin, J.T. Clarke, J. Nichols, J.E.P. Connerney, Auroral evidence of a localized magnetic anomaly in Jupiter's northern hemisphere. J. Geophys. Res. **113**, 9201 (2008)
J. Gustin, S.W.H. Cowley, J.-C. Gérard, G.R. Gladstone, D. Grodent, J.T. Clarke, Characteristics of Jovian morning bright FUV aurora from Hubble Space Telescope/Space Telescope Imaging Spectrograph imaging and spectral observations. J. Geophys. Res. **111**, A09220 (2006)
J. Gustin, J.-C. Gerard, D. Grodent, G. Gladstone, J. Clarke, W. Pryor, V. Dols, B. Bonfond, A. Radioti, L. Lamy, J. Ajello, Effects of methane on giant planets UV emissions and implications for the auroral characteristics. J. Mol. Spectrosc. (2013)
Hansen et al., Space Sci. Rev. (2014, this issue)
S. Hess, P. Zarka, F. Mottez, Io–Jupiter interaction, millisecond bursts and field-aligned potentials. Planet. Space Sci. **55**, 89–99 (2007a)
S. Hess, F. Mottez, P. Zarka, Jovian S burst generation by Alfvén waves. J. Geophys. Res. **112**, A11212 (2007b)
S. Hess, F. Mottez, P. Zarka, T. Chust, Generation of the Jovian radio decametric arcs from the Io flux tube. J. Geophys. Res. **113**, A03209 (2008a)
S. Hess, B. Cecconi, P. Zarka, Modeling of Io-Jupiter decameter arcs, emission beaming and energy source. Geophys. Res. Lett. **35**, L13107 (2008b)
S. Hess, F. Mottez, P. Zarka, Effect of electric potential structures on Jovian S-burst morphology. Geophys. Res. Lett. **36**, L14101 (2009)
S.L.G. Hess, P. Delamere, V. Dols, B. Bonfond, D. Swift, Power transmission and particle acceleration along the Io flux tube. J. Geophys. Res. **115**, 6205 (2010a)
S.L.G. Hess, A. Petin, P. Zarka, B. Bonfond, B. Cecconi, Lead angles and emitting electron energies of Io-controlled decameter radio arcs. Planet. Space Sci. **58**, 1188–1198 (2010b)
S.L.G. Hess, B. Bonfond, P. Zarka, D. Grodent, Model of the Jovian magnetic field topology constrained by the Io auroral emissions. J. Geophys. Res. **116**, 5217 (2011)
S.L.G. Hess, E. Echer, P. Zarka, Solar wind pressure effects on Jupiter decametric radio emissions independent of Io. Planet. Space Sci. **70**, 114–125 (2012)
C.A. Higgins, T.D. Carr, F. Reyes, A new determination of Jupiter's radio rotation period. Geophys. Res. Lett. **23**, 2653–2656 (1996)
C.A. Higgins, T.D. Carr, F. Reyes, W.B. Greenman, G.R. Lebo, A redefinition of Jupiter's rotation period. J. Geophys. Res. **102**, 22033–22042 (1997)
T.W. Hill, Inertial limit on corotation. J. Geophys. Res. **84**, 6554–6558 (1979)
T.W. Hill, The Jovian auroral oval. J. Geophys. Res. **106**, 8101–8108 (2001)
T.W. Hill, D.H. Pontius, Plasma injection near Io. J. Geophys. Res. **103**, 19879 (1998)
T.W. Hill, V.M. Vasyliūnas, Jovian auroral signature of Io's corotational wake. J. Geophys. Res. **107**, 1464 (2002)
T.W. Hill, A.J. Dessler, C.K. Goertz, Magnetospheric models, in *Physics of the Jovian Magnetosphere*, ed. by A.J. Dessler (Cambridge Univ. Press, Cambridge, 1983), pp. 353–394
G.B. Hospodarsky, W.S. Kurth, B. Cecconi, D.A. Gurnett, M.L. Kaiser, M.D. Desch, P. Zarka, Simultaneous observations of Jovian quasi-periodic radio emissions by the Galileo and Cassini spacecraft. J. Geophys. Res. **109**, A09S07 (2004)
T.S. Huang, T.W. Hill, Corotation lag of the Jovian atmosphere, ionosphere, and magnetosphere. J. Geophys. Res. **94**, 3761–3765 (1989)

D.E. Huddleston, C.T. Russell, M.G. Kivelson, K.K. Khurana, L. Bennett, Location and shape of the Jovian magnetopause and bow shock. J. Geophys. Res. **103**, 20075–20082 (1998)

Y. Hui, D.R. Schultz, V.A. Kharchenko, A. Bhardwaj, G. Branduardi-Raymont, P.C. Stancil, T.E. Cravens, C.M. Lisse, A. Dalgarno, Comparative analysis and variability of the Jovian X-ray spectra detected by the Chandra and XMM-Newton observatories. J. Geophys. Res. **115**, 7102 (2010)

C.M. Jackman, N. Achilleos, E.J. Bunce, S.W.H. Cowley, M.K. Dougherty, G.H. Jones, S.E. Milan, Interplanetary magnetic field conditions at ∼9 AU during the declining phase of the solar cycle and its implications for Saturn's magnetospheric dynamics. J. Geophys. Res. **109** (2004)

Janssen et al., Space Sci. Rev. (2014, this issue)

X. Jia, M.G. Kivelson, K.K. Khurana, R. Walker, Magnetic fields of the satellites of Jupiter and Saturn. Space Sci. Rev. **152**, 271–305 (2009)

S.T. Jones, Y.-J. Su, Role of dispersive Alfvén waves in generating parallel electric fields along the Io-Jupiter fluxtube. J. Geophys. Res. **113**, A12205 (2008)

S.P. Joy, M.G. Kivelson, R.J. Walker, K.K. Khurana, C.T. Russell, T. Ogino, Probabilistic models of the Jovian magnetopause and bow shock locations. J. Geophys. Res. **107**, 1309 (2002)

S.J. Kanani, C.S. Arridge, G.H. Jones, A.N. Fazakerley, H.J. McAndrews, N. Sergis, S.M. Krimigis, M.K. Dougherty, A.J. Coates, D.T. Young, K.C. Hansen, N. Krupp, A new form of Saturn's magnetopause using a dynamic pressure balance model, based on in situ, multi-instrument Cassini measurements. J. Geophys. Res. **115**, 6207 (2010)

S. Kasahara, E.A. Kronberg, T. Kimura, C. Tao, S.V. Badman, A. Masters, A. Retino, N. Krupp, M. Fujimoto, Asymmetric distribution of reconnection jet fronts in the Jovian nightside magnetosphere. J. Geophys. Res. **118**, 375–384 (2013)

A. Keiling, E. Donovan, F. Bagenal, T. Karlsson (eds.), *Auroral Phenomenology and Magnetospheric Processes* (AGU, Washington, 2012)

K.K. Khurana, Euler potential models of Jupiter's magnetospheric field. J. Geophys. Res. **102**, 11295–11306 (1997)

K.K. Khurana, Influence of solar wind on Jupiter's magnetosphere deduced from currents in the equatorial plane. J. Geophys. Res. **106**, 25999–26016 (2001)

K.K. Khurana, M.G. Kivelson, On Jovian plasma sheet structure. J. Geophys. Res. **94**, 11791–11803 (1989)

K.K. Khurana, H.K. Schwarzl, Global structure of Jupiter's magnetospheric current sheet. J. Geophys. Res. **110**, 7227 (2005)

K. Khurana, M.G. Kivelson, V. Vasyliunas, N. Krupp, J. Woch, A. Lagg, B. Mauk, W. Kurth, The configuration of Jupiter's magnetosphere, in *Jupiter: Planet, Satellites, Magnetosphere*, ed. by F. Bagenal, T.E. Dowling, W.B. McKinnon (Cambridge University Press, Cambridge, 2004)

T. Kimura, F. Tsuchiya, H. Misawa, A. Morioka, H. Nozawa, Occurrence statistics and ray tracing study of Jovian quasiperiodic radio bursts observed from low latitudes. J. Geophys. Res. **115**, A05217 (2010)

M.G. Kivelson, Planetary magnetospheres, in *Handbook of the Solar-Terrestrial Environment*, ed. by Y. Kamide, A.C.-L. Chian (2007)

M. Kivelson, F. Bagenal, Planetary magnetospheres, in *Encyclopedia of the Solar System*, ed. by McFadden, Weissman, Johnson (2007)

M.G. Kivelson, D.J. Southwood, Dynamical consequences of two modes of centrifugal instability in Jupiter's outer magnetosphere. J. Geophys. Res. **110**, 12209 (2005)

M.G. Kivelson, K.K. Khurana, R.J. Walker, Sheared magnetic field structure in Jupiter's dusk magnetosphere: implications for return currents. J. Geophys. Res. **107**, 1116 (2002)

M.G. Kivelson, F. Bagenal, W.S. Kurth, F.M. Neubauer, C. Paranicas, J. Saur, Magnetospheric interactions with satellites, in *Jupiter: Planet, Satellites, Magnetosphere*, ed. by F. Bagenal, T.E. Dowling, W.B. McKinnon (Cambridge University Press, Cambridge, 2004)

S. Knight, Parallel electric fields. Planet. Space Sci. **21**, 741–750 (1973)

S.M. Krimigis, C.O. Bostrom, E.P. Keath, R.D. Zwickl, J.F. Carbary, T.P. Armstrong, W.I. Axford, C.Y. Fan, G. Gloeckler, L.J. Lanzerotti, Hot plasma environment at Jupiter—Voyager 2 results. Science **206**, 977–984 (1979)

E.A. Kronberg, J. Woch, N. Krupp, A. Lagg, K.K. Khurana, K.-H. Glassmeier, Mass release at Jupiter: substorm-like processes in the Jovian magnetotail. J. Geophys. Res. **110**, 3211 (2005)

E.A. Kronberg, K.-H. Glassmeier, J. Woch, N. Krupp, A. Lagg, M.K. Dougherty, A possible intrinsic mechanism for the quasi-periodic dynamics of the Jovian magnetosphere. J. Geophys. Res. **112**, 5203 (2007)

E.A. Kronberg, J. Woch, N. Krupp, A. Lagg, P.W. Daly, A. Korth, Comparison of periodic substorms at Jupiter and Earth. J. Geophys. Res. **113**, 4212 (2008)

N. Krupp, V. Vasyliunas, J. Woch, A. Lagg, K. Khurana, M. Kivelson, B. Mauk, E. Roelof, D. Williams, S. Krimigis, W. Kurth, L. Frank, W. Paterson, Dynamics of the Jovian magnetosphere, in *Jupiter: Planet, Satellites, Magnetosphere*, ed. by F. Bagenal, T.E. Dowling, W.B. McKinnon (Cambridge University Press, Cambridge, 2004)

W.S. Kurth, Comparative observations of plasma waves at the outer planets. Adv. Space Res. **12**, 83–90 (1992)
W.S. Kurth, D.A. Gurnett, Plasma waves in planetary magnetospheres. J. Geophys. Res. **96**, 18977 (1991)
W.S. Kurth, E.J. Bunce, J.T. Clarke, F.J. Crary, D.C. Grodent, A.P. Ingersoll, U.A. Dyudina, L. Lamy, D.G. Mitchell, A.M. Persoon, W.R. Pryor, J. Saur, T. Stallard, Auroral processes, in *Saturn from Cassini-Huygens*, ed. by M.K. Dougherty, L.W. Esposito, S.M. Krimigis (Springer, Berlin, 2009)
Kurth et al., Space Sci. Rev. (2014, this issue)
H.P. Ladreiter, P. Zarka, A. Lacacheux, Direction finding study of Jovian hectometric and broadband kilometric radio emissions: evidence for their auroral origin. Planet. Space Sci. **42**, 919–931 (1994)
L. Lamy, P. Schippers, P. Zarka, B. Cecconi, C.S. Arridge, M.K. Dougherty, P. Louarn, N. André, W.S. Kurth, R.L. Mutel, D.A. Gurnett, A.J. Coates, Properties of Saturn kilometric radiation measured within its source region. Geophys. Res. Lett. **39**, L12104 (2010)
G.F. Lindal, G.E. Wood, G.S. Levy, J.D. Anderson, D.N. Sweetnam, H.B. Hotz, B.J. Buckles, D.P. Holmes, P.E. Doms, V.R. Eshleman, G.L. Tyler, T.A. Croft, The atmosphere of Jupiter—an analysis of the Voyager radio occultation measurements. J. Geophys. Res. **86**, 8721–8727 (1981)
P. Louarn, A. Roux, S. Perraut, W. Kurth, D. Gurnett, A study of the large scale dynamics of the Jovian magnetosphere using the Galileo plasma wave experiment. Geophys. Res. Lett. **25**, 2905–2908 (1998)
P. Louarn, A. Roux, S. Perraut, W.S. Kurth, D.A. Gurnett, A study of the Jovian "energetic magnetospheric events" observed by Galileo: role in the radial plasma transport. J. Geophys. Res. **105**, 13073–13088 (2000)
P. Louarn, B. Mauk, D.J. Williams, C. Zimmer, M.G. Kivelson, W.S. Kurth, D.A. Gurnett, A. Roux, A multi-instrument study of a Jovian magnetospheric disturbance. J. Geophys. Res. **106**, 29883 (2001)
A. Masters, N. Achilleos, C. Bertucci, M.K. Dougherty, S.J. Kanani, C.S. Arridge, H.J. McAndrews, A.J. Coates, Surface waves on Saturn's dawn flank magnetopause driven by the Kelvin-Helmholtz instability. Planet. Space Sci. **57**, 1769–1778 (2009)
A. Masters, N. Achilleos, M.G. Kivelson, N. Sergis, M.K. Dougherty, M.F. Thomsen, C.S. Arridge, S.M. Krimigis, H.J. McAndrews, S.J. Kanani, N. Krupp, A.J. Coates, Cassini observations of a Kelvin-Helmholtz vortex in Saturn's outer magnetosphere. J. Geophys. Res. **115**, 7225 (2010)
A. Masters, D.G. Mitchell, A.J. Coates, M.K. Dougherty, Saturn's low-latitude boundary layer: 1. Properties and variability. J. Geophys. Res. **116**, 6210 (2011a)
A. Masters, A.P. Walsh, A.N. Fazakerley, A.J. Coates, M.K. Dougherty, Saturn's low-latitude boundary layer: 2. Electron structure. J. Geophys. Res. **116**, 6211 (2011b)
A. Masters, J.P. Eastwood, M. Swisdak, M.F. Thomsen, C.T. Russell, N. Sergis, F.J. Crary, M.K. Dougherty, A.J. Coates, S.M. Krimigis, The importance of plasma β conditions for magnetic reconnection at Saturn's magnetopause. Geophys. Res. Lett. **39**, 8103 (2012)
B. Mauk, F. Bagenal, Auroral phenomenology and magnetospheric processes: Earth and other planets, in *Auroral Phenomenology and Magnetospheric Processes*, ed. by Keiling, Donovan, Bagenal, Karlsson. AGU Monograph Series (AGU, Washington, 2012)
B.H. Mauk, J. Saur, Equatorial electron beams and auroral structuring at Jupiter. J. Geophys. Res. **112**, 10221 (2007)
B.H. Mauk, D.G. Mitchell, R.W. McEntire, C.P. Paranicas, E.C. Roelof, D.J. Williams, S.M. Krimigis, A. Lagg, Energetic ion characteristics and neutral gas interactions in Jupiter's magnetosphere. J. Geophys. Res. **109**, 9 (2004)
B.H. Mauk, D.C. Hamilton, T.W. Hill, G.B. Hospodarsky, R.E. Johnson, C. Paranicas, E. Roussos, C.T. Russell, D.E. Shemansky, E.C. Sittler, R.M. Thorne, Fundamental plasma processes in Saturn's magnetosphere, in *Saturn from Cassini-Huygens*, ed. by M.K. Dougherty, L.W. Esposito, S.M. Krimigis (Springer, Berlin, 2009)
Mauk et al., Space Sci. Rev. (2014, this issue)
D.J. McComas, F. Bagenal, Jupiter: a fundamentally different magnetospheric interaction with the solar wind. Geophys. Res. Lett. **34**, 20106 (2007)
D.J. McComas, F. Allegrini, F. Bagenal, F. Crary, R.W. Ebert, H. Elliott, A. Stern, P. Valek, Diverse plasma populations and structures in Jupiter's magnetotail. Science **318**, 217 (2007)
D.J. McComas, F. Bagenal, Reply to comment by S.W.H. Cowley et al. on "Jupiter: a fundamentally different magnetospheric interaction with the solar wind". Geophys. Res. Lett. **35**, 10103 (2008)
D.J. McComas, N. Angold, H.A. Elliott, G. Livadiotis, N.A. Schwadron, R.M. Skoug, C.W. Smith, Weakest solar wind of the space age and the current "mini" solar maximum. Astrophys. J. **779**, 2 (2013)
D.J. McComas, N. Alexander, F. Allegrini, F. Bagenal, C. Beebe, G. Clark, F. Crary, M.I. Desai, A. De Los Santos, D. Demkee, J. Dickinson, D. Everett, T. Finley, A. Gribanova, R. Hill, J. Johnson, C. Kofoed, C. Loeffler, P. Louarn, M. Maple, W. Mills, C. Pollock, M. Reno, B. Rodriguez, J. Rouzaud, D. Santos-Costa, P. Valek, S. Weidner, P. Wilson, R.J. Wilson, D. White, The Jovian Auroral Distributions Experiment (JADE) on the Juno Mission to Jupiter. Space Sci. Rev. (2014a, this issue). doi:10.1007/s11214-013-9990-9

D.J. McComas, F. Bagenal, R.W. Ebert, Bimodal size of Jupiter's magnetosphere. J. Geophys. Res. (2014b, in review)

J.P. McFadden, C.W. Carlson, R.E. Ergun, Microstructure of the auroral acceleration region as observed by FAST. J. Geophys. Res. **104**, 14453–14480 (1999)

R.L. McNutt Jr., J.W. Belcher, J.D. Sullivan, F. Bagenal, H.S. Bridge, Departure from rigid co-rotation of plasma in Jupiter's dayside magnetosphere. Nature **280**, 803 (1979)

R.L. McNutt, D.K. Haggerty, M.E. Hill, S.M. Krimigis, S. Livi, G.C. Ho, R.S. Gurnee, B.H. Mauk, D.G. Mitchell, E.C. Roelof, D.J. McComas, F. Bagenal, H.A. Elliott, L.E. Brown, M. Kusterer, J. Vandegriff, S.A. Stern, H.A. Weaver, J.R. Spencer, J.M. Moore, Energetic particles in the Jovian magnetotail. Science **318**, 220 (2007)

D.G. Mitchell, J.F. Carbary, S.W.H. Cowley, T.W. Hill, P. Zarka, The dynamics of Saturn's magnetosphere, in *Saturn from Cassini-Huygens*, ed. by M.K. Dougherty, L.W. Esposito, S.M. Krimigis (Springer, Berlin, 2009)

F. Mottez, S.L.G. Hess, P. Zarka, Explanation of dominant oblique radio emission at Jupiter and comparison to the Terrestrial case. Planet. Space Sci. **58**, 1414–1422 (2010)

R.L. Mutel, J.D. Menietti, D.A. Gurnett, W. Kurth, P. Schippers, C. Lynch, L. Lamy, C. Arridge, B. Cecconi, CMI growth rates for saturnian kilometric radiation. Geophys. Res. Lett. **37**, L19105 (2010)

J.D. Nichols, Magnetosphere-ionosphere coupling in Jupiter's middle magnetosphere: computations including a self-consistent current sheet magnetic field model. J. Geophys. Res. **116**, 10232 (2011)

J. Nichols, S. Cowley, Magnetosphere-ionosphere coupling currents in Jupiter's middle magnetosphere: effect of precipitation-induced enhancement of the ionospheric Pedersen conductivity. Ann. Geophys. **22**, 1799–1827 (2004)

J.D. Nichols, S.W.H. Cowley, Magnetosphere-ionosphere coupling currents in Jupiter's middle magnetosphere: effect of magnetosphere-ionosphere decoupling due to field-aligned auroral voltages. Ann. Geophys. **23**, 799–808 (2005)

J.D. Nichols, S.W.H. Cowley, D.J. McComas, Magnetopause reconnection rate estimates for Jupiter's magnetosphere based on interplanetary measurements at ∼5 AU. Ann. Geophys. **24**, 393–406 (2006)

J.D. Nichols, E.J. Bunce, J.T. Clarke, S.W.H. Cowley, J.-C. Gerard, D. Grodent, W.R. Pryor, Response of Jupiter's UV auroras to interplanetary conditions as observed by the Hubble Space Telescope during the Cassini flyby campaign. J. Geophys. Res. **112**, A02203 (2007)

J.D. Nichols, J.T. Clarke, J.C. Gerard, D. Grodent, Observations of Jovian polar auroral filaments. Geophys. Res. Lett. **36**, 8101 (2009a)

J.D. Nichols, J.T. Clarke, J.C. Gerard, D. Grodent, K.C. Hansen, Variation of different components of Jupiter's auroral emission. J. Geophys. Res. **114**, 6210 (2009b)

T.G. Northrop, T.J. Birmingham, Adiabatic charged particle motion in rapidly rotating magnetospheres. J. Geophys. Res. **87**, 661–669 (1982)

N. Ozak, D.R. Schultz, T.E. Cravens, V. Kharchenko, Y.-W. Hui, Auroral X-ray emission at Jupiter: depth effects. J. Geophys. Res. **115**, 11306 (2010)

L. Pallier, R. Prangé, More about the structure of the high latitude Jovian aurorae. Planet. Space Sci. **49**, 1159–1173 (2001)

L. Pallier, R. Prangé, Detection of the southern counterpart of the Jovian northern polar cusp: shared properties. Geophys. Res. Lett. **31**, L06701 (2004)

G. Paschmann, S. Haaland, R. Treumann (eds.), *Auroral Plasma Physics*. Space Sci. Rev. **103** (2002)

D.H. Pontius Jr., T.W. Hill, Departure from corotation of the Io plasma torus: local plasma production. Geophys. Res. Lett. **9**, 1321–1324 (1982)

R. Prange, P. Zarka, G.E. Ballester, T.A. Livengood, L. Denis, T.D. Carr, F. Reyes, S.J. Bame, H.W. Moos, Correlated variations of UV and radio emissions during an outstanding Jovian auroral event. J. Geophys. Res. **98**, 18779–18791 (1993)

J. Queinnec, P. Zarka, Io-controlled decameter arcs and Io-Jupiter interaction. J. Geophys. Res. **103**, 26649–26666 (1998)

A. Radioti, D. Grodent, J.-C. Gerard, B. Bonfond, J.T. Clarke, Auroral polar dawn spots: signatures of internally driven reconnection processes at Jupiter's magnetotail. Geophys. Res. Lett. **35**, 3104 (2008)

A. Radioti, D. Grodent, J.-C. Gerard, B. Bonfond, Auroral signatures of flow bursts released during magnetotail reconnection at Jupiter. J. Geophys. Res. **115**, 7214 (2010)

A. Radioti, D. Grodent, J.-C. Gerard, M.F. Vogt, M. Lystrup, B. Bonfond, Nightside reconnection at Jupiter: auroral and magnetic field observations from 26 July 1998. J. Geophys. Res. **116**, 3221 (2011)

L.C. Ray, R.E. Ergun, P.A. Delamere, F. Bagenal, Magnetosphere-ionosphere coupling at Jupiter: effect of field-aligned potentials on angular momentum transport. J. Geophys. Res. **115**, 9211 (2010)

L.C. Ray, R.E. Ergun, P.A. Delamere, F. Bagenal, Magnetosphere-ionosphere coupling at Jupiter: a parameter space study. J. Geophys. Res. **117**, A01205 (2012)

L.C. Ray, N. Achilleos, Y.N. Yates, Including field-aligned potentials in the coupling between Jupiter's thermosphere, ionosphere, and magnetosphere. Planet. Space Sci. **62** (2014, submitted)

M.J. Reiner, J. Fainberg, R.G. Stone, M.L. Kaiser, M.D. Desch, R. Manning, P. Zarka, B.-M. Pedersen, Source characteristics of Jovian narrow-band kilometric radio emissions. J. Geophys. Res. **98**, 13163–13176 (1993)

E. Roussos, N. Krupp, C.P. Paranicas, P. Kollmann, D.G. Mitchell, S.M. Krimigis, T.P. Armstrong, D.R. Went, M.K. Dougherty, G.H. Jones, and short-term variability of Saturn's ionic radiation belts. J. Geophys. Res. **116**, 2217 (2011)

A. Roux, A. Hilgers, H. de Feraudy, D. Le Queau, P. Louarn, S. Perraut, A. Bahnsen, M. Jespersen, E. Ungstrup, M. Andre, Auroral kilometric radiation sources—in situ and remote observations from Viking. J. Geophys. Res. **98**, 11657–11670 (1993)

C.T. Russell, Outer planet magnetospheres: a tutorial. Adv. Space Res. **33**, 2004–2020 (2004)

C.T. Russell, New horizons in planetary magnetospheres. Adv. Space Res. **37**, 1467–1481 (2006)

C.T. Russell, K.K. Khurana, M.G. Kivelson, D.E. Huddleston, Substorms at Jupiter: Galileo observations of transient reconnection in the near tail. Adv. Space Res. **26**, 1499–1504 (2000)

C.T. Russell, Z.J. Yu, M.G. Kivelson, The rotation period of Jupiter. Geophys. Res. Lett. **28**, 1911–1912 (2001)

V.B. Ryabov, B.P. Ryabov, D.M. Vavriv, P. Zarka, R. Kozhin, V.V. Vinogradov, V.A. Shevchenko, Jupiter S-bursts: narrow-band origin of microsecond subpulses. J. Geophys. Res. **112**, A09206 (2007)

D. Santos-Costa, S.J. Bolton, Discussing the processes constraining the Jovian synchrotron radio emission's features. Planet. Space Sci. **56**, 326–345 (2008)

D. Santos-Costa, S.A. Bourdarie, Modeling the inner Jovian electron radiation belt including non-equatorial particles. Planet. Space Sci. **49**, 303–312 (2001)

D. Santos-Costa, S.J. Bolton, R.M. Thorne, Y. Miyoshi, S.M. Levin, Investigating the origins of the Jovian decimetric emission's variability. J. Geophys. Res. **113**, 1204 (2008)

J. Saur, A. Pouquet, W.H. Matthaeus, An acceleration mechanism for the generation of the main auroral oval on Jupiter. Geophys. Res. Lett. **30**, 1260 (2003)

J. Saur, F.M. Neubauer, J.E.P. Connerney, P. Zarka, M.G. Kivelson, Plasma interaction of Io with its plasma torus, in *Jupiter: Planet, Satellites, Magnetosphere*, ed. by F. Bagenal, T.E. Dowling, W.B. McKinnon (Cambridge University Press, Cambridge, 2004)

A.W. Schardt, C.K. Goertz, High-energy particles, in *Physics of the Jovian Magnetosphere*, ed. by A.J. Dessler (Cambridge University Press, Cambridge, 1983)

P. Schippers, C.S. Arridge, J.D. Menietti, D.A. Gurnett, L. Lamy, B. Cecconi, D.G. Mitchell, N. André, W.S. Kurth, S. Grimald, M.K. Dougherty, A.J. Coates, N. Krupp, D.T. Young, Auroral electron distributions within and close to the Saturn kilometric radiation source region. J. Geophys. Res. **116**, A05203 (2011)

N. Sergis, S.M. Krimigis, E.C. Roelof, C.S. Arridge, A.M. Rymer, D.G. Mitchell, D.C. Hamilton, N. Krupp, M.F. Thomsen, M.K. Dougherty, A.J. Coates, D.T. Young, Particle pressure, inertial force, and ring current density profiles in the magnetosphere of Saturn, based on Cassini measurements. Geophys. Res. Lett. **37**, 2102 (2010)

G.L. Siscoe, Towards a comparative theory of magnetospheres, in *Solar System Plasma Physics*, vol. 2, ed. by Parker, Kennel, Lanzerotti (North-Holland, Amsterdam, 1979)

J.A. Slavin, E.J. Smith, J.R. Spreiter, S.S. Stahara, Solar wind flow about the outer planets: gas dynamic modeling of the Jupiter and Saturn bow shocks. J. Geophys. Res. **90**, 6275–6286 (1985)

C.G.A. Smith, A.D. Aylward, Coupled rotational dynamics of Jupiter's thermosphere and magnetosphere. Ann. Geophys. **23**, 199–230 (2009)

D. Southwood, M. Kivelson, A new perspective concerning the influence of the solar wind on Jupiter. J. Geophys. Res. **106**, 6123–6130 (2001)

T. Stallard, S. Miller, G. Millward, R.D. Joseph, On the dynamics of the Jovian ionosphere and thermosphere. I: the measurement of ion winds. Icarus **154**, 475–491 (2001)

T.S. Stallard, S. Miller, S.W.H. Cowley, E.J. Bunce, Jupiter's polar ionospheric flows: measured intensity and velocity variations poleward of the main auroral oval. Geophys. Res. Lett. **30**, 1221 (2003)

T. Stallard, S. Miller, H. Melin, *Clues on Ionospheric Electrodynamics from IR Aurora at Jupiter and Saturn. Auroral Phenomenology and Magnetospheric Processes: Earth and Other Planets*. Geophys. Mono. Series, vol. 197 (2012), pp. 215–224

A.J. Steffl, A.I.F. Stewart, F. Bagenal, Cassini UVIS observations of the Io plasma torus. I: initial results. Icarus **172**, 78–90 (2004a)

A.J. Steffl, F. Bagenal, A.I.F. Stewart, Cassini UVIS observations of the Io plasma torus. II: radial variations. Icarus **172**, 91–103 (2004b)

A.J. Steffl, P.A. Delamere, F. Bagenal, Cassini UVIS observations of the Io plasma torus. III: observations of temporal and azimuthal variability. Icarus **180**, 124–140 (2006)

A.J. Steffl, P.A. Delamere, F. Bagenal, Cassini UVIS observations of the Io plasma torus. IV: modeling temporal and azimuthal variability. Icarus **194**, 153–165 (2008)
Y.-J. Su, R.E. Ergun, F. Bagenal, P.A. Delamere, Io-related Jovian auroral arcs: modeling parallel electric fields. J. Geophys. Res. **108**, 1094 (2003)
C. Tao, H. Fujiwara, Y. Kasaba, Neutral wind control of the Jovian magnetosphere-ionosphere current system. J. Geophys. Res. **114**, 8307–8323 (2009)
C. Tao, S.V. Badman, M. Fujimoto, UV and IR auroral emission model for the outer planets: Jupiter and Saturn comparison. Icarus **213**, 581–592 (2011)
C. Tao, S.V. Badman, T. Uno, M. Fujimoto, On the feasibility of characterizing Jovian auroral electrons via H_3^+ infrared line-emission analysis. Icarus **221**, 236–247 (2012)
N. Thomas, F. Bagenal, T. Hill, J. Wilson, The Io neutral clouds and plasma torus, in *Jupiter: Planet, Satellites, Magnetosphere*, ed. by F. Bagenal, T.E. Dowling, W.B. McKinnon (Cambridge University Press, Cambridge, 2004)
J.H. Trainor, F.B. McDonald, D.E. Stillwell, B.J. Teegarden, W.R. Webber, Jovian protons and electrons: Pioneer 11. Science **188**, 462–465 (1975)
J.A. Van Allen, F. Bagenal, Planetary magnetospheres and the interplanetary medium, beatty, in *The New Solar System*, ed. by Collins-Petersen, Chaikin (Cambridge University Press, Cambridge, 1999)
A.R. Vasavada, A.H. Bouchez, A.P. Ingersoll, B. Little, C.D. Anger (Galileo SSI Team), Jupiter's visible aurora and Io footprint. J. Geophys. Res. **104**, 27133–27142 (1999)
V.M. Vasyliūnas, Plasma distribution and flow, in *Physics of the Jovian Magnetosphere*, ed. by A.J. Dessler (Cambridge University Press, Cambridge, 1983)
V.M. Vasyliūnas, Role of the plasma acceleration time in the dynamics of the Jovian magnetosphere. Geophys. Res. Lett. **21**, 401–404 (1994)
V.M. Vasyliūnas, Comparative magnetospheres: lessons for Earth. Adv. Space Res. **33**, 2113–2120 (2004)
V.M. Vasyliūnas, Fundamentals of planetary magnetospheres, in *Heliophysics: Plasma Physics of the Local Cosmos*, ed. by C.J. Schrijver, G.L. Siscoe (Cambridge University Press, Cambridge, 2009)
V.M. Vasyliūnas, Comparative magnetospheres: lessons for Earth. Space Sci. Rev. **158**, 91–118 (2011)
M.F. Vogt, M.G. Kivelson, K.K. Khurana, S.P. Joy, R.J. Walker, Reconnection and flows in the Jovian magnetotail as inferred from magnetometer observations. J. Geophys. Res. **115**, 6219 (2010)
M.F. Vogt, M.G. Kivelson, K.K. Khurana, R.J. Walker, B. Bonfond, D. Grodent, A. Radioti, Improved mapping of Jupiter's auroral features to magnetospheric sources. J. Geophys. Res. **116**, 3220 (2011)
M.F. Vogt, M.G. Kivelson, K.K. Khurana, R.J. Walker, M. Ashour-Abdalla, E.J. Bunce, Simulating the effect of centrifugal forces in Jupiter's magnetosphere. J. Geophys. Res. (2013)
J.H. Waite, G.R. Gladstone, W.S. Lewis, R. Goldstein, D.J. McComas, P. Riley, R.J. Walker, P. Robertson, S. Desai, J.T. Clarke, D.T. Young, An auroral flare at Jupiter. Nature **410**, 787–789 (2001)
R.J. Walker, T. Ogino, A simulation study of currents in the Jovian magnetosphere. Planet. Space Sci. **51**, 295–307 (2003)
R.J. Walker, C.T. Russell, Flux transfer events at the Jovian magnetopause. J. Geophys. Res. **90**, 7397–7404 (1985)
R. Walker, C. Russell, Solar wind interactions with magnetized planets, in *Introduction to Space Physics*, ed. by R. Kivelson (Cambridge University Press, Cambridge, 1995)
J. Woch, N. Krupp, A. Lagg, Particle bursts in the Jovian magnetosphere: evidence for a near-Jupiter neutral line. Geophys. Res. Lett. **29**, 1138 (2002)
J.N. Yates, N. Achilleos, P. Guio, Influence of upstream solar wind on thermospheric flows at Jupiter. Planet. Space Sci. **61**, 15–31 (2012)
Z.J. Yu, C.T. Russell, Rotation period of Jupiter from the observation of its magnetic field. Geophys. Res. Lett. **36**, 20202 (2009)
P. Zarka, Auroral radio emissions at the outer planets: observations and theories. J. Geophys. Res. **103**, 20159–20194 (1998)
P. Zarka, Radio emissions from the planets and their moons, in *Radio Astronomy at Long Wavelengths*, ed. by Stone, Weiler, Goldstein, Bougeret (AGU, Washington, 2000)
P. Zarka, Radio and plasma waves at the outer planets. Adv. Space Res. **33**, 2045–2060 (2004)
P. Zarka, R.A. Treumann, B.P. Ryabov, V.B. Ryabov, Magnetically-driven planetary radio emissions and application to extrasolar planets. Astrophys. Space Sci. **277**, 293300 (2001a)
P. Zarka, J. Queinnec, F.J. Crary, Low-frequency limit of Jovian radio emissions and implications on source locations and Io plasma wake. Planet. Space Sci. **49**, 1137–1149 (2001b)
P. Zarka, B. Cecconi, W.S. Kurth, Jupiter's low-frequency radio spectrum from Cassini/radio and plasma wave science (RPWS) absolute flux density measurements. J. Geophys. Res. **109**, A09S15 (2004)